

BOUNCING GAITS AND BICYCLING:
THE BIOMECHANICS AND ENERGETICS OF HUMAN LOCOMOTION
WITH AND WITHOUT ASSISTIVE DEVICES

by

STEPHEN PATRICK ALLEN

B.S., Humboldt State University (now Cal Poly Humboldt), 2013

M.S., University of Colorado Boulder, 2018

A thesis submitted to the
Faculty of the Graduate School of the
University of Colorado in partial fulfillment
of the requirement for the degree of
Doctor of Philosophy
Department of Integrative Physiology

2023

Committee Members:
Alena Grabowski¹, Ph.D. (Faculty Mentor, Chair)
Andrew Tan, Ph.D.
Rodger Kram, Ph.D.
Kristine Snyder, Ph.D.
Richard Neptune, Ph.D.

Allen, Stephen Patrick (Ph.D., Integrative Physiology)

Bouncing Gaits and Bicycling: The Biomechanics and Energetics of Human Locomotion With
and Without Assistive Devices

Thesis directed by Associate Professor Alena M. Grabowski

Wearable assistive devices, such as lower-limb exoskeletons and prostheses, can be used to augment human locomotion and may allow users to perform tasks with reduced metabolic effort, or promote physical activity and improve overall health. The goal of this dissertation is to examine the biomechanics and energetics of bouncing gaits (i.e., hopping and running) and cycling, and determine how assistive devices influence performance. First, I determined how the major biomechanical determinants of metabolic power in hopping and running change across step frequency (Chapter 1), and how hopping biomechanics are influenced by use of a passive, full-leg exoskeleton with linear and non-linear stiffness springs (Chapter 2). Then, I examined how altering bicycle and prosthesis configurations affect the biomechanics and metabolic costs of cyclists with a unilateral transtibial (below-knee) amputation (Chapters 3 & 4).

In Chapter 1, I found that active muscle volume per step decreases as step frequency increases in hopping and running, with the largest reductions attributed to the muscles surrounding the knee joint. I also found that accounting for changes in active muscle volume improves estimates of metabolic power using the ‘cost of generating force’ framework. These results support the general hypothesis that the metabolic cost of bouncing gaits is related to the magnitude of active muscle volume recruited to generate force and the rate at which force is produced.

In Chapter 2, I found that hopping in place using a passive, full-leg exoskeleton primarily assists the muscles surrounding the ankle, followed by the knee and hip, due to the exoskeleton’s

average moment arm about each joint. Moreover, use of degressive stiffness springs within the exoskeleton provides the greatest reduction in the muscle-tendon unit's contribution to overall ankle and knee joint moment and power, likely due to greater elastic energy stored in the spring for a given displacement and the length of the exoskeleton moment arms. These findings suggest that use of a passive full-leg exoskeleton for bouncing gaits may assist multiple joints and provide valuable information for the development of future assistive devices.

In Chapters 3 and 4, I found that in cyclists with a transtibial amputation, shortening the affected side crank arm length and increasing the prosthetic effective leg length while using a daily-use prosthesis did not affect biomechanical asymmetries between legs or influence efficiency. However, shortening the affected side crank arm length when cyclists used a cycling-specific prosthesis (CSP) provided small reductions in hip joint power and hip transfer power asymmetry. Use of a CSP also reduced knee joint angle asymmetry and improved efficiency compared to a daily-use prosthesis. Thus, bicycle and prosthesis configurations influence rider mechanics and performance, and optimizing these configurations could promote cycling as exercise and improve the overall health of athletes with a lower-limb amputation.

Together, these studies improve our understanding of the biomechanical and metabolic effects of integrating assistive devices in human locomotion and may inform the development of future devices aimed at improving human performance.

Acknowledgements

To my wife Greta, thank you for standing with me through it all. Without you, this work would not have been possible.

Words cannot express how grateful I am for the unwavering support of my academic family, loved ones, and friends who have counseled and encouraged me. Alena Grabowski, thank you for your mentorship, constant patience, and belief in me throughout my academic career, even when I doubted myself. Krissy Snyder, thank you for setting the example of the scientist I want to be. Your diligence, selflessness, and empathy in life and in research is what I strive to emulate. Rodger Kram, thank you for welcoming me into your wonderful academic family and encouraging me from afar. To Angela Montgomery, CPO and Todd Carver, thank you for your assistance and technical expertise that made the cycling studies possible. To my parents and family, thank you for the unconditional love you've given me and the courage to always push forward – “nothing in life is wasted”. I would also like to recognize the past and present members of the Applied Biomechanics Lab, Locomotion Laboratory, Neuromechanics Laboratory, and Neurophysiology of Movement Laboratory for building lasting friendships over the years. Your camaraderie through the trials and tribulations of academia was invaluable and something I will forever cherish. Lastly, I would be remiss if I didn't mention the Thursday night D&D crew (Derek Ichien, Kevin Kopp, Jason Pfaff, Trevor Caudle, Colin Korbisch, and Calen Golden) who met almost every week for the last four and half years to shirk our responsibilities for a few hours, roll dice, get into fantastical hijinks, and argue about what constitutes a sandwich. Sharing our lives together has been a true blessing and your steadfast companionship has been a constant (and needed) reminder that there is more to life than work.

The work within these pages is not simply mine, but all of ours. Thank you all.

Contents

Introduction	1
Chapter 1: Evaluating the ‘cost of generating force’ hypothesis across frequency in human running and hopping	6
1.1 Introduction.....	7
1.2 Methods.....	10
1.3 Results.....	15
1.4 Discussion.....	26
1.5 Conclusion	32
Chapter 2: Spring stiffness profile affects lower-limb joint mechanics while hopping using a passive, full-leg exoskeleton	33
2.1 Introduction.....	34
2.2 Methods.....	39
2.3 Results.....	46
2.4 Discussion.....	52
2.5 Conclusion	60
Chapter 3: Effects of asymmetric crank arm lengths and cycling-specific prostheses in riders with a unilateral transtibial amputation	61
3.1 Introduction.....	63
3.2 Methods.....	68
3.3 Results.....	74
3.4 Discussion.....	80
3.5 Conclusion	88
3.6 Supplemental Materials	90
Chapter 4: The effect of increased prosthetic leg length and cycling-specific prostheses in cyclists with a unilateral transtibial amputation	96
4.1 Introduction.....	97
4.2 Methods.....	101
4.3 Results.....	106
4.4 Discussion.....	113
4.5 Conclusion	119
Conclusions	120
References	123

Tables

Table 1.1 Linear mixed-effects model results for effective mechanical advantage and active muscle volume.....	21
Table 1.2 Biomechanical variables for running and hopping in place a different percentages of preferred step frequency.....	21
Table 2.1 Participant characteristics and exoskeleton stiffness organized by body mass.....	45
Table 2.2 Hopping kinematics and kinetics.....	53
Table 3.1 Crank power and cadence while riding with different affected side crank arm lengths.....	83
Table 4.1 Average net efficiency, total mechanical power, and cadence while riding with increased prosthetic effective leg lengths.....	120
Table 4.2 Average asymmetry between affected and unaffected sides.....	123

Figures

Figure 1.1 Active muscle volume across percentage of preferred step frequency.....	19
Figure 1.2 Effective mechanical advantage (EMA) across percentage of preferred Step frequency.....	20
Figure 1.3 Rate of force production across percentage of preferred step frequency.....	22
Figure 1.4 Cost-coefficients across percentage of preferred step frequency.....	23
Figure 1.5 Gross metabolic power across percentage of preferred step frequency.....	24
Figure 1.6 Measured and predicted gross metabolic power across percentage of preferred step frequency.....	25
Figure 1.7 Limits of agreement (Bland-Altman).....	26
Figure 2.1 Illustration of the exoskeleton line of action and spring stiffness profile.....	46
Figure 2.2 Joint angle and range of motion.....	54
Figure 2.3 Instantaneous and cycle-average joint moment.....	55
Figure 2.4 Instantaneous and cycle-average positive joint power.....	57
Figure 2.5 Relative joint contributions to total average positive power.....	58
Figure 2.6 Average sagittal-plane exoskeleton moment arms.....	61
Figure 3.1 Illustration of bicycle ergometer set up and the two prosthesis types.....	74
Figure 3.2 Average instantaneous joint and crank power.....	85
Figure 3.3 Average joint and crank power	86
Figure 3.4 Percent asymmetry for joint and crank power.....	88
Figure 3.5 Average net efficiency.....	89
Figure 3.6 Instantaneous knee joint angle.....	93
Supplementary Content 3.1 2-way repeated-measures SPM ANOVA.....	99
Supplementary Content 3.2 Pairwise SPM t-test of affected side crank arm length.....	100
Supplementary Content 3.3 Pairwise SPM t-test of prosthesis types.....	104
Figure 4.1 Illustration of pylon length and effective leg length in a daily-use prosthesis and cycling-specific prosthesis	112
Figure 4.2 Instantaneous and average hip, knee, and ankle joint angle throughout the crank Cycle	122
Figure 4.3 Average joint and crank power.....	125

Introduction

Biomechanists and physiologists often seek to understand how human movement is related to metabolic energy expenditure. Wearable assistive devices, such as lower-limb exoskeletons or prostheses, may improve a user's performance by reducing the metabolic effort to perform a task (Allen and Grabowski, 2019; Farris and Sawicki, 2012; Grabowski and Herr, 2009; Sawicki et al., 2020) or provide the means for an individual to complete a task and reduce the risk of injury (Childers et al., 2009; Sepp et al., 2020). The central goal of this dissertation is to examine the biomechanics and energetics of bouncing gaits (i.e., hopping and running) and cycling, and determine how wearable assistive devices influence performance.

In bouncing gaits (i.e., hopping and running), the primary determinant of metabolic power is the cost of producing muscle force to support body weight, which is influenced by the rate that muscular force is produced (approximated by the inverse of ground contact time) and the volume of active muscle (Kram and Taylor, 1990; Roberts et al., 1998a; Taylor, 1994). This framework, dubbed the 'cost of generating force' hypothesis, has well-described the rate of metabolic energy expenditure across a four-fold increase in velocity and a 4000-fold increase in body weight in forward hopping, trotting, and running animals (Kram and Taylor, 1990; Roberts et al., 1998b); and accounts for the non-linear increase in the rate of metabolic energy expenditure when humans run up to 5.25 m s^{-1} (Batliner et al., 2018; Kipp et al., 2018). However, if these parameters fundamentally link the biomechanics of bouncing gaits to metabolic energy expenditure, then they should apply to multiple modes of bouncing gaits, such as hopping and running at different step frequencies. In chapter 1, I determined how active muscle volume changes with step frequency during human hopping and running on level ground. I also evaluated how accounting for the changes in active muscle volume affects our estimates of metabolic power under the 'cost of

generating force' framework. This study was published in the *Journal of Applied Physiology* in 2022.

The fundamental mechanics of bouncing gaits can be characterized by a spring-mass model, which represents the leg as a massless linear spring supporting a point mass that represents body mass (Blickhan, 1989; McMahon and Cheng, 1990). During ground contact, the leg spring stores and returns elastic energy, and reduces metabolic energy expenditure by decreasing muscle force production (Kram and Taylor, 1990; Roberts et al., 1998a; Taylor, 1994). The springlike function of the leg during bouncing gaits has inspired the development of a passive, full-leg exoskeleton with springs in parallel to the user's legs. Use of this exoskeleton results in a decrease in the metabolic power required for hopping in place on both feet by 18-28% over multiple frequencies (Grabowski and Herr, 2009). Moreover, the magnitude of the metabolic power reduction while using a passive, full-leg exoskeleton, depends on the stiffness profile of the springs within the exoskeleton (i.e., the continuous slope of the spring's force-displacement curve) (Allen and Grabowski, 2019). While using a passive, full-leg exoskeleton, humans utilize neuromotor adaptations to maintain similar center of mass mechanics compared to unassisted hopping (Allen and Grabowski, 2019; Grabowski and Herr, 2009). However, it is unknown how users adapt their lower-limb joint kinematics and kinetics to the device. In chapter 2, I determined how users adapt their lower-limb joint mechanics while hopping using a passive, full-leg exoskeleton with three different spring stiffness profiles (degressive - initially stiff and becomes less stiff with compression, linear, and progressive - initially compliant and stiffness increases exponentially with compression) while having the same average stiffness at 10 cm of displacement. This manuscript is in preparation, and we intend to submit it to the *Journal of the Royal Society Interface* in the coming weeks.

Cycling offers a low-impact, aerobic exercise option for many people, without incurring the high joint and tissue loads inherent in weight-bearing exercises (such as hopping or running) and provides numerous health benefits over a sedentary lifestyle (Oja et al., 2011; Orekhov et al., 2019; Poonsiri et al., 2021). Cyclists produce power at the crank through the muscles surrounding the ankle, knee, and hip joints, with additional power transferred from the upper body through the hip (Fregly and Zajac, 1996; van Ingen Schenau et al., 1990). Cyclists with a unilateral transtibial amputation (TTA) require the use of a prosthesis to transfer power to the crank. However, a prosthesis is unable to emulate the dorsi- and plantar-flexion of a biological ankle joint, which likely contributes to kinematic and kinetic asymmetries between legs (Childers et al., 2009). Previously, cyclists with a TTA were found to have an ~20% mechanical crank work asymmetry between affected and unaffected sides (Childers and Kogler, 2014), which presumably worsens net efficiency (the ratio of mechanical power to net metabolic power).

The kinematic and kinetic asymmetries in cyclists with a TTA may be addressed by altering the bicycle-rider geometry (“bike fit”) or prosthesis type. Previous work has shown that shortening the affected side crank arm length by 10 mm (from 172 mm to 162 mm), reduces kinematic asymmetries in average knee joint angle and hip joint range of motion, but does not affect joint or crank work asymmetries (Childers and Kogler, 2014). However, standard commercial cranks often have a larger range (160 – 175 mm), and cyclists with a TTA may choose to ride using their daily-use prosthesis (made of a carbon-fiber socket, metal pylon, and a passive-elastic prosthetic foot) or a cycling-specific prosthesis (CSP; similar to a daily-use prosthesis, but with the prosthetic foot removed and the metal pylon lengthened) which may have a different effect with shorter affected side crank arm lengths. In chapter 3, I determined how shorter affected side crank arm lengths and prosthesis type (daily-use prosthesis vs. CSP) influence joint and crank

power, joint and crank power asymmetry, and net efficiency in cyclists with a TTA. This manuscript is in preparation, and we intend to submit it to *Medicine and Science in Sports and Exercise* in the coming weeks.

The kinematic and kinetic asymmetries in cyclists with a TTA may also be addressed by the prosthesis configuration. The biological ankle dorsi- and plantar-flexes by $\sim 20^\circ$ during the crank cycle to assist with transferring power to the crank (Childers and Kogler, 2014), which changes the effective leg length (the distance between the knee joint center to the center of the cycling cleat) by ~ 15 mm. Presumably, the affected side has greater average knee and hip joint angles than the unaffected side so that the leg is more extended to reach the bottom of the crank cycle (Childers et al., 2009), especially if saddle height has been set based on the unaffected side. Increasing the effective leg length of the prosthesis may decrease average knee and hip joint angles and improve kinematic and kinetic asymmetries between sides. Additionally, use of a CSP likely increases average knee and hip joint angles even further due to the absence of the prosthetic foot. These changes in knee and hip joint angles could influence joint and crank power, joint and crank power asymmetry, and net efficiency by altering the muscle force-length-velocity relationship of the knee and hip extensors. In chapter 4, I determined how increased prosthetic effective leg length using a daily-use prosthesis or a CSP influences joint angle, joint and crank power, kinematic and kinetic asymmetries, and net efficiency in cyclists with a TTA. This manuscript is in preparation, and we intend to submit it to *Medicine and Science in Sports and Exercise* in the coming weeks.

In summary, Chapter 1 determined the effects of step frequency on active muscle volume in hopping and running, and how accounting for those changes affect estimates of metabolic power using the ‘cost of generating force’ framework. I found that active muscle volume per step decreases with increasing step frequency, and accounting for these changes improves estimates of

metabolic power using the ‘cost of generating force’ framework. Chapter 2 quantified the effect of hopping using a passive, full-leg exoskeleton on lower-limb joint mechanics. I found that use of a passive full-leg exoskeleton assists multiple joints simultaneously and reduces the muscle-tendon unit contribution to positive joint power, without altering peak joint flexion angle and the distribution of positive power compared to unassisted hopping. Chapters 3 & 4 determined how changes to bicycle-rider geometry or prosthesis type and configurations influence joint kinematics, kinetics, and net efficiency. I found that shorter affected side crank arm lengths offer small improvements in hip joint and hip transfer power asymmetry, but this does not influence net efficiency. Increased prosthetic effective leg length does not influence hip power asymmetry or net efficiency. Instead, use of a CSP may reduce kinematic asymmetries and improve net efficiency compared to a daily-use prosthesis. These findings further our understanding of bouncing gaits and cycling and provide a foundation for future development of assistive devices to improve performance or promote physical activity and improve overall health.

Chapter 1: Evaluating the ‘cost of generating force’ hypothesis across frequency in human running and hopping

Co-authors: Owen N. Beck & Alena M. Grabowski

Published: *Journal of Experimental Biology* (2022)

The volume of active muscle and duration of extensor muscle force well explain the associated metabolic energy expenditure across body mass and velocity during level-ground running and hopping. However, if these parameters fundamentally drive metabolic energy expenditure, then they should pertain to multiple modes of locomotion and provide a simple framework for relating biomechanics to metabolic energy expenditure in bouncing gaits. Therefore, we evaluated the ability of the ‘cost of generating force’ hypothesis to link biomechanics and metabolic energy expenditure during human running and hopping across step frequencies. We asked participants to run and hop at 85%, 92%, 100%, 108% and 115% of preferred running step frequency. We calculated changes in active muscle volume, duration of force production and metabolic energy expenditure. Overall, as step frequency increased, active muscle volume decreased as a result of postural changes via effective mechanical advantage (EMA) or duty factor. Accounting for changes in EMA and muscle volume better related to metabolic energy expenditure during running and hopping at different step frequencies than assuming a constant EMA and muscle volume. Thus, to ultimately develop muscle mechanics models that can explain metabolic energy expenditure across different modes of locomotion, we suggest more precise measures of muscle force production that include the effects of EMA.

1.1 Introduction

For decades, biomechanists and physiologists have sought to link the mechanics of running and hopping with the corresponding metabolic energy expenditure. One prevailing approach is the ‘cost of generating force’ hypothesis, which was proposed by Taylor and colleagues (Kram and Taylor, 1990; Taylor, 1994; Taylor et al., 1980) and posits that the primary determinant of the metabolic energy expenditure required for running and hopping is the cost of generating muscular force to support body weight. This hypothesis is predicated on the fact that animals produce stride-average vertical ground reaction forces equal to body weight when running or hopping on level ground. Previous studies have demonstrated that metabolic energy expenditure depends on animal size, and that metabolic energy expenditure increases in almost direct proportion to the total weight of a running animal (Taylor et al., 1980). Further, per unit of body mass, it is more metabolically costly for smaller animals (e.g. mouse) to generate a unit of force than larger animals (e.g. horse) (Taylor, 1985), because small animals take more frequent strides and use less economical muscle fibers to produce force quickly (Heglund and Taylor, 1988). Thus, the metabolic energy expenditure during running and hopping varies with size and may depend on the number of strides taken per second, or stride frequency.

Kram and Taylor (1990) expanded the ‘cost of generating force’ hypothesis to explain why metabolic energy expenditure increases near linearly when running or hopping at faster velocities. They reasoned that the rate of force generation (i.e. the rate of cross-bridge cycling) could be approximated by the inverse of ground contact time and formally proposed that the rate of metabolic energy expenditure (\dot{E}_{met} in W) during running equals an animal’s body weight (F_{BW}) multiplied by the inverse of ground contact time (t_c^{-1}) and a metabolic cost coefficient (c) (Eqn 1.1):

$$\dot{E}_{met} = F_{BW} \cdot t_c^{-1} \cdot c \quad [1.1]$$

To produce the force needed to support body weight over each stride, animals need to activate a volume of muscle (i.e., the number of active actin–myosin cross-bridges), which is primarily influenced by body weight and the leg’s effective mechanical advantage (EMA). EMA is the ratio of the ground reaction force moment arm to the muscle tendon moment arm. Kram and Taylor (1990) assumed that active muscle volume and EMA were independent of velocity (Biewener, 1989), which is why they simplified the equation to use force in units of body weight. Using this assumption, Eqn 1.1 well describes the increase in metabolic energy expenditure for a four-fold increase in velocity and 4000-fold increase in body weight during forward hopping, trotting and running animals (Kram and Taylor, 1990; Roberts et al., 1998a).

Since Kram and Taylor (1990), multiple studies have shown that active muscle volume and EMA change across running velocity and limb morphology (Kipp et al., 2018b; Roberts et al., 1998b; Wright and Weyand, 2001). Notably, Roberts et al. (1998b) demonstrated that running bipeds have a greater EMA than size-matched quadrupeds as a result of their upright posture, which influences active muscle volume and metabolic energy expenditure. Thus, the authors proposed a refined version of the ‘cost of generating force’ hypothesis to account for changes in active muscle volume where the rate of metabolic energy expenditure equals the product of active muscle volume (V_m), the inverse of ground contact time and a new cost coefficient (k) (Eqn 1.2):

$$\dot{E}_{met} = V_m \cdot t_c^{-1} \cdot k \quad [1.2]$$

Kipp et al. (2018b) applied this refined version of the ‘cost of generating force’ hypothesis (Eqn 1.2) to human running and found that humans decrease their EMA and increase active muscle volume by as much as 53% from 2.2 m s⁻¹ to 5.0 m s⁻¹. Thus, the authors concluded that the curvilinear increase in metabolic energy expenditure with running velocity (Batliner et al., 2018)

results from an increase in active muscle volume and an increase in the rate of force production as a result of shorter ground contact times.

Though the rate of force generation and active muscle volume well explain metabolic energy expenditure across different running and hopping velocities, it is unknown whether these biomechanical variables adequately account for changes in metabolic energy expenditure across different stride and step frequencies, where during running, a step equals ground contact and the subsequent aerial time and two steps comprise a stride. Previous studies have shown that humans have a preferred step frequency when running at a constant velocity and hopping in place that minimizes metabolic energy expenditure, and deviating from the preferred step frequency increases metabolic energy expenditure (Allen and Grabowski, 2019; Cavagna et al., 1988; Cavanagh and Williams, 1982; Farris and Sawicki, 2012; Grabowski and Herr, 2009; Högberg, 1952; Raburn et al., 2011; Swinnen et al., 2021) – exhibiting a U-shaped relationship between metabolic energy expenditure and step frequency (Doke and Kuo, 2007; Snyder and Farley, 2011; Swinnen et al., 2021) under these conditions. Previous studies have suggested that the U-shaped relationship is due to simultaneous increasing and decreasing metabolic costs (Doke and Kuo, 2007; Snyder and Farley, 2011; Swinnen et al., 2021), where ground contact time decreases with increased step frequency during human running and hopping, which implies that humans must produce forces at a faster rate and increase metabolic cost (Farley et al., 1991). When considering the ‘cost of generating force’ hypothesis, Gutmann and Bertram (2017a,b) suggest that the rate of force production alone (Eqn 1.1) cannot fully account for the U-shaped changes in metabolic energy expenditure with hopping frequency, unless conditions are highly constrained (e.g. fixed hopping frequency and changing hop height), and may also depend on the cost of activating a given muscle volume. Therefore, accounting for changes in active muscle volume along with the

rate of force production (Eqn 1.2) may better explain the U-shaped relationship between metabolic energy expenditure and step frequency. An increase in step frequency is simultaneously accompanied by shorter steps when running at a constant velocity, and a decrease in center of mass displacement during running and hopping – both of which may increase EMA, reduce active muscle volume and decrease metabolic cost (Monte et al., 2021). Thus, accounting for changes in the rate of force production and active muscle volume through EMA may better describe metabolic energy expenditure across step frequencies than the cost of generating force alone.

The purpose of this study was to determine how active muscle volume changes across step frequency in running and hopping, and to evaluate the ‘cost of generating force’ equations (Eqns 1 and 2), when changes in active muscle volume are accounted for. Both equations well characterize changes in metabolic energy expenditure across different velocities; however, accounting for changes in active muscle volume due to running and hopping mechanics may better account for the U-shaped changes in metabolic energy expenditure across different frequencies. We hypothesized that active muscle volume would decrease as step frequency increases in running and hopping as a result of increased EMA. Further, we hypothesized that accounting for changes in active muscle volume and the rate of force production (Eqn 1.2) would better explain changes in metabolic energy expenditure across step frequencies compared with the original ‘cost of generating force’ equation, which estimates active muscle volume from body weight (Eqn 1.1) for both running and hopping.

1.2 Methods

1.2.1 Participants

Ten healthy runners (6 female, 4 male; mean±s.d. mass 60.7±8.9 kg, height 1.72±0.09 m, age 24.5±3.4 years) with no reported cardiovascular, neurological or musculoskeletal impairments

participated in the study. All participants reported running for exercise at least 30 min per day, 3 times per week, for at least 6 months. Each participant provided written informed consent to participate in the study according to the University of Colorado Boulder Institutional Review Board.

1.2.2 Experimental Protocol

Over two separate days, participants performed a series of running trials on a force-measuring treadmill (Treadmetrix, Park City, UT, USA; 1000 Hz) and stationary, two-legged hopping trials on force plates (Bertec, Columbus, OH, USA; 1000 Hz) while we simultaneously measured ground reaction forces, lower limb kinematics, and metabolic energy expenditure throughout each trial. On the first day, participants performed six, 5 min running trials at 3ms⁻¹. During the first trial, we determined each participant's preferred step frequency (PSF). We collected ground reaction forces (GRFs) for 15 s during the third and fifth minute of the first trial and determined average PSF from ground contact events identified by a 20 N vertical GRF threshold. We then instructed participants to complete the remaining running trials while matching their step frequency to the timing of an audible metronome. The metronome was set to 85%, 92%, 100%, 108% and 115% of their PSF, similar to previous studies (Snyder and Farley, 2011; Swinnen et al., 2021), and the order of the trials was randomized. On the second day, participants performed five, 5 min stationary hopping trials, on both feet. To account for the effects of frequency on metabolic energy expenditure and given the similarity of frequencies that minimize metabolic energy expenditure during hopping and running (Allen and Grabowski, 2019; Cavagna et al., 1997; Farris and Sawicki, 2012; Grabowski and Herr, 2009; Kaneko et al., 1987), we instructed participants to hop in place while matching their step frequency to the audible

metronome set to 85%, 92%, 100%, 108% and 115% of their PSF from day 1. The order of the hopping trials was randomized, and we did not determine preferred hopping frequency.

1.2.3 Metabolic energy expenditure

We measured participants' rates of oxygen consumption and carbon dioxide production via indirect calorimetry (TrueOne 2400, ParvoMedics, Sandy, UT, USA) throughout each running and hopping trial. We instructed participants to refrain from exercising before each experimental session or ingesting caffeine 4 h before each experimental session to minimize day-to-day variability in metabolic rate. Additionally, participants were instructed to be at least 2 h postprandial at the start of each experimental session to mitigate potential effects of diet on metabolic measurements. Further, each experimental session was performed at the same time each day and separated by at least 24 h to eliminate any potential effects of day-to-day variability or fatigue. We calculated gross steady-state metabolic power from the average metabolic rates during the last 2 min of each 5 min trial using a standard equation (Kipp et al., 2018a; Péronnet and Massicotte, 1991).

1.2.4 Kinematics and kinetics

We positioned 40 reflective markers bilaterally on both legs and the pelvis. Markers on the ankles and knees were used to define joint centers and clusters of 3–4 markers were placed on each segment prior to experimental trials. We collected lower limb kinematic data for 15 s during the last minute of each trial using 3D motion capture (Vicon Nexus 2.3, Oxford, UK; 200 Hz) simultaneously with GRFs. We analyzed 20 steps from each trial and used a 4th order low-pass Butterworth filter with a 20 Hz cut-off to process analog GRF signals and marker trajectories (Alcantara, 2019; Mai and Willwacher, 2019). We determined ground contact using a 20 N vertical GRF threshold for both running and hopping and calculated the rate of force production as the

inverse of ground contact time (t_{c-1}). To calculate EMA and V_m , we estimated the average extensor muscle–tendon unit force (F_{mtu}) about each joint assuming a constant muscle–tendon moment arm (r) for each muscle group and using instantaneous ankle, knee and hip sagittal joint moments from Visual 3D (Visual 3D, C-Motion Inc., Germantown, MD, USA) (Biewener et al., 2004; Kipp et al., 2018b). We only included joint moment values that exceeded 25% of the maximum extensor moment because of the inherently noisy center of pressure measurements caused by low force values at the beginning and end of the ground contact phase (Biewener et al., 2004; Griffin et al., 2003; Kipp et al., 2018b). Because the net joint moments of the knee and hip include flexion moments from bi-articular muscles, we accounted for forces in bi-articular muscles by assuming F_{mtu} was proportional to the physiological cross-sectional area of active muscle fibers (Eqns 1.3–1.5).

$$M_{ankle} = r_{ankle} \cdot F_{mtu,ankle} \quad [1.3]$$

$$M_{knee} = r_{knee} \cdot F_{mtu,knee} - \left(r_{BF} \cdot F_{mtu,hip} \frac{PCSA_{BF}}{\sum PCSA_{hip}} \right) - \left(r_{Gas} \cdot F_{mtu,ankle} \frac{PCSA_{Gas}}{\sum PCSA_{ankle}} \right) \quad [1.4]$$

$$M_{hip} = r_{hip} \cdot F_{mtu,hip} - \left(r_{RF} \cdot F_{mtu,knee} \frac{PCSA_{RF}}{\sum PCSA_{knee}} \right) \quad [1.5]$$

where M is the net joint moment, r is a weighted-average muscle–tendon moment arm and PCSA is the physiological cross-sectional area. Gas, BF and RF represent the properties of the gastrocnemius, biceps femoris and rectus femoris muscles, respectively. We calculated $F_{mtu,ankle}$ from Eqn 1.3, and solved Eqns 1.4 and 1.5 simultaneously because of the two unknown quantities of $F_{mtu,knee}$ and $F_{mtu,hip}$. We considered moments that extend joints to be positive. Values for r and PCSA were taken from the anthropometric data of four male human cadavers reported in Biewener et al. (2004) and previously used in Kipp et al. (2018b). We then used the quotient of the average

sagittal plane resultant GRF magnitude and F_{mtu} at each joint during ground contact to calculate EMA, which equals the quotient of r and the GRF moment arm (R).

$$EMA = \frac{GRF}{F_{mtu}} = \frac{r}{R} \quad [1.6]$$

We calculated V_m separately for each joint (Eqn 1.7) and then summed them to estimate the total average V_m per leg. To do this, we assumed the muscles produced force isometrically with a constant stress ($\sigma=20 \text{ N cm}^{-2}$) (Perry et al., 1988) and combined this with our estimates of F_{mtu} and weighted-average fascicle length (L) from Biewener et al. (2004):

$$V_m = \frac{F_{mtu} \cdot L}{\sigma} \quad [1.7]$$

1.2.5 Estimating cost-coefficients and metabolic energy expenditure

We calculated the metabolic cost coefficients, c and k , for each trial during running and hopping using Eqns 1.1 and 1.2. We averaged each cost coefficient across the range of frequencies (separately for running and hopping). Then we implemented the respective cost coefficient averages in addition to V_m , t_c^{-1} and F_{BW} to predict metabolic power for each step frequency during running and hopping using Eqns 1.1 and 1.2.

1.2.6 Statistics

To evaluate the agreement between measured metabolic power and predicted metabolic power from Eqns 1.1 and 1.2, we performed limits of agreement analyses (Bland–Altman) for each target step frequency and calculated the systematic bias (mean differences) and 95% limits of agreement. In conjunction, we also provide the minimum detectable change (Dontje et al., 2018) for each model. We also constructed linear mixed-effects models ($\alpha=0.05$) to determine the effect of measured step frequency relative to PSF on t_c^{-1} , c , k , EMA, V_m , average joint extensor moment

and average sagittal plane resultant GRF magnitude. In each linear mixed-effects model, we considered measured step frequency relative to PSF as a fixed effect and participant as a random effect. Model coefficients are reported alongside their P-values and represent the change in the dependent variable per a 1% change in measured step frequency relative to PSF. We performed all statistical analyses in R (v3.6.3; <http://www.R-project.org/>) using custom scripts and packages (<https://github.com/deepankardatta/blandr/>; <https://CRAN.R-project.org/package=nlme>; <https://CRAN.R-project.org/package=psych>; <https://CRAN.R-project.org/package=ggplot2>).

1.3 Results

We removed data for one participant at the 85% PSF and 92% PSF running trials because they were >3% off the target step frequencies.

1.3.1 Running

The linear mixed-effects model showed that total V_m decreased by $0.32 \text{ cm}^3 \cdot \text{kg}^{-1}$ for every 1% increase in step frequency relative to PSF ($p < 0.001$; **Figure 1.1B**; **Table 1.1**). Specifically, participants decreased ankle, knee, and hip V_m by $0.06 \text{ cm}^3 \cdot \text{kg}^{-1}$, $0.17 \text{ cm}^3 \cdot \text{kg}^{-1}$, and $0.09 \text{ cm}^3 \cdot \text{kg}^{-1}$, respectively, for every 1% increase in step frequency ($p < 0.001$ for each; **Figure 1.1A**; **Table 1.1**). Despite the reduction in joint-specific V_m , we did not detect significant changes in ankle, knee, or hip EMA across step frequency ($p = 0.66$; $p = 0.05$; $p = 0.59$, respectively). Average (\pm s.d.) EMA across step frequencies for the ankle, knee, and hip was 0.314 ± 0.017 , 0.393 ± 0.084 , and 0.714 ± 0.117 , respectively (**Figure 1.2**, **Table 1.1**). Rather, the changes in joint-specific V_m may have been due to the decrease in average ankle, knee, and hip extensor moments as step frequency increased.

Average ankle, knee, and hip extensor moments decreased by $0.01 \text{ N}\cdot\text{m}\cdot\text{kg}^{-1}$ ($p<0.001$), $0.02 \text{ N}\cdot\text{m}\cdot\text{kg}^{-1}$ ($p<0.001$), and $0.01 \text{ N}\cdot\text{m}\cdot\text{kg}^{-1}$ ($p=0.002$), respectively, for every 1% increase in step frequency (**Table 1.2**). Finally, t_c^{-1} increased by 0.02 s^{-1} for every 1% increase in step frequency relative to PSF during running ($p<0.001$; **Figure 1.3A**). We used these variables to solve for the cost-coefficient and found that c decreased by $0.003 \text{ J}\cdot\text{N}^{-1}$ for every 1% increase in step frequency ($p<0.001$; **Figure 1.4A**), but k did not change across step frequency, and averaged (\pm s.d.) $0.087 \pm 0.003 \text{ J}\cdot\text{cm}^{-3}$ ($p=0.18$; **Figure 1.4A**).

On average, measured metabolic power was minimized when participants ran at their PSF (**Figure 1.5A**), which was an average (\pm s.d.) step frequency of $2.90 \pm 0.09 \text{ Hz}$ (**Table 1.2**). As participants deviated from their PSF, average measured metabolic power increased by 19% and 10% when running at 85% of PSF and 115% of PSF, respectively (**Figure 1.5A**). Overall, metabolic power estimated with Eqn. 1 underestimated average metabolic power for step frequencies slower than PSF (up to 13% at 85% PSF) but overestimated average metabolic power for step frequencies equal to or greater than PSF (up to 9% greater at 108% PSF) (**Figure 1.6A, 1.6C & 1.7A**). The Limits of Agreement analysis shows that the metabolic power estimated with Eqn. 1.2 had a bias closer to zero and lower than Eqn. 1.1 at each step frequency, however, the magnitude of the upper and lower limits of agreement for Eqn. 1.2 were greater than those of Eqn. 1.1 (**Figure 1.7A**). The minimum detectable change was 3.1 W kg^{-1} and 3.8 W kg^{-1} using Eqns. 1.1 and 1.2, respectively.

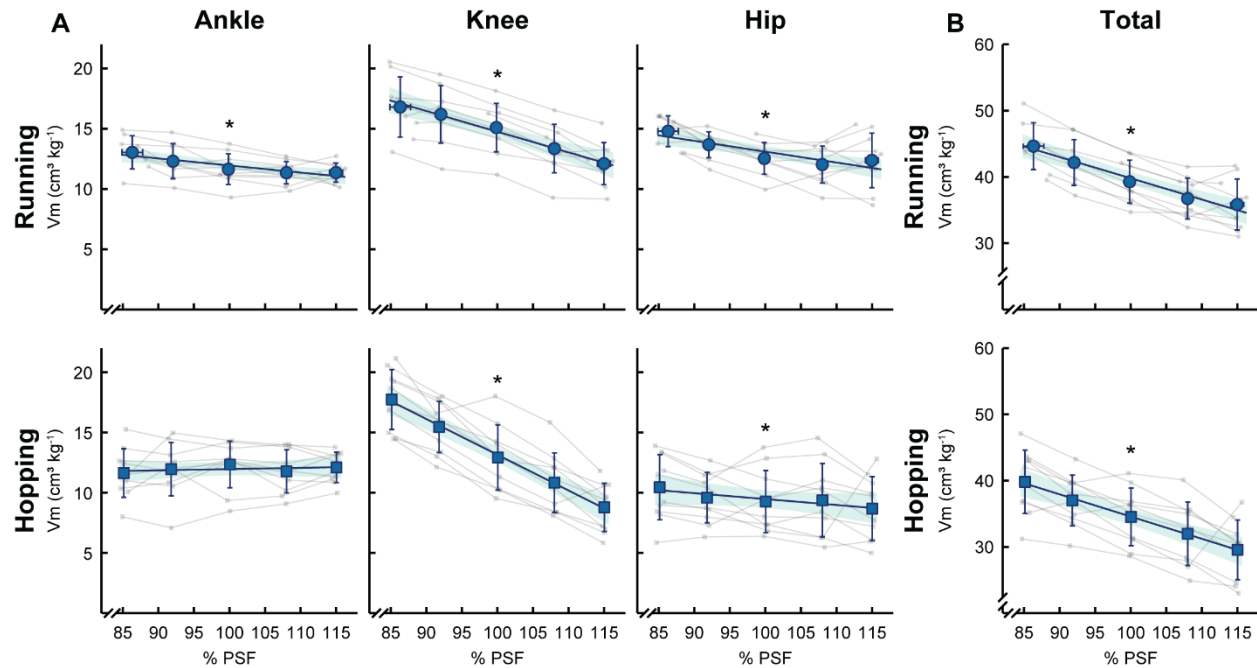


Figure 1.1 Active muscle volume across percentage of preferred step frequency. Mean \pm s.d. active muscle volume (V_m) of the leg extensors during ground contact (blue symbols) and values from individual subjects (gray symbols) versus the percentage of running preferred step frequency (% PSF) for running and hopping. (A) V_m of the muscles surrounding the ankle, knee and hip joints during running (top) and hopping (bottom), and (B) the summed total of the ankle, knee and hip joint V_m . The dark lines represent the results of linear mixed-effects models, and the shaded regions represent the model's 95% confidence intervals. Coefficients and intercepts for each of the linear mixed-effects models are presented in **Table 1.1**. Asterisks indicate the model slope is significantly different from zero. Vertical and horizontal error bars may not be visible behind data points.

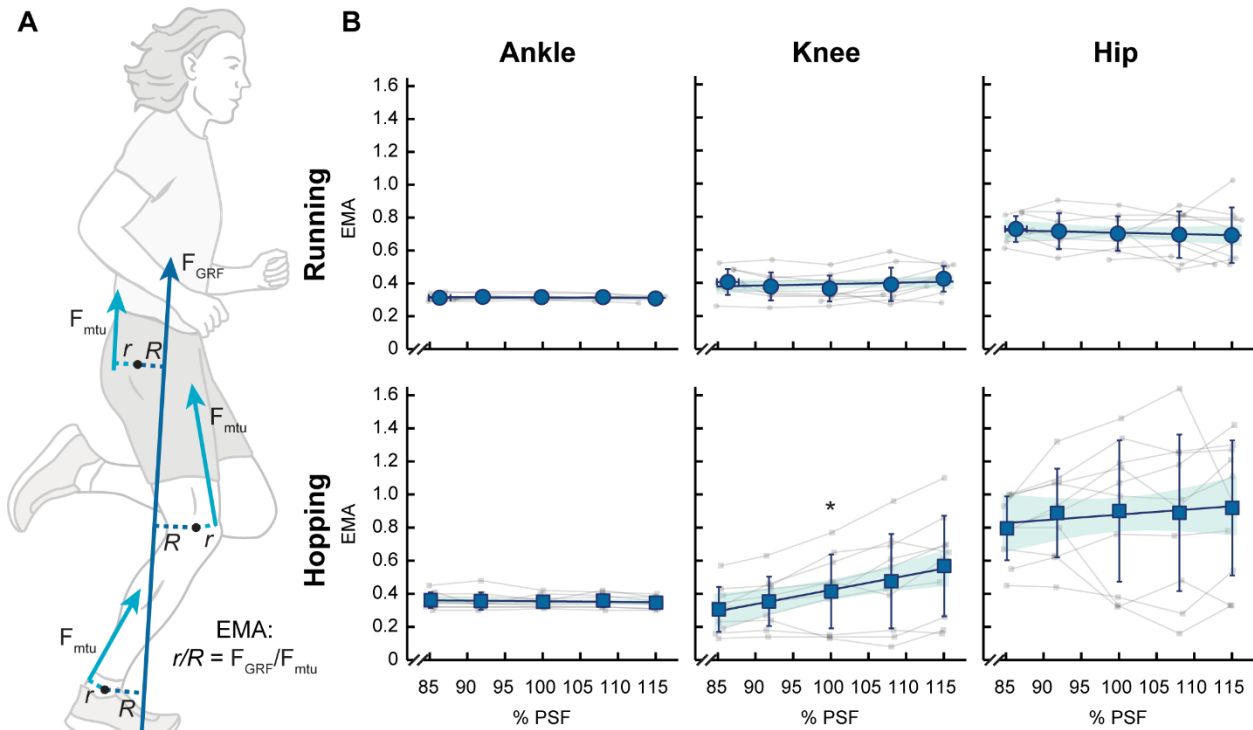


Figure 1.2 Effective mechanical advantage (EMA) across percentage of preferred step frequency. (A) Illustration of EMA during running, which equals the ratio of the *muscle tendon* moment arm (r) and the external resultant ground reaction force moment arm (R) or the ratio of resultant ground reaction force (F_{GRF}) and muscle force (F_{mtu}). (B) Mean \pm s.d. EMA for the ankle, knee and hip joints (blue symbols) with values for individual subjects (gray symbols) versus the percentage of running PSF. The dark lines represent the results of linear mixed-effects models and the shaded regions represent the model's 95% confidence intervals. Coefficients and intercepts for each of the linear mixed-effects models are presented in **Table 1.1**. Asterisks indicate the model slope is significantly different from zero. Vertical and horizontal error bars may not be visible behind data points.

Table 1.1 Linear mixed-effects model results for effective mechanical advantage and active muscle volume

	Joint	V_m			EMA		
		Intercept	Slope	p-value	Intercept	Slope	p-value
Running	Ankle	17.6	-0.06	<0.001	0.32	$-0.24 \cdot 10^{-5}$	0.87
	Knee	31.9	-0.17	<0.001	0.29	$1.0 \cdot 10^{-3}$	0.07
	Hip	22.5	-0.09	<0.001	0.76	$-4.9 \cdot 10^{-4}$	0.67
	Total	72.2	-0.32	<0.001	-	-	-
Hopping	Ankle	11	0.01	0.43	0.39	$-3.6 \cdot 10^{-4}$	0.06
	Knee	42.7	-0.3	0.001	-0.4	$8.4 \cdot 10^{-3}$	<0.001
	Hip	14.4	-0.05	0.0275	0.63	$2.7 \cdot 10^{-3}$	0.35
	Total	68.1	-0.34	<0.001	-	-	-

V_m : active muscle volume; EMA: effective mechanical advantage; p-value < 0.05 indicates a slope significantly different from zero with respect to percent of preferred running stride frequency. Linear mixed-effects model is in the form of $Y = \text{Intercept} + \%PSF \cdot \text{Slope}$.

Table 1.2 Biomechanical variables for running ($3 \text{ m} \cdot \text{s}^{-1}$) and hopping in place at different percentages of preferred running step frequency.

	Target % PSF	Achieved % PSF	Achieved step frequency (Hz)	Stance Avg. resultant GRF (BW)	Avg. extension moment ($\text{N} \cdot \text{m} \cdot \text{kg}^{-1}$)		
					Ankle	Knee	Hip
Running	85	86.3 ± 1.5	2.50 ± 0.1	1.60 ± 0.12	2.35 ± 0.25	1.77 ± 0.37	1.06 ± 0.13
	92	92.0 ± 0.2	2.67 ± 0.1	1.52 ± 0.09	2.22 ± 0.26	1.73 ± 0.35	0.97 ± 0.10
	100	100.0 ± 0.1	2.90 ± 0.1	1.42 ± 0.09	2.10 ± 0.23	1.62 ± 0.29	0.88 ± 0.12
	108	108.1 ± 0.3	3.13 ± 0.1	1.40 ± 0.09	2.05 ± 0.17	1.37 ± 0.30	0.87 ± 0.16
	115	115.2 ± 0.5	3.34 ± 0.1	1.36 ± 0.13	2.05 ± 0.14	1.17 ± 0.23	0.93 ± 0.21
Hopping	85	85.1 ± 0.4	2.46 ± 0.1	1.49 ± 0.11	2.10 ± 0.36	2.04 ± 0.37	0.63 ± 0.25
	92	91.8 ± 0.3	2.66 ± 0.1	1.47 ± 0.08	2.16 ± 0.40	1.71 ± 0.33	0.59 ± 0.20
	100	100.1 ± 0.2	2.90 ± 0.1	1.49 ± 0.09	2.23 ± 0.35	1.33 ± 0.40	0.62 ± 0.22
	108	108.1 ± 0.2	3.13 ± 0.1	1.46 ± 0.05	2.12 ± 0.32	1.02 ± 0.35	0.67 ± 0.26
	115	115.1 ± 0.3	3.33 ± 0.1	1.46 ± 0.08	2.18 ± 0.28	0.73 ± 0.26	0.65 ± 0.23

Average \pm SD.; PSF, preferred running step frequency; GRF, ground reaction force; Avg. joint moment is defined when extension moments are greater than 25% of the peak joint moment.

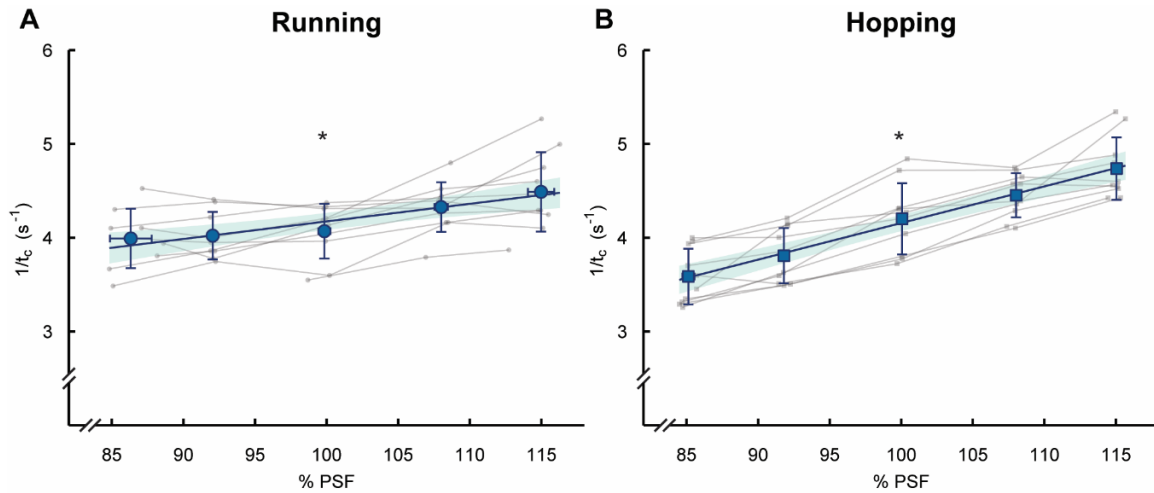


Figure 1.3 Rate of force production across percentage of preferred step frequency. Average \pm SD rate of force production (t_c^{-1} ; large, blue symbols) and values from individual subjects (small, grey symbols) versus the percentage of running preferred step frequency (% PSF) for A) running and B) hopping. The dark lines represent the model prediction across percentage of preferred step frequency (running: $t_c^{-1} = 0.021 \cdot \text{PSF} + 2.160$, hopping: $t_c^{-1} = 0.040 \cdot \text{PSF} + 0.216$) and the shaded areas represent the 95% confidence interval. * indicates if the model slope is significantly different from zero. Vertical and horizontal error bars may not be visible behind data points.

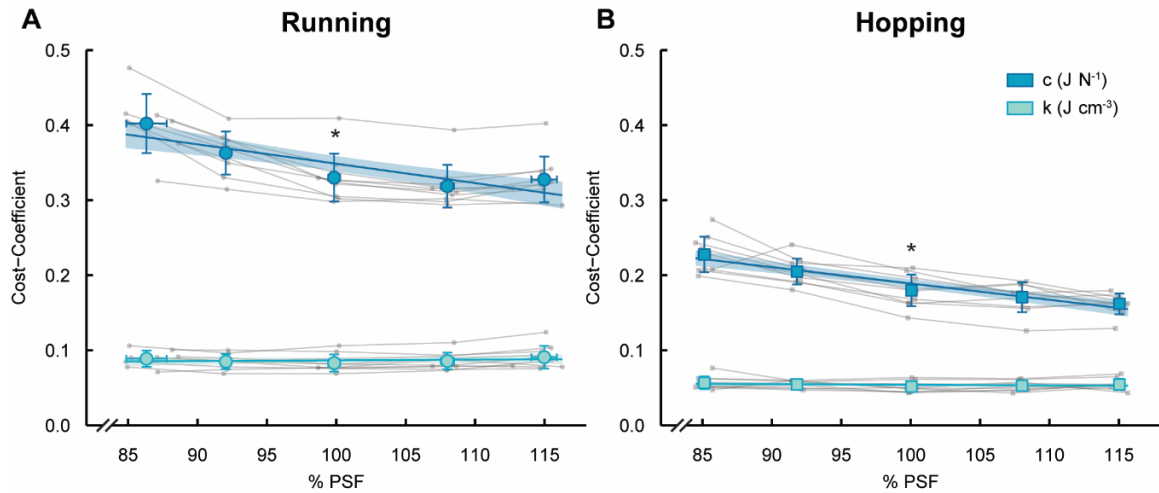


Figure 1.4 Cost-coefficient across percentage of preferred step frequency. Average \pm SD cost coefficients (c – large, dark blue symbols and k – large, light blue symbols) and values from individual subjects (small, grey symbols) versus the percentage of running preferred step frequency (% PSF) in A) running and B) hopping. The lines represent the results of the linear mixed-effects model where $c = -0.003 \cdot \text{PSF} + 0.601$ ($p < 0.001$) and $k = 1.16 \times 10^{-4} \cdot \text{PSF} + 0.075$ ($p = 0.18$) for running, and $c = -0.0022 \cdot \text{PSF} + 0.407$ ($p < 0.001$) and $k = 0.001 \cdot \text{PSF} + 0.045$ ($p = 0.20$) for hopping. The p-values indicate if the slope is significantly different than zero. The dark lines represent the results of linear mixed-effects models, and the shaded regions represent the model's 95% confidence intervals. Vertical and horizontal error bars may not be visible behind data points.

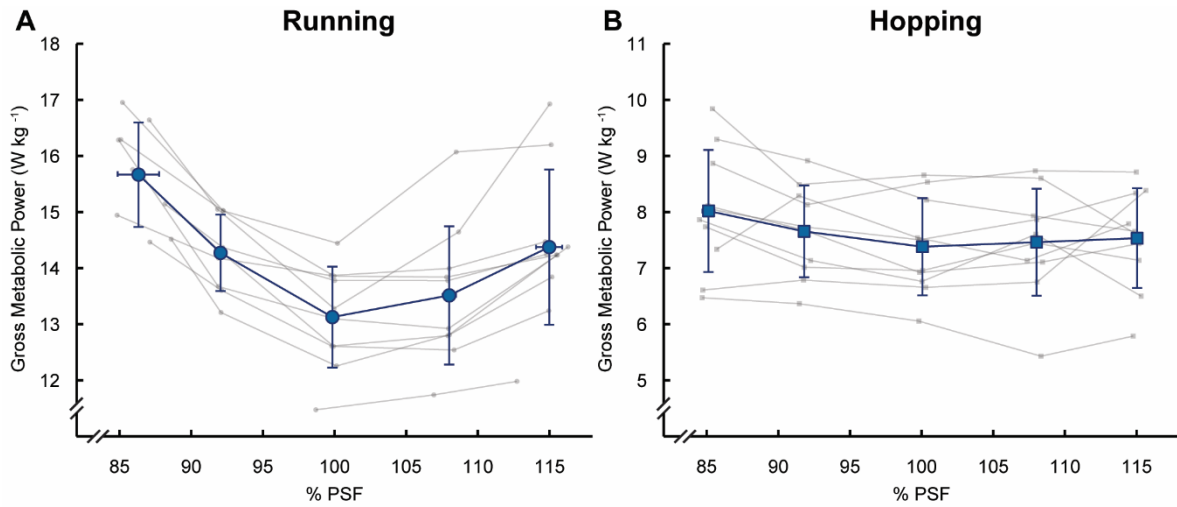


Figure 1.5 Gross metabolic power across percentage of preferred step frequency. Average \pm SD metabolic power (large, blue symbols) and values from individual subjects (small, grey symbols) versus the percentage of running preferred step frequency (% PSF) in A) running and B) hopping. Vertical and horizontal error bars may not be visible behind data points.

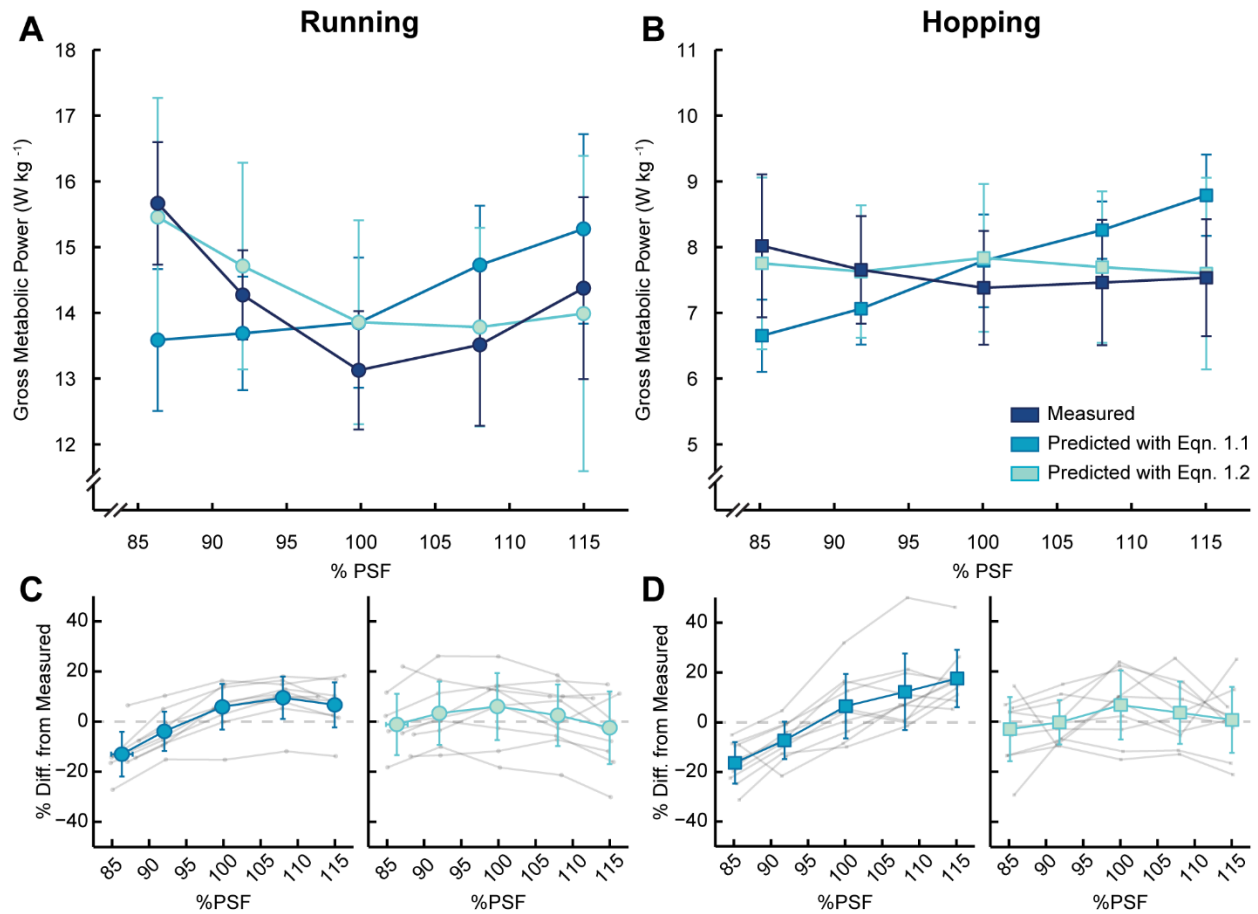


Figure 1.6 Measured and predicted gross metabolic power across percentage of preferred step frequency. Average \pm SD (large, colored symbols) gross metabolic power for measured (dark blue) and predicted values using Eqn.1.1 (blue) and Eqn. 1.2 (light blue) versus the percentage of running preferred step frequency (% PSF) in A) running and B) hopping. Vertical and horizontal error bars may not be visible behind the data points. C) Running and D) hopping percent difference between each equation and measured metabolic power for average \pm SD and participants (small, grey symbols).

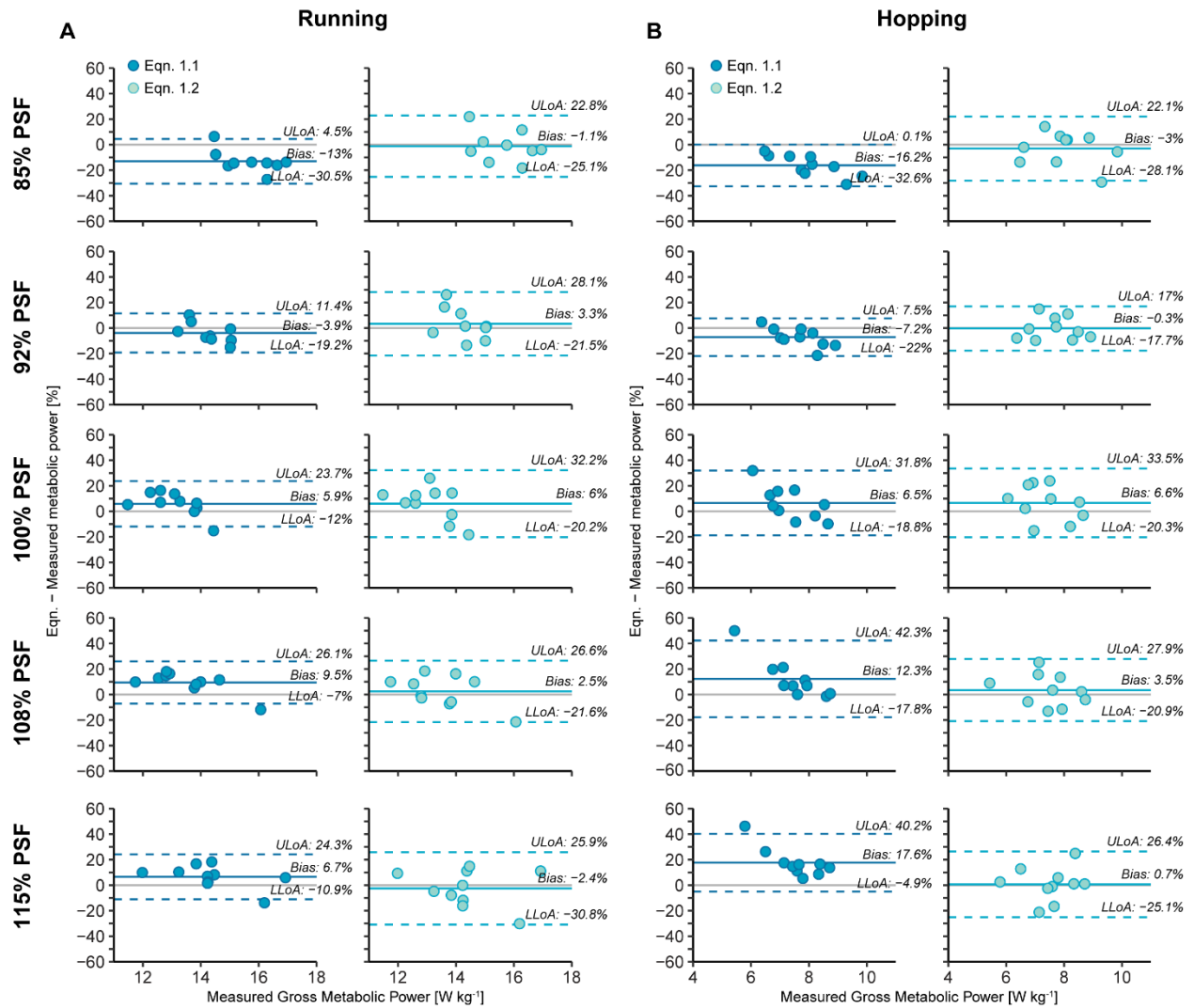


Figure 1.7 Limits of Agreement (Bland-Altman). Limits of agreement analysis comparing the percent difference between Eqn. 1 (blue symbols) or Eqn. 2 (light blue symbols) and gross metabolic power measured via indirect calorimetry. Mean differences (Bias) are indicated by the solid-colored lines, while the lower and upper limits of agreement (LLoA/ULoA) are denoted by dashed-colored lines. LLoA/ULoA were calculated using 1.96 SD.

1.3.2 Hopping

The linear mixed-effects models showed that total V_m decreased by $0.34 \text{ cm}^3 \cdot \text{kg}^{-1}$ for every 1% increase in step frequency relative to PSF ($p < 0.001$; **Figure 1.1B**; **Table 1.1**). Participants decreased joint-specific V_m at the knee and hip by $0.30 \text{ cm}^3 \cdot \text{kg}^{-1}$ and $0.05 \text{ cm}^3 \cdot \text{kg}^{-1}$ for every 1% increase in step frequency ($p < 0.001$ and $p = 0.028$, respectively; **Figure 1.1A**; **Table 1.1**), whereas ankle V_m did not change across step frequency and averaged (\pm s.d.) $11.96 \pm 1.81 \text{ cm}^3 \cdot \text{kg}^{-1}$ ($p = 0.43$; **Figure 1.1A**; **Table 1.1**). We found that knee EMA increased by 0.008 for every 1% increase in step frequency ($p < 0.001$; **Figure 1.2**, **Table 1.1**). However, ankle and hip EMA did not change across step frequency and averaged (\pm s.d.) 0.35 ± 0.04 ($p = 0.06$) and 0.88 ± 0.36 ($p = 0.22$), respectively (**Figure 1.2**; **Table 1.2**). Similarly, participants decreased average knee extensor moment by $0.04 \text{ N} \cdot \text{m} \cdot \text{kg}^{-1}$ for every 1% increase in step frequency ($p < 0.001$; **Table 1.2**). However, average ankle and hip extensor moments did not change across step frequency and averaged (\pm s.d.) $2.16 \pm 0.33 \text{ N} \cdot \text{m}$ ($p = 0.43$) and $0.63 \pm 0.22 \text{ N} \cdot \text{m} \cdot \text{kg}^{-1}$ ($p = 0.34$), respectively. Finally, t_c^{-1} increased by 0.04 s^{-1} for every 1% increase in step frequency relative to PSF during stationary hopping ($p < 0.001$; **Fig 1.3B**). We used these variables to solve for the cost-coefficients and found that c decreased by $0.0022 \text{ J} \cdot \text{N}^{-1}$ for every 1% increase in step frequency ($p < 0.001$; **Figure 1.4B**), but k did not change across step frequency and averaged (\pm s.d.) $0.054 \pm 0.007 \text{ J} \cdot \text{cm}^{-3}$ ($p = 0.20$; **Figure 1.4B**).

On average, measured metabolic power numerically increased by 9% and 2% when hopping at 85% of PSF and 115% of PSF, respectively, relative to 100% PSF ($p > 0.9$; **Figure 1.5B**). On average, metabolic power estimated with Eqn. 1.1 underestimated metabolic power for step frequencies slower than PSF (up to 17% at 85% PSF) but overestimated metabolic power for step frequencies greater than PSF (up to 17% at 115% PSF) (**Figure 1.6B**, **1.6D** & **1.7B**).

Metabolic power estimated with Eqn. 1.2 had a bias closer to zero and lower than Eqn. 1.1 at each step frequency (**Figure 1.7B**). The magnitude of the upper and lower limits of agreement for Eqn. 1.2 were greater than those of Eqn. 1.1. (**Figure 1.7B**). The minimum detectable change was 2.6 W kg⁻¹ and 2.1 W kg⁻¹ using Eqns. 1.1 and 1.2, respectively.

1.4 Discussion

Our data partially support our first hypothesis as active muscle volume (V_m) per step decreased as step frequency increased when running at a constant velocity and hopping in place. When step frequency increased from 85% PSF to 115% PSF, we found that V_m decreased by 20% and 26% during running and hopping, respectively. This reduction predominantly occurred as a result of changes in V_m at the knee in both running and hopping, with smaller or non-significant contributions from the ankle and hip during both tasks (**Figure 1.1, Table 1.1**). We found that the V_m at the knee accounted for ~53% and ~88% of the change in total V_m during running and hopping, respectively, whereas, when humans run at faster velocities from 2.2 to 5.0 m s⁻¹, V_m at the knee accounts for ~20% of the change in total active muscle volume (Kipp et al., 2018b).

The mechanism by which total V_m decreased with step frequency differed between running and hopping. We found that joint-specific EMA was independent of step frequency during running (**Figure 1.1, Table 1.1**). Therefore, the reductions in total V_m during running were likely due to greater duty factors (product of contact time and frequency), which resulted in reduced stance-average resultant GRFs and the corresponding joint moments (**Table 1.2**). In comparison, during hopping, EMA at the knee increased by 86% when step frequency increased from 85% to 115% PSF, while the magnitude of stance-average resultant GRF did not change (**Figure 1.2, Tables 1.1 and 1.2**). This might imply that participants decreased total V_m during hopping by altering their lower limb position to hop with a straighter leg and extended knee as step frequency increased.

When taken together, these results suggest that humans may utilize two different mechanisms to alter total V_m during bouncing gaits, duty factor (Beck et al., 2020) and EMA. Previously, Kipp et al. (2018b) demonstrated that humans utilize the two mechanisms simultaneously to increase total V_m when running at different velocities. They found that runners increased total V_m by 53% with faster running velocities from 2.2 to 5.0 m s⁻¹ as a result of a concurrent increase in GRFs and decrease in hip EMA, which is likely due to the increased step frequency that accompanies faster running velocity (Heglund and Taylor, 1988).

Our knee and ankle EMA results during two-legged, stationary hopping conflict with those of Monte et al. (2021), who suggest that knee EMA is independent of step frequency (2.0–3.5 Hz). Our results may differ from those of Monte et al. (2021) because of a difference in methodology. We calculated joint-specific average EMA during the stance phase when joint moments exceeded 25% of their peak value, whereas Monte et al. (2021) separated stance into two phases and included EMA values obtained when GRF and center of pressure are noisy (near ground contact or toe off), which may increase variability in EMA and obscure changes that occur with step frequency (Griffin et al., 2003). There may have also been differences in inter-participant hopping strategies between studies, where participants adopt a strategy of hopping with their knees ‘locked’ or ‘unlocked’. While our average knee EMA data suggest that participants straightened their legs to hop at faster frequencies, three of our participants did not appreciably change their knee EMA across frequency (**Figure 1.2**), which could be interpreted as choosing a ‘locked’ knee strategy.

Our results provide mixed support of our second hypothesis, that accounting for changes in V_m (Eqn 1.2) better explains changes in metabolic energy expenditure across step frequencies compared with the original ‘cost of generating force’ equation, which estimates V_m through body weight alone (Eqn 1.1). Eqn 1.1 exhibited a bias for running and hopping that systematically varied

with step frequency – underestimating metabolic power for step frequencies lower than preferred and overestimating metabolic power for step frequencies higher than preferred (**Figure 1.7**), which was likely due to the linear increase in the rate of force production (t_c^{-1}). In contrast, Eqn 1.2 had a lower bias across all step frequencies for running and hopping, but wider limits of agreement (**Figure 1.7**) that encompassed the average metabolic power between any two step frequencies. Additionally, the minimum detectable change for Eqns 1.1 and 1.2 was greater than the overall range of average measured metabolic power in running (2.6 W kg^{-1}) and hopping (0.6 W kg^{-1}). Together, these results might suggest that neither Eqn 1.1 or 1.2 is sensitive to the changes in metabolic power that occur with step frequency and they have limited usefulness when considering participant-specific responses. However, we found Eqn 1.2's cost coefficient (k) to be near-constant across step frequency for running and hopping (**Figure 1.4**), which suggests a better performing model because changes in metabolic power are proportional to changes in the rate of force produced and the total volume of active muscle (Griffin et al., 2003; Kipp et al., 2018a; Kram and Taylor, 1990; Roberts et al., 1998a,b). Thus, including changes in active muscle volume in the 'cost of generating force' equation may better account for changes in average metabolic power during running and hopping across different frequencies, but may require further refinement to be used to describe participant-specific responses.

1.4.1 Variation in the cost coefficient

The 'cost of generating force' hypothesis originally put forth by Kram and Taylor (1990) provides a simple equation (Eqn 1.1) that links biomechanics to metabolic energy expenditure across running velocities. However, this framework assumes animals employ a constant EMA, while muscles operate at consistent relative shortening velocities and lengths. Changes in the cost coefficient may result from differences in one of these assumptions (Full et al., 1990; Roberts et

al., 1998a), whereas a constant cost coefficient implies that the primary mechanical determinants of metabolic energy expenditure have been accounted for. Here, we found that accounting for changes in V_m (Eqn 1.2) due to running or hopping mechanics results in a near-constant cost coefficient, k (**Figure 1.4**), across step frequencies and is in line with previous research reported for human running (0.079 J cm^{-3}) at different velocities (Kipp et al., 2018b).

Despite a near-constant cost coefficient while running and hopping at different step frequencies, the wide limits of agreement suggest that neither equation is sensitive to changes in metabolic energy expenditure, and this could be due to other factors that our study did not account for. For instance, Eqns 1.1 and 1.2 are not able to account for changes in the influence of muscle contractile dynamics (i.e., relative shortening velocity and fiber length) on metabolic energy expenditure. In a recent study, Beck et al. (2020) demonstrated that producing the same cycle-average force with a decreasing duty factor during cyclic soleus contractions requires greater peak muscle force, a decrease in fascicle operating length, and a general increase in active muscle volume and metabolic energy expenditure. Future studies might improve predictions of the ‘cost of generating force’ hypothesis by utilizing duty factor as a proxy for muscle contractile dynamics and validate it against ultrasound or modeling approaches.

In addition, although the ‘cost of generating force’ equations account for the majority of the metabolic cost of a muscle contraction, these equations are unable to account for 30–40% of the metabolic cost, which has been primarily attributed to ion pumping (Barclay, 2017; Rall, 1985) and cycling activating/ deactivating muscles per unit time (Bergstrom and Hultman, 1988; Doke et al., 2005; Hogan et al., 1998). Cyclically activating and deactivating muscles at faster frequencies, such as in our study, should incur a large metabolic cost for ion pumping. Therefore, while these simple equations can be used to estimate metabolic energy expenditure in exercising

animals, they do not fully account for all aspects of muscle metabolism that might be found in more detailed approaches (Umberger et al., 2003), and may contribute to variation in the cost coefficient and wide limits of agreement.

1.4.2 Running versus hopping

We evaluated how active muscle volume changes with step frequency during running and hopping, and how well changes in metabolic energy expenditure could be explained when accounting for these changes. We did not intend to compare running and hopping, yet it is interesting to note that the cost coefficient (k) is almost twice as large in running compared with hopping. One possible reason for this may be the metabolic cost of leg swing during running (Arellano and Kram, 2014; Doke et al., 2005; Marsh et al., 2004; Moed and Kram, 2005), which is estimated to comprise ~10–25% of the total metabolic cost of running, and is not accounted for in the ‘cost of generating force’ equation.

Previous research suggests that the metabolic cost surface of hopping (in the height–frequency domain) is different from that of running (Gutmann and Bertram, 2017b), where metabolic energy expenditure increases with hop height at a given frequency, likely as a result of an increase in the rate of force production and active muscle volume. Here, we did not constrain hop height in order to evaluate the ‘cost of generating force’ hypothesis on U-shaped metabolic energy expenditure data. However, future studies could determine how well these ‘cost of generating force’ equations predict metabolic cost when hopping frequency and height are constrained.

1.4.3 Limitations

A potential limitation of our study is the use of static internal muscle–tendon moment arms, fascicle lengths and pennation angles to estimate active muscle volume. We intentionally did this

to allow a direct comparison of our results with those of previous studies (Biewener et al., 2004; Kipp et al., 2018a) that account for active muscle volume changes during human locomotion. Previous studies have shown that muscle–tendon moment arms change with joint angle (Arnold et al., 2010; Hoy et al., 1990; Rasske et al., 2017). We found that accounting for active muscle volume increases interparticipant variability of predicted metabolic energy expenditure compared with assuming a constant active muscle volume (Figs 1.6 and 1.7). This increase in variability may be due to the assumption of fixed-length muscle moment arms. Inter-participant variability in total active muscle volume and predicted metabolic energy expenditure using Eqn 1.2 might be reduced by accounting for changes in muscle moment arms during the stance phase and/or scaling moment arms to leg lengths (Griffin et al., 2003). Thus, using variable muscle–tendon moment arms that change with joint angle could further improve the estimate of active muscle volume and metabolic energy expenditure during running and hopping.

Finally, we intentionally set out to investigate the changes in active muscle volume and evaluate the ‘cost of generating force’ equations when metabolic power demonstrates a U-shaped relationship with step frequency in two types of bouncing gaits running and hopping. When running, this U-shaped relationship is observed at a constant velocity (Cavagna and Kaneko, 1977; Cavagna and Legramandi, 2015; Cavagna et al., 1997; Cavanagh and Williams, 1982; Heglund and Taylor, 1988; Högberg, 1952; Snyder and Farley, 2011; Swinnen et al., 2021); however, a change in step frequency is accompanied by a proportional change in step length. Therefore, we were unable to separate the effect of changing step frequency from step length and present the combined effects. Nonetheless, we provide information on the influence of changes in active muscle volume and the generalizability of a simple equation that relates metabolic energy expenditure to biomechanics.

1.5 Conclusion

In this study, we investigated changes in active muscle volume and evaluated the ‘cost of generating force’ hypothesis for predicting metabolic energy expenditure across different step frequencies during running and hopping. We found that accounting for changes in effective mechanical advantage to compute active muscle volume resulted in a near-constant cost coefficient, k , and may improve the estimation of average metabolic energy expenditure. Our data, along with previous studies, support the general hypothesis that the metabolic energy expenditure required for bouncing gaits is related to the magnitude of active muscle volume recruited to generate force and the rate that the force is produced, but further considerations of the model’s assumptions need to be addressed to further refine and account for variation in metabolic energy that occur with changes in step frequency.

Chapter 2: Spring stiffness profile affects lower-limb joint mechanics while hopping using a passive, full-leg exoskeleton

In preparation - with intent to submit to *Journal of Royal Society Interface*

Passive, full-leg exoskeletons that act in-parallel with the legs can reduce the metabolic power of bouncing gaits like hopping. However, the magnitude of metabolic power reduction depends on the spring stiffness profile of the exoskeleton and is presumably affected by how users adapt their lower-limb joint mechanics. We determined the effects of using a passive, full-leg exoskeleton with degressive, linear, and progressive stiffness springs on lower-limb joint kinematics and kinetics during stationary, bilateral hopping at 2.4 Hz. We found that use of a passive, full-leg exoskeleton did not affect peak lower-limb joint flexion compared to unassisted hopping, but reduced the muscle-tendon unit contributions at the ankle and knee, due to the average exoskeleton moment arm about each joint and the elastic energy returned by the exoskeleton springs. The greatest reduction in the muscle-tendon unit contribution to average ankle and knee joint moment and power occurred with degressive, followed by linear and progressive stiffness springs, likely due to differences in elastic energy return. Moreover, the relative distribution of positive joint power for each joint did not change when using a passive, full-leg exoskeleton compared to unassisted hopping. Passive, full-leg exoskeletons simultaneously assist multiple lower-limb joints and future assistive devices should consider the effects of spring stiffness profile in their design.

2.1 Introduction

The mechanics of bouncing gaits, such as hopping and running, can be characterized by a spring-mass model, where the leg is represented as a massless linear spring and body mass is represented as a point mass (Blickhan, 1989; Farley and González, 1996; McMahon and Cheng, 1990). During ground contact, the leg spring stores and returns elastic energy in series-elastic tissues like tendon, which contributes to a reduction in muscle mechanical work and metabolic energy expenditure (Alexander and Bennet-Clark, 1977; Roberts et al., 1997). Humans and animals utilize neuromuscular control to adapt the mechanics of the lower-limb in response to locomotor demands, such as modulating leg stiffness to hop or run at different step frequencies or speeds (Arampatzis et al., 1999; Farley and González, 1996; Farley and Morgenroth, 1999; Kuitunen et al., 2011), or increasing effective mechanical advantage and leg stiffness to hop or run on compliant surfaces (Ferris and Farley, 1997; Kerdok et al., 2002). These neuromotor adaptations allow humans to maintain consistent center of mass mechanics and utilize the return of stored elastic energy during hopping and running.

The spring-like function of the leg has inspired the development of lower-limb passive exoskeletons to assist human hopping and running, often with the goal of reducing metabolic power (Sawicki et al., 2020). Similar to series-elastic elements like tendon, passive exoskeletons utilize springs or other elastic materials to store and return mechanical energy to the user. These wearable devices cannot produce net positive work but are able to provide a portion of the overall joint moment and power during hopping and running so that the contribution from the muscle-tendon units (MTUs) surrounding the joint is reduced (Farris and Sawicki, 2012a; Farris et al., 2013). In turn, a passive exoskeleton can reduce whole-body metabolic power by decreasing the

muscle force (Farris et al., 2013) and hence, active muscle volume (Beck et al., 2019; Sawicki et al., 2020).

Previous research has often targeted the lower limb joint with the greatest positive mechanical power during either the ground contact or swing phases of level-ground hopping and running (Farris and Sawicki, 2012a; Nasiri et al., 2018; Witte et al., 2020). During unassisted hopping, the MTUs surrounding the ankle and knee joints provide 53-80% and 18-46% of the total positive mechanical power generated by the leg from 2.2 – 3.2 Hz, respectively (Farris and Sawicki, 2012a). Similarly, when running without an exoskeleton at 2.0 – 3.25 m s⁻¹, the MTUs surrounding the ankle, knee, and hip joint account for 42-47%, 19-21%, and 32-39% of the total positive power over a stride, respectively (Farris and Sawicki, 2012b). Thus, several passive exoskeletons have been designed to assist the ankle joint during the ground contact phase of hopping and running (Farris and Sawicki, 2012a; Ferris et al., 2006; Witte et al., 2020) or the hip joint during the swing phase of running (Nasiri et al., 2018; Zhou et al., 2021). For example, Farris and colleagues found that two-legged hopping in place at 2.5 Hz with a passive exoskeleton in parallel with both ankles reduced metabolic power by 13% (Farris and Sawicki, 2012a; Farris et al., 2013). Use of the ankle-only exoskeleton also reduced the average plantarflexor MTU moment by 30-50%, so that the positive ankle power supplied by the biological tissues was decreased by approximately 50% while users maintained similar spring-mass mechanics compared to unassisted hopping (Farris and Sawicki, 2012a; Farris et al., 2013). However, despite utilizing neuromotor control to adapt to exoskeletal assistance and reduce musculoskeletal demands (Farris and Sawicki, 2012a; Ferris et al., 2006; Witte et al., 2020), metabolic power reductions are not guaranteed (Cherry et al., 2016; Witte et al., 2020).

Passive exoskeleton designs that act during the ground contact phase of hopping and running may need to simultaneously assist multiple joints to achieve greater reductions in muscle force, active muscle volume, and metabolic power (Farris and Sawicki, 2012a; Grabowski and Herr, 2009; Malcolm et al., 2018; van den Bogert, 2003). While the MTUs surrounding the ankle contribute the most to total positive mechanical power during hopping and running, the MTUs that surround the knee and hip joints also significantly contribute to total positive mechanical power during hopping and running. Previously, Farris and colleagues (Farris and Sawicki, 2012a; Farris et al., 2013; Farris et al., 2014) found that hopping using the passive ankle-only exoskeleton resulted in small mechanical changes at the knee, where 6% of the total positive power was redistributed from the knee to the ankle, and almost half of the 13% reduction in metabolic power could be attributed to this small change. Proximal leg muscles that surround the knee and hip joints are thought to be less efficient than distal leg muscles, such as the plantarflexors (Sawicki et al., 2009; Umberger and Rubenson, 2011). Thus, an exoskeleton that spans the ankle, knee, and hip joints may further reduce the metabolic power required for hopping and running by providing greater assistance at the knee or hip compared to an exoskeleton that only spans one joint. Previously, Grabowski and Herr (Grabowski and Herr, 2009) found that a passive full-leg exoskeleton that acted in-parallel with the leg and spanned the ankle, knee, and hip reduced the metabolic power of stationary two-legged hopping by 18-28% across frequencies of 2.2 - 2.8 Hz and users reduced their biological leg stiffness to maintain total overall leg stiffness that was not different from unassisted hopping (Grabowski and Herr, 2009). However, it is not known how users adjusted their lower-limb joint mechanics while hopping using the passive full-leg exoskeleton, and if there is a redistribution of total positive power amongst the lower-limb joints.

Determining biological joint power while using a passive full-leg exoskeleton may provide valuable insight for the future design of passive exoskeletons that augment hopping and running.

The metabolic cost of hopping while using a passive exoskeleton depends on the spring's elastic properties. For example, exoskeleton springs that are more stiff than the leg during stationary hopping can increase metabolic cost and compromise neuromotor control (i.e., changes in hopping frequency or increased difficulty maintaining balance) (Grabowski and Herr, 2009; Robertson et al., 2014). In addition, the decrease in metabolic power reductions depend on the exoskeleton spring stiffness profile, which refers to the continuous slope of the force-displacement curve (Allen and Grabowski, 2019). Previous research of passive ankle-only exoskeletons for hopping and running have utilized a linear-tension spring, where stiffness is constant throughout the spring's displacement (Farris and Sawicki, 2012a; Farris et al., 2013; Farris et al., 2014; Robertson et al., 2014; Witte et al., 2020). However, experiments using a passive, full-leg exoskeleton during stationary hopping have shown that the magnitude of metabolic power reduction depends on the spring's stiffness profile and the amount of elastic energy stored and returned, despite the springs exhibiting the same average stiffness for a given displacement (Allen and Grabowski, 2019). Compared to unassisted hopping at 2.4 Hz, use of a passive full-leg exoskeleton with degressive stiffness springs (initially stiff but becomes less stiff with compression) and linear stiffness springs decreased metabolic power by 24% and 16%, respectively, while the use of progressive springs (initially compliant but stiffness increases non-linearly with compression) did not significantly change metabolic power (Allen and Grabowski, 2019). Users maintained consistent spring-mass mechanics when using each spring stiffness profile, where there were no changes in ground contact time, hop height, or overall leg stiffness compared to unassisted hopping. However, other measures, such as center of mass displacement

during the ground contact phase and peak vertical ground reaction force, were reduced while hopping using a passive full-leg exoskeleton with degressive or linear stiffness springs, which indicates that the spring stiffness profile may elicit different effects on lower-limb joint angles, moments, and powers compared to unassisted hopping. The design of the passive full-leg exoskeleton includes springs that span the entire leg and attach to a waist harness with mounts near the hip joint center of rotation and to a shoe with mounts near the metatarsal joint center of rotation in the sagittal plane. Presumably, this design primarily affects the MTUs surrounding the ankle and knee given that the exoskeleton's sagittal plane moment arm about the hip joint is designed to be smaller than at the ankle or knee joint, and the MTUs surrounding the hip joint provide a negligible contribution to total leg power during hopping (Farris and Sawicki, 2012a). The influence of using a full-leg exoskeleton with different spring stiffness profiles on joint mechanics is not known but may provide further insight into differences in metabolic power during bouncing gaits.

We determined the effects of hopping using a passive full-leg exoskeleton with three different spring stiffness profiles on lower-limb joint mechanics. We hypothesized that peak flexion angles and range of motion at the ankle, knee, and hip joints would decrease while hopping using a passive full-leg exoskeleton compared to unassisted hopping. We also hypothesized that hopping using a passive full-leg exoskeleton would reduce the MTU joint moment and power compared to unassisted hopping, with the greatest reductions occurring with the degressive stiffness springs, followed by linear and progressive stiffness springs, respectively. Finally, we hypothesized that hopping using a passive full-leg exoskeleton would redistribute overall joint power from the knee to the ankle, compared to unassisted hopping.

2.2 Methods

2.2.1 Participants

14 individuals (**Table 2.1**) with no reported cardiovascular, neurological, or musculoskeletal impairments participated in the study. All participants self-reported exercising at least 30 minutes per day at or above a moderate intensity, three times per week, for the last 6 months, and provided written informed consent according to the University of Colorado Boulder Institutional Review Board.

Table 2.1 Participant characteristics and exoskeleton stiffness organized by body mass.

Sex	Age [yr.]	Height [m]	Leg length [m]	Mass [kg]	k_{calc} [kN/m]	k_{DG} [kN/m]	k_{LN} [kN/m]	k_{PG} [kN/m]
F	37	1.70	0.92	58.9	7.84	7.8	7.00	8.00
F	22	1.53	0.86	60.0	7.98	8.4	8.44	8.00
F	23	1.70	0.87	60.6	8.08	7.8	8.44	8.00
F	25	1.65	0.87	62.0	8.24	7.8	8.44	8.00
F	26	1.73	0.93	62.8	8.36	8.2	8.44	8.00
F	26	1.62	0.84	62.9	8.38	7.8	8.44	8.00
F	23	1.59	0.85	63.6	8.46	7.8	8.44	8.00
M	43	1.63	0.94	65.4	8.70	8.2	8.44	8.00
M	20	1.67	0.90	65.9	8.80	9.0	8.44	9.00
M	24	1.73	0.94	67.5	8.98	8.2	8.44	9.00
M	30	1.79	0.94	69.2	9.22	8.2	9.46	9.00
M	25	1.80	0.98	71.6	9.50	9.4	9.46	10.00
M	20	1.64	0.86	75.3	9.96	10.6	9.46	10.00
M	30	1.73	0.88	77.7	10.34	10.6	10.6	10.00
Avg.	26.7	1.68	0.90	66.0	8.77	8.56	8.71	8.64
s.d.	6.5	0.08	0.04	5.7	0.75	0.99	0.82	0.84

Leg length was measured from the greater trochanter to the floor; k_{calc} is calculated exoskeleton stiffness for the sum of both legs; k_{DG} is degressive spring stiffness; k_{LN} is linear spring stiffness; k_{PG} is progressive spring stiffness. All stiffness values represent the sum of both springs and are calculated for 10 cm of displacement. Differences in k_{DG} relative to mass are caused by variations in leg length.

2.2.2 Exoskeleton Design

The full-leg exoskeleton design consists of a waist mount, foot mounts on each shoe, and two exoskeleton “legs” that each incorporate a spring and are compressed in parallel with the legs during the stance phase of stationary, two-legged hopping (**Figure 2.1**). The waist mount is

comprised of an adjustable aluminum frame that is secured tightly around the user's waist with a padded hip belt and nylon webbing harness that wraps beneath the pelvis and around the thighs. The frame includes a 3 degree-of-freedom exoskeleton hip joint (flexion/extension, ab/adduction, and internal/external rotation) positioned near the hip joint's center of rotation in the sagittal plane. The foot mounts are comprised of aluminum pin joints secured to a steel plate that is fastened to the bottom of clipless mountain biking shoes via the cleat mounting holes (Gavin MTB Cycling Shoe, Elkton, FL or Trace MTB Shoe, Diamondback, Kent, WA). The pin joint allows 1 degree-of-freedom (plantar/dorsiflexion) and is positioned near the metatarsal-phalangeal joint's center of rotation in the sagittal plane. The exoskeleton springs act in parallel with the legs and connect to the exoskeleton hip joints and foot mounts.

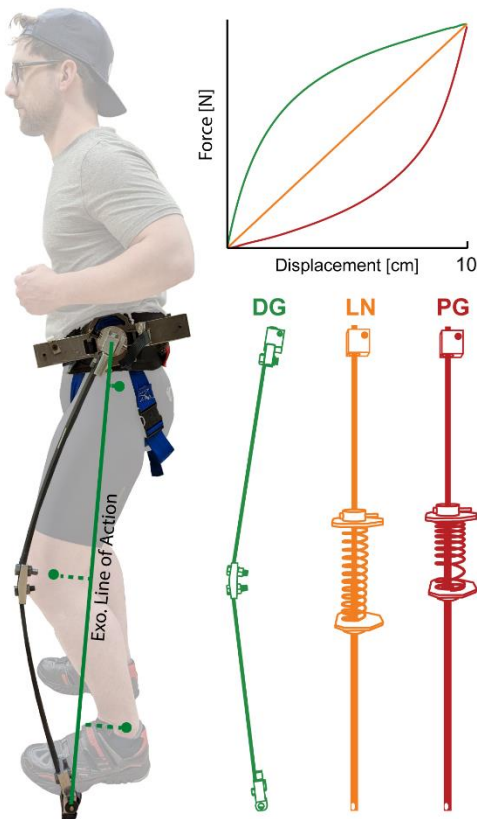


Figure 2.1 Illustration of the exoskeleton line of action relative to the lower-limb joints and the degressive (DG; green), linear (LN; orange), and progressive (PG; red) spring stiffness profiles used in the exoskeleton. Dashed lines from the exoskeleton's line of action to the ankle, knee, and hip joints represent the exoskeleton's moment arm about each joint. The line of action was measured via markers placed on the exoskeleton hip and foot attachment points; motion capture markers are not pictured.

We used three different sets of springs with different stiffness profiles (**Figure 2.1**). We custom-made leaf springs from fiberglass (GC067 UB; Gordon Composites, Montrose, CO) to

create degressive stiffness springs, which are characterized by a high initial stiffness that becomes compliant with further compression (Grabowski and Herr, 2009). The leaf springs consisted of “thigh” and “shank” segments that varied in length by 2.54 cm, where the “thigh” segment was always 2.54 cm longer than the “shank” segment. The two segments were attached together by a piece of aluminum with a 165° angle when unloaded to ensure that the leaf springs would always bend anteriorly to the user. We used metal compression springs with even pitch coils for the linear stiffness springs and variable pitch coils for the progressive stiffness springs, which are characterized by a low initial stiffness that increases exponentially with compression (Allen and Grabowski, 2019). The compression springs were placed between two aluminum plates that could be positioned along the length of two telescoping rods to accommodate different lengths and diameters of the coil springs. When the telescoping rods were attached to the waist harness and foot mounts, the springs could be compressed by the aluminum plates during the stance phase.

We measured the stiffness of each fully assembled exoskeleton “leg” prior to the experimental tests using a materials testing machine to measure instantaneous force and displacement (Series 5859; Instron, Norwood, MA) (Allen and Grabowski, 2019). Because of the non-linear stiffness profiles of the degressive and progressive springs, we characterized the discrete stiffness value for all of the springs at 10 cm of compression, as this approximates the average center of mass displacement while hopping without an exoskeleton at 2.4 Hz (Allen and Grabowski, 2019; Farley et al., 1998; Grabowski and Herr, 2009). We provided participants with springs of the same body mass-normalized stiffness ($\sim 0.132 \text{ kN}\cdot\text{m}^{-1}\cdot\text{kg}^{-1}$ for both springs) at 10 cm of compression (**Table 2.1**), which was the stiffness previously determined to provide the greatest reduction in metabolic power compared to unassisted hopping at 2.4 Hz (Allen and

Grabowski, 2019). A detailed explanation of how this mass-normalized stiffness was calculated can be found in previous papers (23, 24).

We sized each exoskeleton to each participant while their ankles were plantarflexed, and their knees and hips extended, so that they were standing on their toes. We measured the distance from the greater trochanter to the floor under the metatarsal heads to set the exoskeleton “leg” length. This allowed the springs to compress at the instant of ground contact. For the degressive springs, we selected fiberglass segments that achieved the same approximate exoskeleton “leg” length when the spring was fully assembled. The stiffness of the degressive springs is affected by their length, where longer leaf springs are more compliant and shorter leaf springs are stiffer. We controlled for this effect by increasing or decreasing the thickness of the fiberglass by increments of ~0.05 cm to achieve a spring with a stiffness close to the body mass-normalized stiffness. When affixed to the waist harness and foot mounts, the telescoping rods for the linear and progressive springs were able to match the measured exoskeleton “leg” length by sliding past each other. Pre-drilled holes on the “thigh” segment that were ~1.27 cm apart allowed us to set the height of the aluminum plates to accommodate different lengths of coil springs and ensure that compression began at the instant of ground contact.

2.2.3 Experimental Protocol

We simultaneously measured ground reaction forces (GRFs) and lower body kinematics while participants hopped in place, with both feet, at 2.4 Hz in four conditions: normal hopping without an exoskeleton (NH), and using passive full-leg exoskeletons with degressive (DG), linear (LN), and progressive (PG) stiffness springs. Each trial was two minutes long, and we analyzed 20 hops from the last 30 seconds of each trial.

Participants hopped in place on both legs on a stationary, split-belt treadmill (Bertec, Columbus, OH; 1000 Hz) with a force plate under each foot so that separate GRF vectors could be attributed to each leg. Lower body kinematics were recorded with a 10-camera motion capture system (Vicon, Centennial, CO; 200 Hz) using a total of 38 reflective markers placed on the pelvis and both legs. We placed markers on the skin or form-fitted clothes over the anterior and posterior iliac spines, superior aspect of the iliac crests, greater trochanters, bilaterally on the femoral condyles and malleoli, and on the shoes over the first and fifth metatarsal heads, and the posterior aspect of the calcaneus. Rigid clusters of 4 markers were placed on the thigh and shank segments and secured with a soft Velcro wrap. During the exoskeleton conditions the padded waistbelt covered the pelvis, so we placed markers on the outside of the belt over the pelvis anatomical landmarks. Additionally, we placed markers on the exoskeleton hip and shoe attachments to measure spring displacement and orientation.

Participants were given a short acclimatization period (1 – 3 min.) to hop at 2.4 Hz prior to each condition until they reported they were comfortable using each exoskeleton and the research team visually confirmed that participants were able to match the target hopping frequency consistently while maintaining an aerial phase between hops. We randomized the order of conditions and used an audible metronome to enforce the hopping frequency. Participants were given at least 2 minutes of rest between trials due to donning, doffing, and assembly of the exoskeleton “legs”.

2.2.4 Data analysis

We labeled marker trajectories in Vicon Nexus and exported them to Visual 3D (C-motion, Germantown, MD) with GRFs for inverse dynamics analysis. We up-sampled the marker data to match the GRF data, filtered both using a fourth order, lowpass Butterworth filter with a 20 Hz

cutoff (Mai and Willwacher, 2019), and applied a 20 N vertical GRF threshold to detect ground contact. We calculated sagittal plane joint angles, moments, and powers for the ankle, knee, and hip. We measured joint angle as the inter-segment angle between proximal and distal segments, where an increase in joint angle represents extension or plantarflexion, and range of motion was measured as the minimum joint angle subtracted from the maximum joint angle throughout the hop cycle.

In the exoskeleton conditions, a portion of the overall joint moment and power is provided by the exoskeleton and the rest is supplied by the MTUs. To estimate the exoskeleton contributions to overall joint moment and power in the sagittal plane, we first assumed that there was no soft-tissue artifact and estimated the instantaneous exoskeleton force for each leg by combining the displacement of the spring (via the markers at the hip and shoe attachments) with the *a-priori* measured force-displacement data. Because the exoskeleton attachments are low friction pin joints that allow rotation and ~99% of the resultant GRF is directed vertically in hopping (Veilleux et al., 2012), we used the markers on the exoskeleton attachments to define the line of action for exoskeleton force (**Figure 2.1**). We then determined the exoskeleton moment arms about each joint as the perpendicular distance from the joint center to the exoskeleton line of action (**Figure 2.1**). For each joint, we estimated the exoskeleton contribution to the overall joint moment as the cross product of exoskeleton moment arms relative to each joint and the estimated exoskeleton force. We resolved both joint and exoskeleton moments in the proximal segment coordinate system (Schache and Baker, 2007). Then, we estimated the exoskeleton contribution to overall joint power by multiplying the estimated exoskeleton moment by the joint's angular velocity (Malcolm et al., 2018; van den Bogert, 2003). The average joint moments and powers provided by the MTUs were estimated as the difference between the overall joint moments and powers, and the average joint

moment and powers provided by the exoskeleton. We considered moments that acted to extend the joints or plantarflex the ankle to be positive.

At each joint, we separately calculated the MTUs' and exoskeleton's contributions to overall average positive mechanical power according to Farris & Sawicki (Farris and Sawicki, 2012a). First, we used the trapezium method to integrate joint positive power over the hop cycle, and then summed all periods of positive joint work to determine total positive joint work. Next, total positive joint work was divided by the duration of the hop cycle to determine average positive joint power over the hop cycle. The average positive power was then summed across each joint and MTU or exoskeleton contributions to estimate the total average positive power (\bar{P}_{tot}) of the leg (Equation 2.1),

$$\bar{P}_{tot} = \bar{P}_{ankle,mtu} + \bar{P}_{ankle,exo} + \bar{P}_{knee,mtu} + \bar{P}_{knee,exo} + \bar{P}_{hip,mtu} + \bar{P}_{hip,exo} \quad [2.1]$$

where \bar{P}_{ankle} , \bar{P}_{knee} , and \bar{P}_{hip} are the average positive powers from the ankle, knee, and hip joints, respectively, with separate contributions from the MTUs or exoskeleton denoted as 'mtu' or 'exo'. The distribution of total average positive power from each term of Eq. 2.1, could then be expressed as a percentage (P%) of total average positive leg power (Equation 2.2),

$$P\% = \frac{\bar{P}_{j,c}}{\bar{P}_{tot}} \cdot 100\%. \quad [2.2]$$

where $\bar{P}_{j,c}$ is the average positive power from any joint and contribution. We performed all kinetic calculations separately for each leg before summing the two legs together.

2.2.5 Statistical analysis

We performed a repeated-measures analysis of variance (ANOVA) in R (v4.2.2, Vienna, Austria) using the nlme (Pinheiro et al., 2020) and anova (R Core Team, 2022) packages to

determine the effect of hopping condition on peak joint flexion and range of motion, the MTU average moment and power at each joint, and the distribution of overall average positive power between the ankle, knee, and hip. We considered hopping condition as a fixed categorical effect and participant as a random effect. If a significant main effect of hopping condition was found, we performed Tukey *post hoc* tests ($\alpha = 0.05$) using the `glht` function from the `multcomp` package (Hothorn et al., 2008). While not a part of our hypotheses, we also performed the same analysis on hopping frequency, ground contact time, peak vGRF (summed from the two plates), and hop height (calculated according to Cavagna (Cavagna, 1975)), to determine if participants completed the same hopping task with the full-leg exoskeletons compared to NH.

2.3 Results

We found that participants maintained a consistent hopping frequency ($F_{3,39}=1.0$, $p=0.30$) and ground contact time ($F_{3,39}=1.38$, $p=0.26$) across all conditions (**Table 2.2**). However, there was an effect of hopping condition on peak vGRF ($F_{3,39} = 7.96$, $p<0.001$), where hopping using a full-leg exoskeleton with PG stiffness springs increased peak vGRF by 12.2% (271 ± 131 N [avg. \pm s.d.], $p<0.001$) compared to NH, and 14.3% (276 ± 333 N, $p<0.001$) compared to using an exoskeleton with DG stiffness springs. We also found an effect of condition on hop height ($F_{3,39}=3.024$, $p=0.04$), where there were no significant differences between NH and any of the exoskeleton conditions ($p\geq 0.42$ for all) but hopping using a full-leg exoskeleton with DG stiffness springs increased hop height by 31.6% (0.7 ± 1.1 cm, $p=0.015$) compared to with PG stiffness springs.

Table 2.2 Hopping Kinematics and Kinetics

Condition	Frequency [Hz]	Contact Time [s]	Peak vGRF [N]	Hop Height [cm]
NH	2.40 ± 0.01	0.26 ± 0.03	2253 ± 289	3.1 ± 1.0
DG	2.40 ± 0.01	0.25 ± 0.03	2248 ± 380 [#]	3.4 ± 1.2
LN	2.41 ± 0.01	0.26 ± 0.03	2387 ± 287	2.9 ± 1.1
PG	2.41 ± 0.01	0.26 ± 0.03	2524 ± 310 [*]	2.8 ± 1.0 [#]

Group means ± s.d. vGRF: vertical ground reaction force. Conditions are normal hopping (NH) and hopping using an exoskeleton with degressive (DG), linear (LN), and progressive (PG) stiffness springs. * different from NH, # different from DG.

2.3.1 Joint Angles

We found no significant difference in peak flexion angle between any condition at the ankle (**Figure 2.2**; $F_{3,39}=0.522$, $p=0.70$), knee ($F_{3,39}=1.672$, $p=0.19$) or hip joints ($F_{3,39}=2.683$, $p=0.06$). Additionally, we found no significant difference in ankle or hip joint range of motion between any condition ($F_{3,39}=1.380$, $p=0.26$ and $F_{3,39}=0.272$, $p=0.85$, respectively). However, there was a difference in knee joint range of motion ($F_{3,39}=9.644$, $p < 0.001$), where hopping using a full-leg exoskeleton with DG stiffness springs decreased knee joint range of motion by 10.5% ($3.5 \pm 3.0^\circ$, $p < 0.001$) compared to NH, 6.6% ($2.4 \pm 3.5^\circ$, $p=0.003$) compared to an exoskeleton with LN stiffness springs, and 11.2% ($3.8 \pm 2.9^\circ$, $p < 0.001$) compared to an exoskeleton with PG stiffness springs.

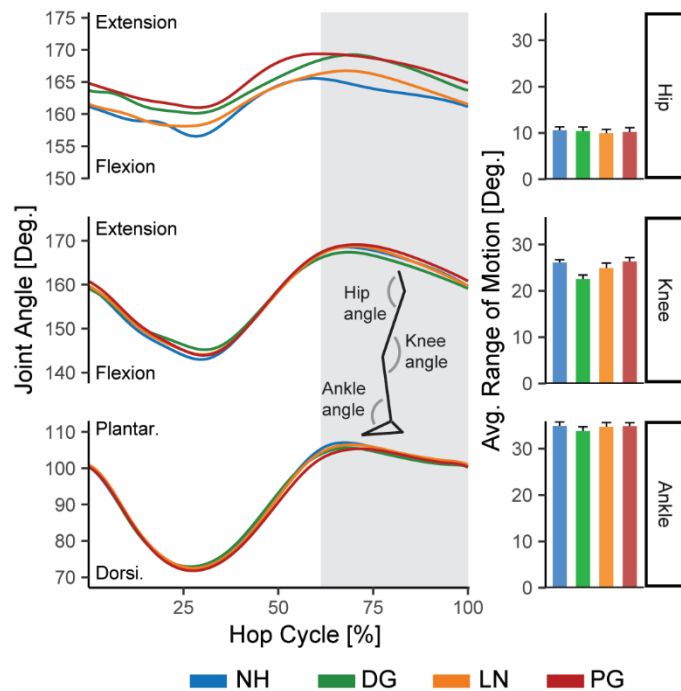


Figure 2.2 Average joint angle and range of motion (\pm s.e.) for the hip (top row), knee (middle row), and ankle (bottom row) during normal hopping (NH; blue) and hopping using an exoskeleton with degressive (DG; green), linear (LN; orange), and progressive (PG; red) stiffness springs. Data are time normalized over the hop cycle and represent the average of both legs. The shaded area represents the average aerial phase across all conditions.

2.3.2 Joint Moments

While hopping using a full-leg exoskeleton, participants decreased the MTU contribution to overall average joint moment at the ankle (**Figure 2.3**; $F_{3,39}=90.927$, $p=0.0002$), knee ($F_{3,39}=21.724$, $p<0.001$), and hip ($F_{3,39}=8.113$, $p<0.001$). We found that hopping using a full-leg exoskeleton with DG stiffness springs reduced the MTU average ankle plantarflexion moment by 36% ($0.38 \pm 0.13 \text{ Nm kg}^{-1}$, $p<0.001$), average knee extension moment by 27.4% ($0.18 \pm 0.11 \text{ Nm kg}^{-1}$, $p<0.001$), and average hip flexion moment by 128.6% ($0.09 \pm 0.15 \text{ Nm kg}^{-1}$, $p<0.03$) compared to NH. Similarly, hopping using a full-leg exoskeleton with LN stiffness springs reduced the MTU average ankle plantarflexion moment and knee extension moment by 24.0% ($0.26 \pm 0.05 \text{ Nm kg}^{-1}$, $p<0.001$) and 22.4% ($0.15 \pm 0.12 \text{ Nm kg}^{-1}$, $p<0.001$) compared to NH. Finally, hopping using a full-leg exoskeleton with PG stiffness springs reduced the MTU average ankle plantarflexion moment by 9.4% ($0.10 \pm 0.04 \text{ Nm kg}^{-1}$, $p<0.001$) compared to NH.

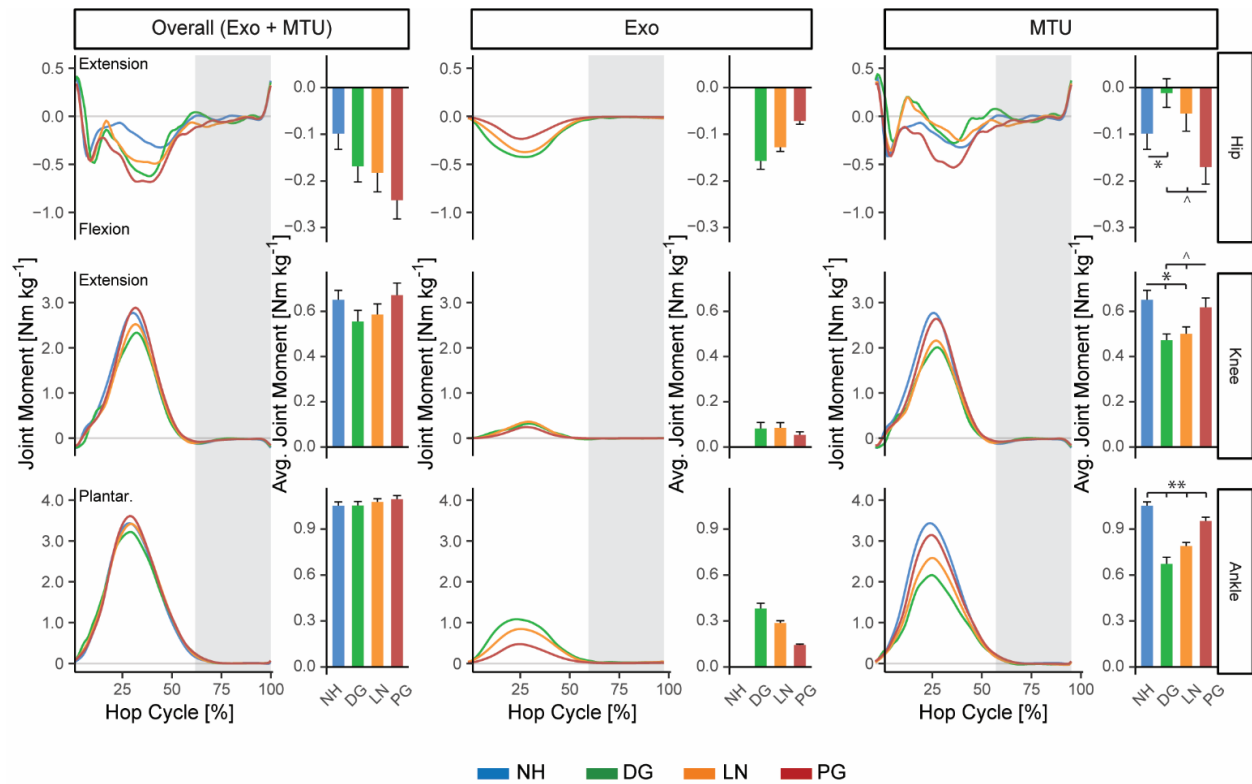


Figure 2.3 Instantaneous and cycle-average joint moment (\pm s.e.). Overall (left column) is the sum of the exoskeleton (exo; middle column) and muscle-tendon unit (MTU; right column) contributions to joint moment for the hip (top row), knee (middle row), and ankle (bottom row). Colors represent different conditions of normal hopping (NH; blue) and hopping using an exoskeleton with degenerative (DG; green), linear (LN; orange), and progressive (PG; red) stiffness springs. Joint moment is normalized to biological mass and represents both legs. Shaded grey region represents the average aerial phase across all conditions. ** all conditions different, * different from NH, ^ different from PG. Note the different y-axis scales for each joint.

2.3.3 Joint Powers

Participants maintained constant total average positive power between conditions ($F_{3,39}=1.029$, $p=0.39$). Hopping using a full-leg exoskeleton resulted in significant reductions to the MTU average positive power at the ankle and knee joints (**Figure 2.4**; $F_{3,39}=22.05$, $p<0.001$ and $F_{3,39}=10.46$, $p<0.001$, respectively). Compared to NH, we found that hopping using a full-leg exoskeleton with DG or LN stiffness springs decreased the MTU average positive ankle power by 26.6% (0.57 ± 0.30 W kg⁻¹, $p<0.001$) and 19.5% (0.43 ± 0.13 W kg⁻¹, $p<0.001$), respectively. Additionally, use of the exoskeleton with the DG and LN stiffness springs decreased the MTU average positive knee power by 24.6% (0.25 ± 0.23 W kg⁻¹, $p<0.001$) and 20.0% (0.21 ± 0.23 W kg⁻¹, $p<0.001$) compared to NH. We also found an effect of condition on the MTU average positive hip power ($F_{3,39}=4.22$, $p=0.011$). However, pairwise comparisons of the MTU average positive hip power revealed that none of the exoskeleton conditions differed from NH ($p \geq 0.07$ for all). Instead, we found that the MTU average positive hip power increased by 48.7% (0.03 ± 0.03 W kg⁻¹, $p=0.004$) and 50.7% (0.02 ± 0.03 W kg⁻¹, $p=0.041$) when using an exoskeleton with DG stiffness springs compared to LN and PG stiffness springs, respectively. Use of an exoskeleton with PG stiffness springs did not significantly reduce the MTU average positive power compared to NH for any lower-limb joint (ankle: $p=0.0614$, knee: $p=0.972$, hip: $p=0.458$).

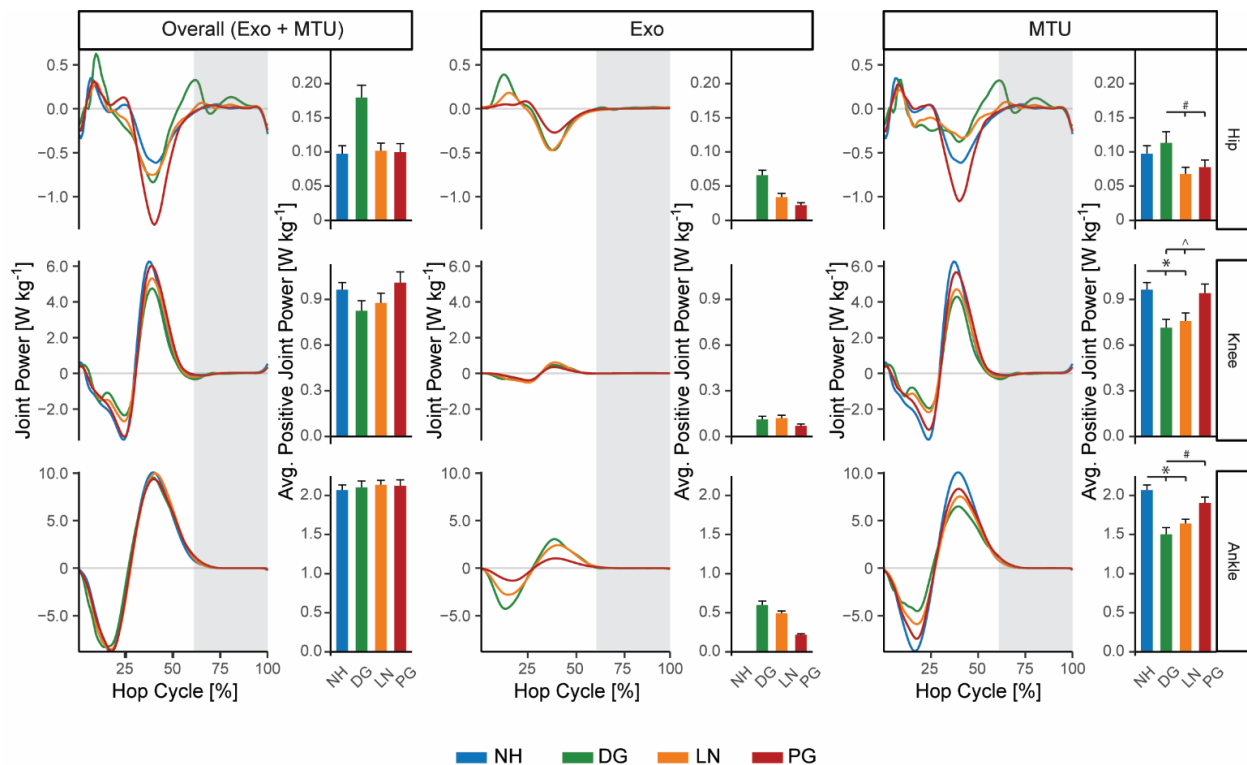


Figure 2.4 Instantaneous and cycle-average positive joint power (\pm s.e.). Overall (left column) is the sum of exoskeleton (exo; middle column) and muscle-tendon unit (MTU; right column) contributions to joint power for the hip (top row), knee (middle row), and ankle (bottom row). Colors represent different conditions with normal hopping (NH; blue) and hopping using an exoskeleton with degressive (DG; green), linear (LN; orange), and progressive (PG; red) stiffness springs. Joint power is normalized to biological mass and represents both legs. Shaded grey region represents the average aerial phase across all conditions. * different from NH, # different from DG, ^ different from PG. Note the different y-axis scales for each joint.

The distribution of total average positive power was nearly constant across conditions (**Figure 2.5**). We found that participants did not change the relative proportion of overall average positive ankle power to total positive leg power (**Figure 2.5**, $F_{3,39}=0.282$, $p=0.84$). There was an effect of condition on the relative proportion of overall average positive knee power to total positive leg power ($F_{3,39}=3.56$, $p=0.03$), but exoskeleton conditions were not different from NH ($p \geq 0.10$ for all). There was also an effect of condition on the relative proportion of overall average positive hip power to total positive leg power ($F_{3,39}=12.12$, $p < 0.001$), where hopping using a

passive full-leg exoskeleton with DG stiffness springs increased the relative proportion of overall average positive hip power from 3% to 5% compared to all other conditions.

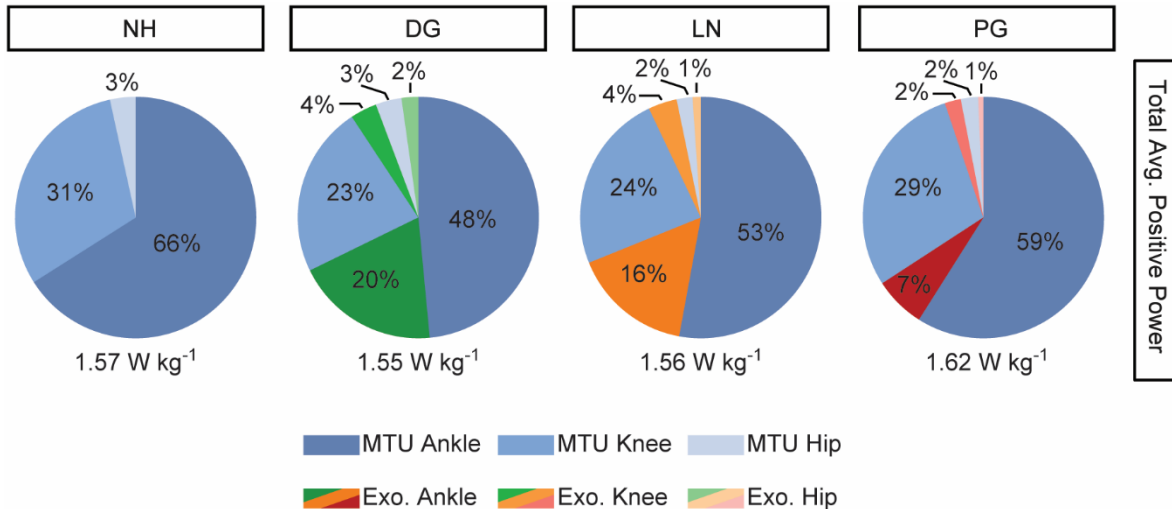


Figure 2.5 Relative joint average positive power contributions to total average positive leg power during normal hopping (NH; blue) and hopping using an exoskeleton with degressive (DG; green), linear (LN; orange), and progressive (PG; red) stiffness springs. Total average positive leg power is displayed below each chart and normalized to biological mass.

2.4 Discussion

In this study, we quantified the joint-level mechanics of two-legged stationary hopping at 2.4 Hz while using a passive full-leg exoskeleton with three different spring stiffness profiles: degressive, linear, and progressive (**Figure 2.1**), compared to normal hopping without an exoskeleton. Overall, our findings indicate that use of a passive full-leg exoskeleton primarily assists the ankle and knee by reducing the MTU average joint moment and power compared to unassisted hopping. However, spring stiffness profile affects the magnitude of assistance, so that MTU average joint moment and power is lowest with DG stiffness springs, followed by LN and PG stiffness springs, respectively.

Our data provide partial support of our first hypothesis, that hopping using a passive full-leg exoskeleton with any spring stiffness profile would decrease peak flexion angles and range of

motion at the ankle, knee, and hip compared to NH. We found that peak flexion angles for each of the joints were not significantly different from NH when hopping using a passive full-leg exoskeleton with any of the three spring stiffness profiles (**Figure 2.2**). However, we also found that use of an exoskeleton with DG stiffness springs reduced knee range of motion compared to all other conditions (**Figure 2.2**). The reduction in knee range of motion with DG stiffness springs was small ($\sim 4^\circ$) but can likely be attributed to reductions in peak knee extension angle during the aerial phase and may be indicative of the design of the exoskeleton with DG stiffness springs.

The DG stiffness springs had a fixed resting length and spanned the entire leg (**Figure 2.1**; **Table 2.1**). We sized each spring to each participant so that the spring would begin to compress at the instant of ground contact, however, the spring may have limited the extension of the leg during the aerial phase if we set the resting length to be too short. Participants may have reduced their knee joint range of motion to prevent the DG stiffness springs from stretching beyond their resting length and absorbing some of the positive power needed to achieve an aerial phase. Alternatively, if we set the resting length of the DG stiffness springs to be too long, we observed that participants had difficulty maintaining balance or achieving the target hopping frequency during the acclimatization period before the experimental trial. In contrast, the LN and PG stiffness springs were mounted between adjustable aluminum plates on telescoping rods so that the exoskeleton “leg” length always matched the participant’s leg length at any point in the hop cycle. The LN and PG stiffness springs were not fixed to the aluminum plates, which allowed the springs to be compressed during the stance phase but never stretched beyond their resting length during the aerial phase. This design likely allowed participants to have the same joint range of motion as the NH condition. These results add to previous literature suggesting that a spring’s resting length should be optimized to the participant on an individual basis (Cherry et al., 2016; Farris and

Sawicki, 2012a; Ferris et al., 2006), and add that studies utilizing a large spring as the exoskeleton “leg” should strive to carefully match the resting spring length to a participant’s extended leg length so that elastic energy stored in the spring during compression is not lost to stretching the spring beyond its resting length during the aerial phase.

Our findings support our second hypothesis that hopping using a passive full-leg exoskeleton would decrease MTU average joint moment and power compared to NH, with the greatest reductions occurring with the DG stiffness springs, followed by the LN and PG stiffness springs, respectively. We found that hopping using a passive full-leg exoskeleton reduced the MTU average ankle plantarflexor moment by 36%, 24%, and 9% while using DG, LN, and PG stiffness springs, respectively. Additionally, use of the exoskeleton with DG and LN stiffness springs decreased the MTU average knee extensor moment by 24-27%, while the PG stiffness springs did not (**Figure 2.3**). Ultimately, these changes allowed participants to reduce the MTU average positive joint power, with the largest reductions at the ankle then the knee (**Figures 2.4 & 2.5**). We also found that hopping using a full-leg exoskeleton with DG stiffness springs provided 26% of the total average positive leg power (**Figure 2.5**), while the LN and DG stiffness springs provided 19% and 10%, respectively. The differences in total average positive leg power between spring stiffness profiles are likely due to the magnitude of elastic energy that can be stored and returned by the spring for a given displacement (Allen and Grabowski, 2019). For example, a degressive stiffness spring can store 36% more elastic energy per hop than an LN stiffness spring, and 186% more than a PG stiffness spring for the same displacement (Allen and Grabowski, 2019).

The full-leg exoskeleton had the greatest influence on the ankle due in part to the average length of the exoskeleton moment arm throughout the stance phase. The attachment points of the exoskeleton “leg” are placed close to the hip and metatarsal heads, and the pin joints allow a direct

line of action between them. As the joints of the lower limb flex and extend throughout the stance phase, the ankle and knee joint centers move relative to the exoskeleton's line of action. We found that the longest average exoskeleton moment arm in the sagittal plane was at the ankle, followed by the knee and hip, respectively, despite the moment arm about the knee having the largest range (**Figure 2.6**). We also found that the exoskeleton provided a flexion moment about the hip (**Figure 2.3**), suggesting that the exoskeleton's line of action was oriented at a slight angle that is posterior to the hip joint center in the sagittal plane. However, this did not translate to any significant changes in positive power at the hip compared to NH.

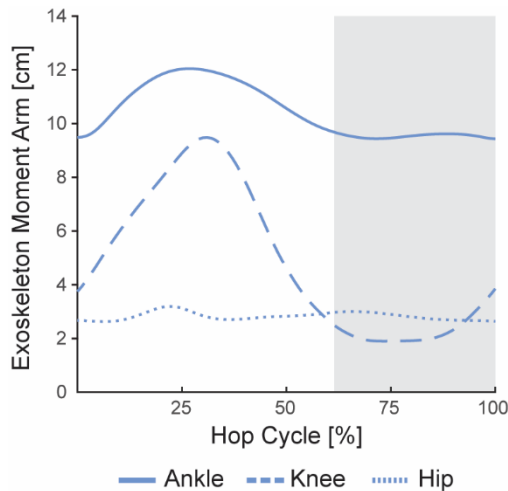


Figure 2.6 Average sagittal-plane exoskeleton moment arms while hopping using the passive, full-leg exoskeleton. Data are averaged across degressive, linear, and progressive stiffness springs. Grey area represents the average aerial phase across all exoskeleton conditions.

Finally, our data do not support the hypothesis that hopping using a full-leg exoskeleton would result in a redistribution of overall joint power from the knee to the ankle. Similar to hopping using a passive, ankle-only exoskeleton with LN stiffness springs (Farris and Sawicki, 2012a), humans adopt a neuromotor control strategy to maintain the distribution of joint power for normal hopping and hopping using a passive, full-leg exoskeleton with DG, LN, or PG stiffness springs. Across all conditions, we found that the ankle and knee joints provided approximately 66-69% and 26-31% of the total average positive leg power across all conditions, with the remainder coming from the hip (**Figure 2.5**). Presumably, maintaining the distribution of average overall positive

joint power allowed participants to hop with constant ground contact times, peak vGRF, and hop heights while using a passive full-leg exoskeleton with DG and LN stiffness springs (**Table 2.2**). We found an increase in peak vGRF and a decrease in hop height while using the exoskeleton with PG stiffness springs, which is consistent with results from our previous study (Allen and Grabowski, 2019). These changes likely occurred because the PG stiffness springs cannot store and return as much elastic energy as the DG and LN stiffness springs, which is reflected by the increase in total average positive leg power (**Figure 2.5**).

However, contrary to our expectations, hopping using a passive, full-leg exoskeleton did not provide greater relative contributions to total average positive leg power compared to a passive, ankle-only exoskeleton (**Figure 2.5**). Use of the full-leg exoskeleton with LN stiffness springs provided 21% of the total average positive leg power when hopping at 2.4 Hz and was previously shown to reduce metabolic power by 16% (Allen and Grabowski, 2019) compared to unassisted hopping. However, Farris et al. (Farris and Sawicki, 2012a) found that use of an ankle-only exoskeleton with LN stiffness springs provided 38% of the total average positive leg power when hopping at 2.5 Hz, and reduced metabolic power by 13% compared to unassisted hopping. One possible explanation for the differences between the percentage of positive power and metabolic power reduction due to using a full-leg versus ankle only exoskeleton is that the demands of hopping differed between studies. Participants in the current study had a 2.5-fold increase in hop height and 0.27 body-weight increase in peak vGRF compared to our previous study (Allen and Grabowski, 2019), and may have increased their MTU relative contribution to total average positive leg power to hop higher. Another possible explanation may be that the assistance provided by a full leg exoskeleton affects the underlying muscle mechanics differently compared to an ankle-only exoskeleton, especially when considering that the two studies used LN stiffness springs

with similar body mass-normalized stiffness (full-leg: $\sim 0.132 \text{ kN}\cdot\text{m}^{-1}\cdot\text{kg}^{-1}$; ankle-only: $\sim 0.125 \text{ kN}\cdot\text{m}^{-1}\cdot\text{kg}^{-1}$, for both springs). Previously, the use of a passive ankle-only exoskeleton has been shown to sub-optimally shift where the plantarflexors operate along the force-length and force-velocity curves compared to unassisted hopping, which may reduce the metabolic benefits of reducing muscle force (Farris et al., 2013; Farris et al., 2014). For example, Farris and colleagues (Farris et al., 2013; Farris et al., 2014) found that hopping at 2.5 Hz using an ankle-only exoskeleton with LN stiffness springs reduced average plantarflexor muscle force by $\sim 45\%$ compared to unassisted hopping, but it also shifted the average operating length of the muscle fascicles leftward down the ascending arm of the force-length curve, increasing fascicle excursion, increasing the relative shortening velocity and placing the fascicles in a sub-optimal state for producing force economically. It is possible that by distributing exoskeletal assistance over the entire leg, the average operating length of the ankle plantarflexors and knee extensors remained closer to the plateau-region of their respective force-length curves, similar to unassisted hopping, and reduced the magnitude of a leftward shift down the ascending arm of the force-length curve. Thus, any changes in metabolic power due to a change in the muscle's average operating length when using a passive full-leg exoskeleton might be mitigated and muscle force produced more economically compared to an ankle-only exoskeleton (Lai et al., 2015). Future studies are needed to determine muscle dynamics using full-leg and ankle-only exoskeletons.

2.4.1 Towards a full-leg running exoskeleton

Similar to hopping, the MTUs surrounding the ankle and knee joints provide the greatest contribution to total average positive leg power during the stance phase of running (Farris and Sawicki, 2012b). Therefore, use of a passive, full-leg exoskeleton with DG spring stiffness that simultaneously assists multiple joints during the stance phase may also reduce ankle and knee joint

positive power in running. However, while the center-of-mass mechanics in bouncing gaits are similarly described by a spring-mass model, there are differences in joint mechanics between hopping and running that should be considered for future passive, full-leg running exoskeletons. For example, the passive, full-leg exoskeleton in the present study utilized springs that span the entire leg as exoskeleton “legs” and do not allow the knee to flex during the swing phase. Previously, Cherry et al. (Cherry et al., 2016) used a friction-lock clutch controlled by participant-specific inputs from thigh velocity and foot switches that enabled a two segment exoskeleton “leg” to lock during the stance phase and release during the swing phase so that the knee could flex with minimal resistance. A similar clutch mechanism placed between the “thigh” and “shank” segments of the DG stiffness springs could allow the spring to store and return elastic energy during the stance phase and provide assistance to the ankle and knee joint, and also allow the knee to flex freely and prevent users from working against the spring during the swing phase.

The hip joint also provides a large proportion (32-39%) of the total average positive leg power during the swing phase when running on level ground at 2.25-3.25 m s⁻¹, but does not significantly contribute positive power during the stance phase (Farris and Sawicki, 2012b). While previous research has shown that passive assistive devices can reduce the metabolic cost of running by 6.5-8% through hip flexion assistance during the swing phase using tension springs (Nasiri et al., 2018; Simpson et al., 2019; Zhou et al., 2021), a passive, full-leg exoskeleton that acts during the stance phase with compression springs may not significantly contribute to positive hip power. Therefore, minimizing the exoskeleton moment arm about the hip might allow the exoskeleton to provide assistance to the ankle and knee joints during stance phase without interfering with hip joint mechanics. Additionally, distal mass carried by the legs incurs a metabolic penalty, owing to the increased muscular effort to raise the foot off the ground, move the leg forward during swing

phase, and decelerate the leg before the next ground contact (Franz et al., 2012; Frederick et al., 1984). Use of lighter weight materials or redistribution of the exoskeleton mass more proximally would reduce the inertia of the device during swing phase (Cherry et al., 2016), which could further reduce metabolic cost.

Finally, the passive, full-leg exoskeleton springs are placed lateral to the legs and likely apply a frontal plane moment to the lower-limb joints. In stationary, two-legged hopping, these exoskeleton frontal plane moments are equal and opposite. However, running with one foot on the ground at a time using a passive, full-leg exoskeleton spring lateral to the leg would apply a frontal plane moment that would need to be counteracted by the user. As such as, users might increase hip abductor moment to help maintain balance, compress the spring, and limit frontal plane hip drop during running. A lower profile design that reduces the frontal plane joint moment arms would mitigate these potentially adverse effects.

2.4.2 Potential Limitations

We assumed a rigid connection between the user and exoskeleton with no soft-tissue displacement. However, it is likely that there was soft-tissue displacement and some energy loss due to the interface between the user and exoskeleton. Previous studies have identified that user-device interfaces are a significant challenge to the development of successful lower-body wearable devices because of the energy lost to soft-tissue displacement (Cherry et al., 2016; Yandell et al., 2017). We placed the hip markers in the same positions for each exoskeleton condition to minimize the error between exoskeleton trials. Future passive, full-leg exoskeleton designs may benefit from alternative user interfaces that distribute force over a larger surface area to maximize effective power transfer between the user and the device. Additionally, the mountain bike shoes given to the participants provided an easy method of attaching the exoskeleton legs. However, due in part

to the thickness and rigidity of the shoes, we modelled the foot as a single segment and previous studies have shown that this simplification of the foot may over-estimate angular displacement (by as much as 10°) and ankle power (Kessler et al., 2020). Participants used the same rigid mountain bike shoes in all conditions, including NH, and we assumed the same error in a repeated-measures design to mitigate this potential limitation.

2.5 Conclusion

Hopping using a passive, full-leg exoskeleton assists the ankle and knee by reducing the MTU average joint moment and power. Moreover, the magnitude of reductions depend on the spring stiffness profile, where use of a full-leg exoskeleton with DG spring stiffness provides significantly greater assistance at the ankle than LN or PG spring stiffness, and may explain why previous studies (Allen and Grabowski, 2019) found that the spring stiffness profile within an exoskeleton affects the magnitude of metabolic power reductions. Our data add to the increasing number of studies that show the elastic properties of an exoskeleton spring have a significant effect on hopping mechanics (Allen and Grabowski, 2019; Grabowski and Herr, 2009; Robertson et al., 2014). Therefore, future studies that examine the design of a passive exoskeleton or investigate the effects of springs in human locomotion should consider and report the spring stiffness profile.

Chapter 3: Effects of asymmetric crank arm lengths and cycling-specific prostheses in riders with a unilateral transtibial amputation

Co-authors: Gabriela B. Diaz & Alena M. Grabowski

In preparation – with intent to submit to *Medicine and Science in Sports and Exercise*

Due in part to structural and musculoskeletal differences between a biological leg and prosthesis, cyclists with a unilateral transtibial amputation (TTA) exhibit kinematic and kinetic asymmetries that may reduce efficiency. Use of asymmetric crank arm lengths or a cycling-specific prosthesis (CSP) could reduce asymmetries and improve efficiency. **Purpose:** We determined the effects of shorter crank arm lengths on the affected side and cycling with two different prostheses on joint and crank power, joint and crank power asymmetry, and net efficiency. **Methods:** 12 cyclists with a TTA rode at $1.5 \text{ W}\cdot\text{kg}^{-1}$ with symmetric (175 mm) and shorter affected side crank arms (160, 165, 170 mm) using a daily-use prosthesis and CSP. We used statistical parametric mapping to determine differences in instantaneous joint and crank power between prostheses, and compared average joint and crank power, joint and crank power asymmetry, and net efficiency with linear mixed-effect models. **Results:** Shorter affected side crank arm lengths reduced the magnitude of peak positive ($p \leq 0.001$) and negative ($p < 0.001$) crank power compared to symmetric crank arms. Use of a CSP increased the magnitude of peak positive knee power ($p < 0.001$) and decreased the magnitude of peak negative crank power ($p < 0.001$) compared to a daily-use prosthesis. Shorter affected side crank arm lengths while using a CSP reduced hip joint power and hip transfer power asymmetry ($p = 0.002$). However, we found no significant differences in affected side average crank or joint power, crank or knee joint power asymmetry, or net efficiency. **Conclusions:** At a moderate mechanical power output ($1.5 \text{ W}\cdot\text{kg}^{-1}$), cycling with asymmetric crank arm lengths or CSPs offer small improvements in hip joint power

and hip transfer power asymmetry, but does not alter crank asymmetry or efficiency in cyclists with a TTA.

3.1 Introduction

Cycling for recreation or exercise provides numerous health benefits over a sedentary lifestyle, such as a lower incidence of type-2 diabetes and heart disease, and a reduced risk of all-cause mortality (Oja et al., 2011; Poonsiri et al., 2021). In addition, cycling is a low impact aerobic exercise option that does not incur high joint and tissue loads inherent in weight-bearing exercises such as running (Orekhov et al., 2019). Compared to 60% of people without amputation, only 32-37% of people with a unilateral transtibial amputation (TTA) engage in enough vigorous physical activity to elicit health benefits (Deans et al., 2012). Engagement in physical activity is generally lower in people with versus without TTA due to barriers such as increased pain, physical limitations, and a lack of access to appropriate equipment (Deans et al., 2012; Poonsiri et al., 2021). Cycling may pose greater barriers for people with versus without a TTA such as pain and discomfort that may be due to bike fit, and asymmetric joint range of motion and/or mechanical work between legs (Childers et al., 2009). Addressing these barriers and allowing people with a TTA to participate in cycling for exercise may improve engagement in vigorous exercise and promote improvements in overall health.

During cycling, the mechanical power delivered to the crank is produced by the muscles surrounding the ankle, knee, and hip joints, as well as the upper body (transferred across the hip joint) (van Ingen Schenau et al., 1990). The biological ankle dorsi- and plantarflexes throughout the crank cycle with a range of motion of $\sim 20^\circ$ (Barrat et al., 2016; Heil et al., 1997) and assists with transferring power from the proximal segments to the crank (Fregly and Zajac, 1996). However, riding with the ankle constrained to a neutral position reduces resultant crank forces (Pierson-Carey et al., 1997) and crank power in cyclists without an amputation. A cyclist with a TTA often uses their daily-use prosthesis on their affected side, which is comprised of a socket

that surrounds the residual limb and connects to a carbon fiber prosthetic foot via a metal pylon (**Figure 3.1**). The length of a daily-use prosthesis is typically set so that the length of the affected side matches the unaffected side during standing. A cyclist with a TTA is unable to dorsi- or plantarflex the prosthetic foot and must compensate by altering the knee and hip kinematics and kinetics of their affected side (Childers et al., 2009). These compensations, in addition to strength imbalances between legs due to muscular atrophy (Hewson et al., 2020), contribute to asymmetric lower-limb kinematics, pedal forces, joint moments, and crank work between legs (Childers and Gregor, 2011; Childers et al., 2009; Dyer, 2016; Pierson-Carey et al., 1997). Biomechanical symmetry is often used as a goal for performance and rehabilitation, and while small to moderate pedaling asymmetries (i.e., 5-10% asymmetry in pedal force, crank moment, or crank work) exist in cyclists without an amputation (Carpes et al., 2010; Daly and Cavanagh, 1976; Sargeant and Davies, 1977; Smak et al., 1999), cyclists with a TTA may experience greater asymmetries, such as a 20% asymmetry in mechanical work between legs (Childers et al., 2009). Presumably, these biomechanical asymmetries worsen efficiency, performance, comfort, and participation in exercise for cyclists with a TTA (Childers and Kogler, 2014; Forte et al., 2020), but might be addressed by manipulating the bicycle fit or the prosthesis configuration to better account for the mechanical differences between legs.

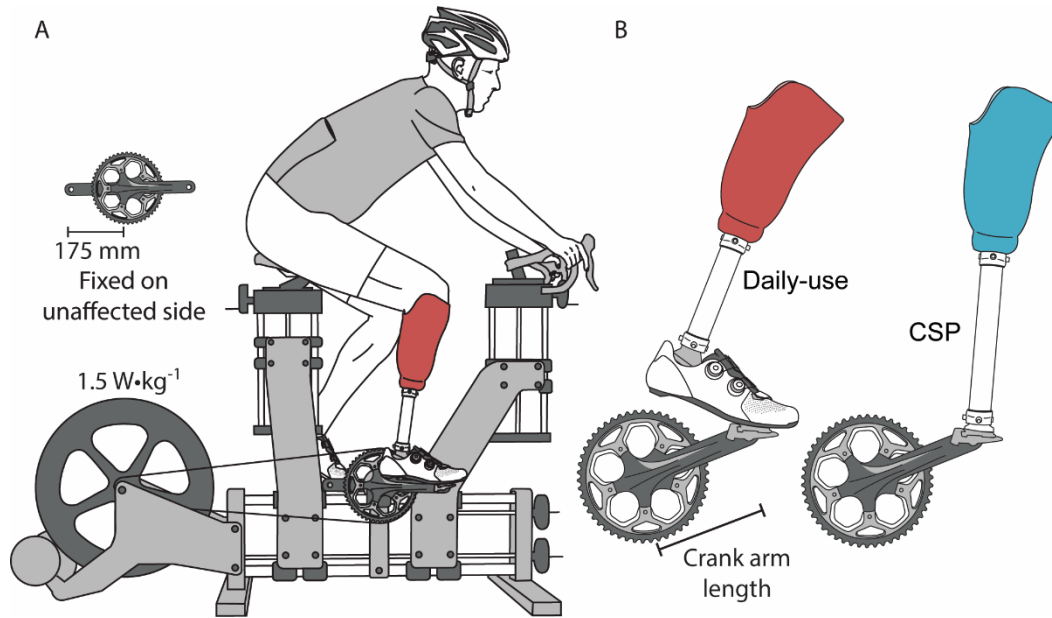


Figure 3.1 Illustration of A) the bicycle ergometer set up and B) the two prosthesis types, a daily-use prosthesis (left; red) and cycling-specific prosthesis (CSP; right; blue).

A common way to influence bicycle fit and potentially address the asymmetries between legs is to adjust crank arm length, the distance between the bottom bracket and pedal spindle (**Figure 3.1**). In cyclists without an amputation, increasing crank arm length increases effective crank moment during submaximal cycling, and peak crank power can be maximized during sprints with crank arm lengths of 170-180 mm depending on cadence (Ferrer-Roca et al., 2017; Hull and Gonzalez, 1988; Martin and Spirduso, 2001; Too and Landwer, 2000). Changes in crank arm length may alter muscle fascicle operating lengths and influence joint moments if the muscle operates in a different region of the force-length curve (Barrat et al., 2016; Elmer et al., 2011). Yet, joint-level analyses of non-amputee steady-state cycling have shown that average joint power and the distribution of power amongst the lower-limb joints when riding at 240 W may not significantly change when riding with equal crank arm lengths between 150-190 mm (Barrat et al., 2016). This likely contributes to previous findings that suggest efficiency, the ratio of mechanical

power to metabolic power, is independent of changes in crank arm length in cyclists without an amputation (Ferrer-Roca et al., 2017; McDaniel et al., 2002) or is specific to the individual (Morris and Londeree, 1997). However, in cyclists with a TTA, there is ~23% difference in crank work where the affected side contributes significantly less to total power output than the unaffected side (Childers and Kogler, 2014). Previous research proposed that utilizing asymmetric crank arm lengths may mitigate the kinematic and kinetic asymmetries between legs (Childers and Kogler, 2014; Childers et al., 2009) and potentially improve efficiency. Previously, Childers and colleagues (Childers and Kogler, 2014; Childers et al., 2009) hypothesized that shortening the crank arm length on the affected side would allow cyclists with a TTA to elicit more symmetric kinematics by reducing peak knee and hip joint flexion over the top of the crank cycle and peak extension at the bottom of the crank cycle. They found that cyclists with a TTA reduced kinematic asymmetries using asymmetric (172mm - unaffected side, 162mm – affected side) compared to symmetric (172 mm) crank arms while riding at 150 W, but found that half of the participants reduced crank work asymmetry while the other half increased crank work asymmetry (Childers and Kogler, 2014). Thus, it remains unclear if asymmetric crank arm lengths do or do not influence kinetic asymmetries of cyclists with a TTA or if there is a bimodal distribution of responders. Moreover, it is unknown if riding with asymmetric crank arm lengths alters efficiency in cyclists with a TTA.

The mechanical asymmetries in cyclists with a TTA might also be affected by the prosthesis used. Relative to daily-use prostheses, sport-specific prostheses may improve performance and/or reduce the risk of injury during exercise in athletes with a TTA (Sepp et al., 2020). Several elite para-cyclists and triathletes with a TTA prefer to use a cycling-specific prosthesis (CSP), which directly connects the prosthetic pylon to the pedal and effectively removes

the lever arm provided by the prosthetic foot (**Figure 3.1**). While cycling performance can be improved by utilizing CSPs that have reduced weight and/or aerodynamic drag compared to a daily-use prosthesis (Dyer and Disley, 2020; Dyer and Woolley, 2017), the influence of a CSP on asymmetry and efficiency is not well understood. A pervasive belief in para-cycling culture is that CSPs may provide a stiff attachment between the residuum and crank, potentially allowing mechanical energy loss to be minimized and thereby improving performance compared to a daily-use prosthesis (Bragaru et al., 2012; Childers et al., 2009; Dyer, 2016). Previous research has shown that cycling with a stiffer prosthetic foot reduced crank asymmetry by ~8% compared to an energy-storing prosthetic foot commonly prescribed for walking (Childers et al., 2011). However, removing the prosthetic foot's lever arm may alter knee and hip joint angles and further influence mechanical asymmetries and efficiency (Rankin and Neptune, 2010).

To our knowledge, no study has determined efficiency while cyclists with a TTA ride using a CSP compared to a daily-use prosthesis. Previous research in competitive, non-amputee cyclists has shown that pedaling with the midfoot compared to the forefoot does not elicit any change in metabolic energy expenditure during submaximal cycling. Additionally, Bartlett and Kram (Bartlett, 2007) simulated the effects of a CSP by asking 10 cyclists without an amputation to pedal with their heel rather than their fore-foot while riding at 75, 100, 125, and 150 W and found no differences in efficiency between normal pedaling, unilateral heel pedaling, and bilateral heel pedaling. Moreover, they report that three additional cyclists with a TTA showed no difference in efficiency while using their preferred prosthetic device compared to cyclists without an amputation, however, the prosthesis type (daily-use or CSP) was not described. Therefore, it is unknown whether use of a CSP improves asymmetry and/or efficiency in cyclists with a TTA

compared to a daily-use prosthesis, or if there is an interaction between riding using a CSP or daily-use prosthesis with asymmetrical crank arm lengths.

There is a need to determine the effects of bicycle fit and prosthesis configuration in cyclists with a TTA so individuals, coaches, and clinicians can make informed decisions of what equipment to select or prescribe. It is unclear if recreational cyclists with a TTA, who desire to cycle as a mode of transportation or low-impact form of exercise, should invest in specialized cycling equipment such as asymmetric crank arms or CSPs. Additionally, such specialized equipment, like CSPs, may not be readily accessible to recreational cyclists; the cost of sport-specific prostheses is often not covered by insurance, so the financial burden is placed directly on the individual. Additionally, reducing the large asymmetries between legs may increase engagement in physical activity and promote improvements in overall health. We determined how joint and crank power, joint and crank power asymmetry, and efficiency are affected by shorter affected side crank arm lengths and prosthesis type. We hypothesized that riding with shorter crank arm lengths on the affected side or using a CSP would increase joint and crank power of the affected limb, reduce joint and crank power asymmetry, and improve efficiency compared to riding with equal crank arm lengths or a daily-use prosthesis.

3.2 Methods

3.2.1 Participants

12 healthy individuals with a TTA (6 males/6 females, mean \pm S.D. age: 39.4 ± 8.7 years, height: 1.72 ± 0.08 m, mass: 73.2 ± 17.9 kg) and no additional reported cardiovascular, neurological, or musculoskeletal impairments enrolled in the study. Since we did not have a prior estimate of effect size, the number of participants was chosen based on previous cycling studies that showed significant differences in crank work asymmetry for 2-8 cyclists with a TTA (Childers

and Gregor, 2011; Childers and Kogler, 2014; Childers et al., 2011; Childers et al., 2012). Participants for this study were not required to have previous cycling experience, but self-reported at least 30 minutes of moderate exercise 3 times per week while using a prosthesis for at least 3 years. All participants provided written informed consent according to the protocol approved by the Colorado Multiple Institutional Review Board and the Department of Veterans Affairs (COMIRB 18-2783).

3.2.2 Ergometer setup

All participants rode a fully adjustable bicycle ergometer (Retül Müve; Boulder, CO, USA; **Figure 3.1**). We sized the bicycle ergometer to match each participant's personal bike fit if measurements were provided, or according to a standard fitting protocol developed by Retül for individuals without an amputation based on the participant's unaffected side. The ergometer was initially set to default measures based on a web-based sizing app developed by Retül that uses sex and standing height as input measures (Bike Sizing App | Specialized.com). Both crank arm lengths were set to 175 mm, and we adjusted the saddle height and fore-aft position so that seat tube angle was kept constant, and knee angle was 150-160 degrees when the crank was at dead bottom center. We then allowed minor adjustments for comfort. The handlebar position and stem angle were set so the elbows were slightly bent when the cyclist's hands were resting on the handlebars and their torso was leaning forward. Because there is no influence of aerodynamics on the stationary ergometer, torso angle was not standardized, which allowed for individual participant comfort. Simultaneously with the bike fit, a certified prosthetist evaluated and adjusted the prosthesis socket and foot alignment in the frontal plane to ensure the participant's knee was oriented vertically over the pedal throughout the crank cycle and their shoe did not hit or rub against the crank due to pedal float.

The bicycle ergometer was equipped with an electronic stationary trainer (CycleOps PowerBeam Pro Electronic Trainer; Saris; Madison, WI, USA) that provided a constant, target mechanical power output of $1.5 \text{ W}\cdot\text{kg}^{-1}$. In addition, the ergometer was equipped with 6-component, instrumented clip-in pedals (I-CrankSet; ICS-RM Look Keo2; Sensix, Poitiers, France; 1000 Hz) that measured individual pedal forces and moments. For trials with the daily-use prosthesis, participants wore their own road cycling shoes on both feet, or we provided shoes (S-Works 7; Specialized Bicycle Components; Morgan Hill, CA, USA) and cleats (Keo Cleat; Look; Nevers, France; 9° float) if participants did not have their own. For the trials with the CSP, we removed the prosthetic foot and created a CSP by securing a cleat directly to the bottom of the pylon (**Figure 3.1**). We also lengthened the CSP pylon to match the effective lower-leg length of their daily-use prosthesis, which was defined as the linear distance from the knee joint center to the cleat on the bottom of the shoe (Childers et al., 2009). After six participants successfully completed the protocol with this setup, the trainer stopped working so we replaced it with a different trainer (Kickr Smart Trainer, Wahoo, Atlanta, GA, USA) for the remaining participants. A member of the research team calibrated the trainers prior to each testing session by riding the bike for at least 15 minutes and performing a roll-down calibration per manufacturer instructions.

3.2.3 Experimental protocol

The participants performed a total of eight, 5-minute trials of seated cycling at $1.5 \text{ W}\cdot\text{kg}^{-1}$ over two days, wearing their daily-use prosthesis and a CSP. We selected $1.5 \text{ W}\cdot\text{kg}^{-1}$ as a mechanical power output, because it is achievable by a wide population of cyclists using aerobic metabolism. For each prosthesis, participants rode with four different crank arm lengths on the affected side (160, 165, 170, and 175 mm) in a randomized order, while the crank arm length for the unaffected side was fixed at 175 mm. The ergometer gear ratio was kept constant (53:24),

however the trainers dynamically adjusted resistance to match the desired power output and we did not restrict cadence. Participants were given at least five minutes rest between trials.

3.2.4 Data collection

Before beginning the experimental trials, we secured 42 reflective markers to both legs and the pelvis using double-sided tape and marker clusters with self-adhesive bandages. We placed markers bilaterally on the ankles and knees to define the joint centers, and marker clusters on each leg segment. We positioned markers on the prosthesis to mirror the unaffected side: bilateral knee markers were placed on the outside of the prosthetic socket at the visual axis of rotation while the participant flexed and extended their knee in a seated position, 1st and 5th metatarsal head markers were placed on the shoe to match the markers on the unaffected side, and bilateral “malleoli” markers were placed on the distal pyramid, where the prosthetic foot connects with the metal pylon. We also placed four markers on the base of the ergometer to establish a global coordinate system relative to the bicycle, and four markers on each pedal square to track pedal position and orientation. We collected 15 seconds of lower-body kinematic data from the first, fourth, and fifth minute of each trial using a 10-camera motion capture system (Vicon Nexus 2.3, Oxford, UK; 200 Hz) simultaneously with left and right pedal forces and moments.

We measured each participant’s rates of oxygen consumption and carbon dioxide production using indirect calorimetry (TrueOne 2400, Parvo Medics, Salt Lake City, UT). At the beginning of each experimental session, we measured resting metabolic rate while the participant was seated on the ergometer and then continuously throughout each trial. We instructed participants to refrain from exercising 24 hours and to be at least two hours post-prandial prior to the experimental sessions and conducted the experiments at the same time of day to minimize variability in metabolic rates.

3.2.5 Data analysis

The 3D motion capture marker trajectories were labeled in Vicon and exported to Visual 3D (C-Motion Inc., Germantown, MD) along with pedal forces for inverse dynamics analysis. Marker trajectories and pedal forces were filtered using a zero-lag, 2nd-order lowpass Butterworth filter with a 12 Hz cut-off (Wilkinson et al., 2020). We calculated joint angle as the inter-segment angle between proximal and distal segments, where an increased angle represents extension. We converted local pedal forces to the global coordinate system using a 3D rotation matrix that accounted for the crank and pedal positions. The origin of the global pedal forces was determined by a marker on the pedal square in line with the pedal spindle, and then offset to the midline of the pedal. We assumed the pedal free-moment to be zero and calculated lower limb joint kinematics and kinetics for each leg using 10 crank cycles from the last minute of each trial. We calculated instantaneous crank forces (tangential and radial) by transforming the global pedal forces with respect to crank position, and then multiplied tangential crank force by the length of the crank arm and its angular velocity to calculate instantaneous crank power for each leg. We calculated joint power at the ankle, knee, and hip as the dot product of joint moment and angular velocity, and hip transfer power from the upper body was calculated as the dot product of hip joint reaction force and linear velocity (van Ingen Schenau et al., 1990). We defined positive power when joint moment and angular velocity, or joint reaction force and linear velocity, were in the same direction and negative power when they were in opposite directions (Vigotsky et al., 2019).

We defined the total mechanical power output of the trial as the average of summed instantaneous crank powers over a complete crank cycle, where the crank starts and finishes at top-dead-center and is oriented vertically above the bottom bracket. We defined average joint and crank power separately for each leg, as the average power over a complete crank cycle. We did

not calculate ankle joint power during the CSP trials. We quantified percent asymmetry (Eq. 1) (Herzog et al., 1989) for average joint and crank power as the percent difference between the affected side (AS) and unaffected side (US) where perfect symmetry between legs is represented as 0%,

$$\% \text{ Asymmetry} = \left| \frac{US - AS}{0.5(US + AS)} \right| \cdot 100 \quad [3.1]$$

Finally, we calculated metabolic power (Péronnet and Massicotte, 1991) from the rates of oxygen consumption and carbon dioxide production averaged during the last two minutes of each trial, and determined net metabolic power by subtracting resting metabolic power. We calculated net efficiency as the quotient of average total mechanical power output and net metabolic power.

3.2.6 Statistics

We utilized statistical parametric mapping (SPM) (Pataky, 2010) to identify differences in instantaneous joint and crank joint powers on the affected side due to crank arm length and prosthesis type. For each participant and trial, 10 crank cycles were analyzed to create participant-average waveforms. We performed a 2-way, repeated measures SPM ANOVA with crank arm length and prosthesis type as factors ($\alpha=0.05$), and used post-hoc, two-tailed SPM paired t-tests with a Dunn-Šidák correction if a significant main effect was observed. We did not perform SPM analyses on ankle power because the ankle joint is fixed on a daily-use prosthesis and could not be defined on a CSP. We also evaluated the effect of shortened crank arm length on the affected side and prosthesis type on average joint and crank power, joint and crank power asymmetry, and net efficiency by constructing linear mixed-effects models ($\alpha=0.05$). We considered prosthesis type (categorical), the shortened crank arm length (continuous), and side (affected vs. unaffected, categorical) as fixed effects, and participant as a random effect. We performed the SPM analyses

in Matlab (Mathworks Inc., Natick, MA) and constructed the linear mixed-effects models in R (R Foundation for Statistical Computing, Vienna, Austria; version 4.2.2) using publicly-available scripts and packages (Pinheiro et al., 2020; Revelle, 2019; Wickham, 2016). SPM source code was provided from spm1d (version M.0.04.8; www.spm1d.org).

3.3 Results

When subjects used a daily-use prosthesis and CSP, total mechanical power output for all crank arm lengths was 1.54 ± 0.02 (mean \pm s.e.) and 1.56 ± 0.02 $\text{W}\cdot\text{kg}^{-1}$, with a cadence of 74.1 ± 1.7 and 73.3 ± 1.4 rpm, respectively (**Table 3.1**). For hip transfer power asymmetry with equal crank arm lengths, we removed one outlier trial from one participant while they used a daily-use prosthesis. The outlier was determined as greater than three standard deviations away from the median, and if included, it significantly altered the results of the linear-mixed effect model.

Table 3.1. Average \pm s.e. crank power and cadence while riding with different affected side crank arm lengths

CAL [mm]	Crank Power [$\text{W}\cdot\text{kg}^{-1}$]		Cadence [rpm]	
	Daily-Use	CSP	Daily-Use	CSP
160	1.54 ± 0.04	1.58 ± 0.04	73.8 ± 3.6	73.8 ± 2.8
165	1.54 ± 0.04	1.58 ± 0.03	74.8 ± 3.4	73.7 ± 2.8
170	1.53 ± 0.04	1.54 ± 0.04	73.8 ± 3.5	73.6 ± 2.8
175	1.55 ± 0.03	1.55 ± 0.04	74.2 ± 3.7	72.3 ± 3.0

CAL: Crank arm length on the affected side, crank arm length on the unaffected side was 175 mm. Daily-Use: Daily-use prosthesis. CSP: Cycling-specific prosthesis

3.3.1 Mechanical Power

We found a main effect of shorter affected side crank arm length on instantaneous hip joint, knee joint, hip transfer, and crank power of the affected side using a two-way, repeated measures SPM ANOVA (**Figures, Supplemental Digital Content 3.1**, Summarizes the main and interaction effects of asymmetric crank arm lengths and prosthesis types). However, we found no

significant differences for instantaneous hip joint, knee joint, and hip transfer between crank arm lengths when we performed post-hoc, SPM pairwise comparisons (**Figures, Supplemental Digital Content 3.2**, Pairwise comparisons of asymmetric crank arm length on instantaneous power). Instead, we found an effect of shortened crank arm length on crank power, where a shorter affected side crank arm length (160 mm) resulted in a decreased magnitude of affected side positive crank power during the downstroke (from $\sim 45\text{-}94^\circ$) and decreased magnitude of affected side negative crank power during the upstroke (from $\sim 270\text{-}360^\circ$) compared to a longer affected side crank arm length (170 and 175 mm; $p \leq 0.001$ for both) (**Figures, Supplemental Digital Content 3.3**, Pairwise comparisons of prosthesis type on instantaneous power). We also found a main effect of prosthesis type on instantaneous knee joint and crank power using a two-way, repeated measures SPM ANOVA. Pairwise comparisons revealed that use of a CSP increased the magnitude of affected side knee joint power during the downstroke (from $\sim 50\text{-}175^\circ$) compared to a daily-use prosthesis ($p \leq 0.01$), however, this was not simultaneously reflected in crank power. Instead, the magnitude of affected side negative crank power during the upstroke ($\sim 180\text{-}345^\circ$) was reduced while cycling using a CSP ($p < 0.001$).

Despite the effects of shorter affected side crank arm lengths and prosthesis type on instantaneous knee joint and crank power of the affected side, shorter affected side crank arm length and/or using different prosthesis types did not significantly affect average crank power or average joint power for either leg ($p \geq 0.25$ for all; **Figures 3.2 & 3.3**). We found that average joint and crank power were influenced by side. Across all affected side crank arm lengths and each prosthesis type, average ankle joint, knee joint, and hip transfer power on the affected side produced $0.09 \pm 0.01 \text{ W}\cdot\text{kg}^{-1}$, $0.23 \pm 0.02 \text{ W}\cdot\text{kg}^{-1}$, and $0.01 \pm 0.00 \text{ W}\cdot\text{kg}^{-1}$ less than the unaffected

side, respectively ($p < 0.001$ for all). Finally, average crank power on the affected side was $0.39 \pm 0.02 \text{ W}\cdot\text{kg}^{-1}$ less than the unaffected side ($p < 0.001$).

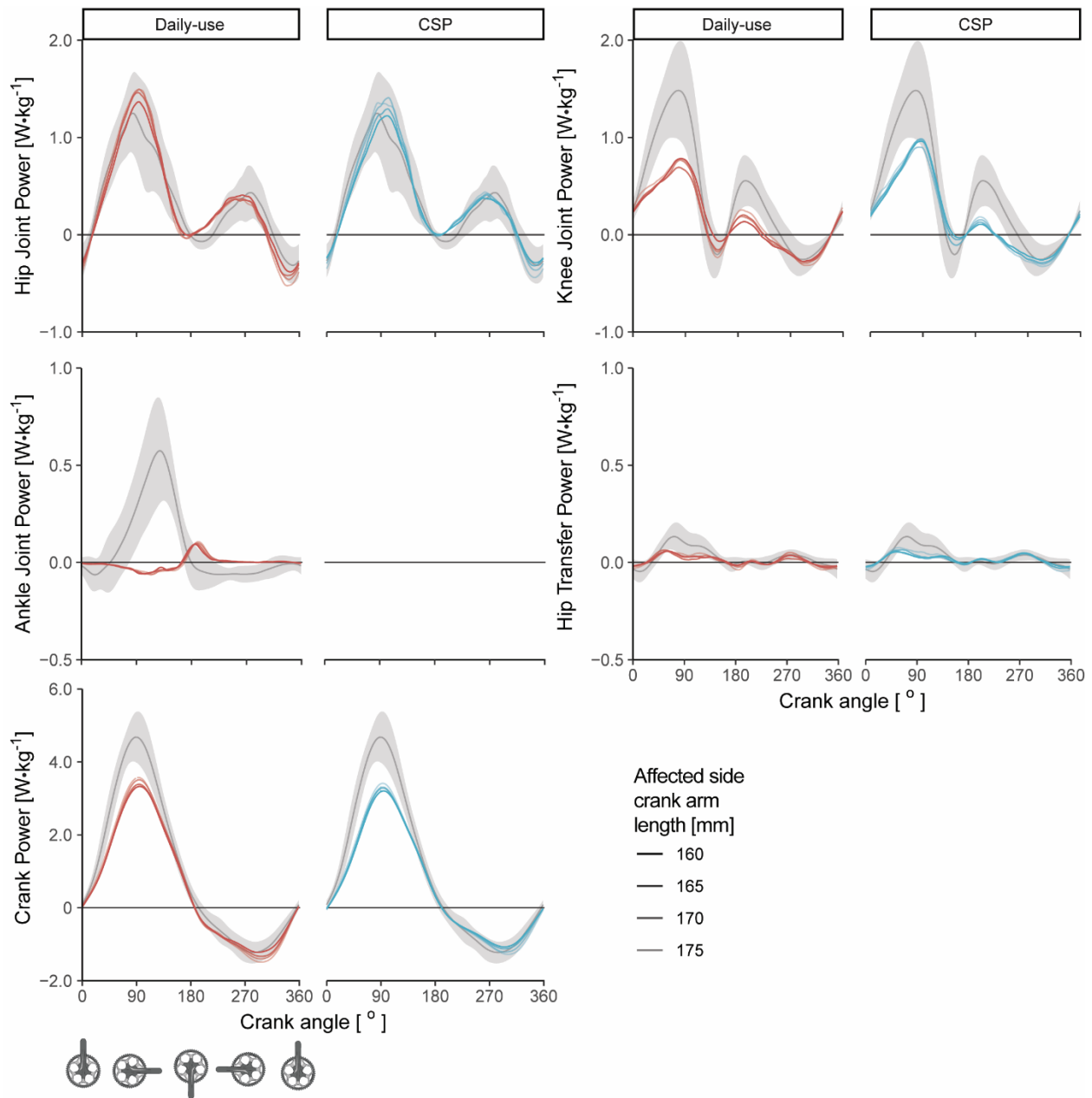


Figure 3.2 Average instantaneous hip joint, knee joint, ankle joint, hip transfer, and crank power for cyclists with a unilateral transtibial amputation using a daily-use (red) or cycling-specific (CSP; blue) prosthesis. The unaffected side (gray) is shown as a visual reference of asymmetry and represents the average power \pm s.d. across all conditions. Changes in crank arm length were applied to the affected side only, while the crank arm length on the unaffected side was held constant at 175 mm. Note the different y-axes along each row.

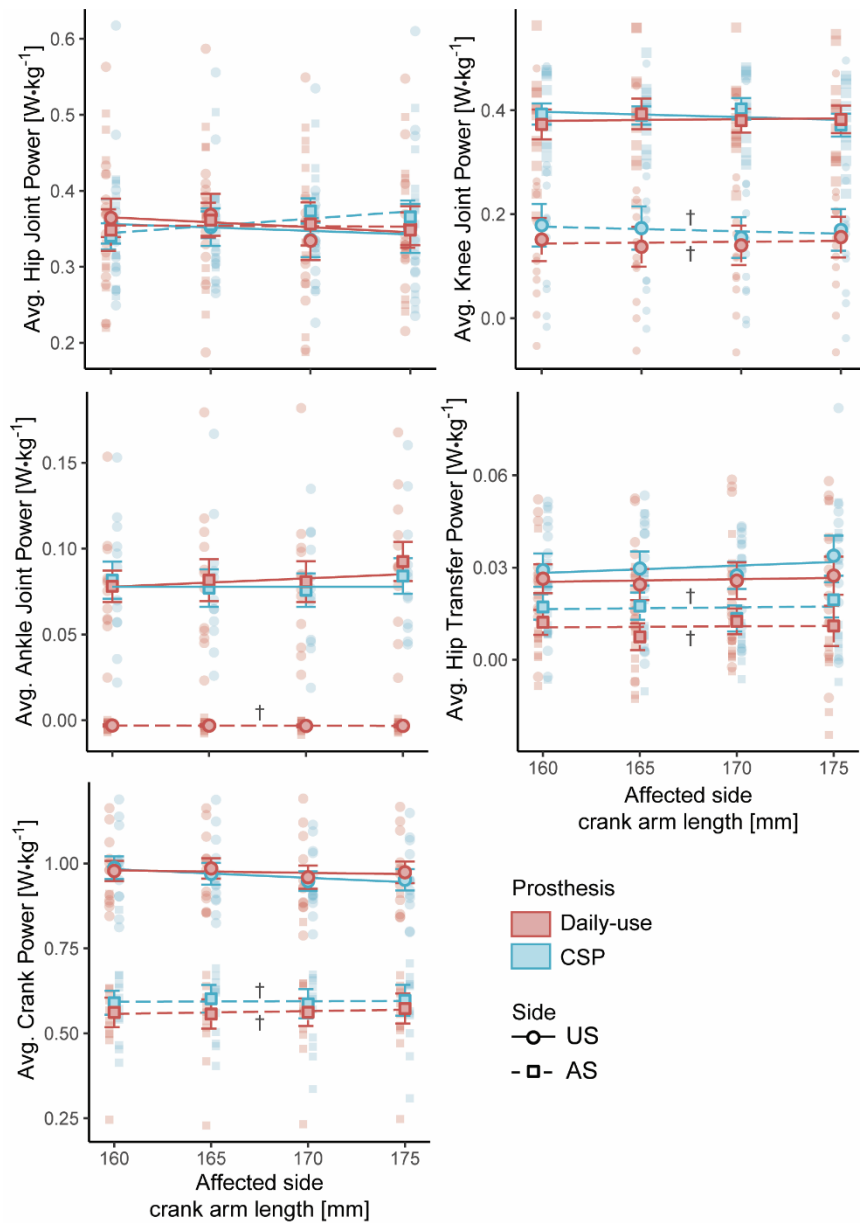


Figure 3.3 Average \pm s.e. hip joint, knee joint, ankle joint, hip transfer, and crank power for cyclists with a unilateral transtibial amputation using a daily-use (red) and cycling-specific (CSP; blue) prosthesis. The unaffected side (US) is indicated with circles and the affected side (AS) is indicated with squares. Ankle joint power with a CSP was not calculated because an ‘ankle’ could not be defined. Lines represent the linear mixed-effect models. Small points represent participant responses with ± 0.25 mm offset along the x-axis for visual clarity. Note the different y-axes for each subpanel. † indicates a significant effect of side.

3.3.2 Asymmetry

With the exception of hip joint power and hip transfer power, we found no effect of shorter affected side crank arm length or prosthesis type on crank or joint power asymmetry (**Figure 3.4;** $p \geq 0.26$ for crank, ankle joint, and knee joint power asymmetry). While using a daily-use prosthesis or CSP, crank power asymmetry was $54.8 \pm 9.2\%$ and $48.6 \pm 8.3\%$, ankle joint power asymmetry was $223.4 \pm 30.3\%$ and not calculated for a CSP, and knee joint power asymmetry was $105.3 \pm 20.2\%$ and $95.1 \pm 19.9\%$, respectively. We found an interaction effect of shorter affected side crank arm length and prosthesis type on hip joint power asymmetry ($p=0.014$) and hip transfer power asymmetry ($p=0.025$), where shorter affected crank arm length had no effect on hip joint power asymmetry ($p=0.44$) or hip transfer power asymmetry ($p=0.41$) while using a daily-use prosthesis. However, when using a CSP, hip joint power asymmetry and hip transfer power asymmetry decreased by $0.96 \pm 0.29\%$ ($p=0.002$), and $4.40 \pm 1.68\%$ ($p=0.013$) for every 1 mm decrease in affected side crank arm length, respectively.

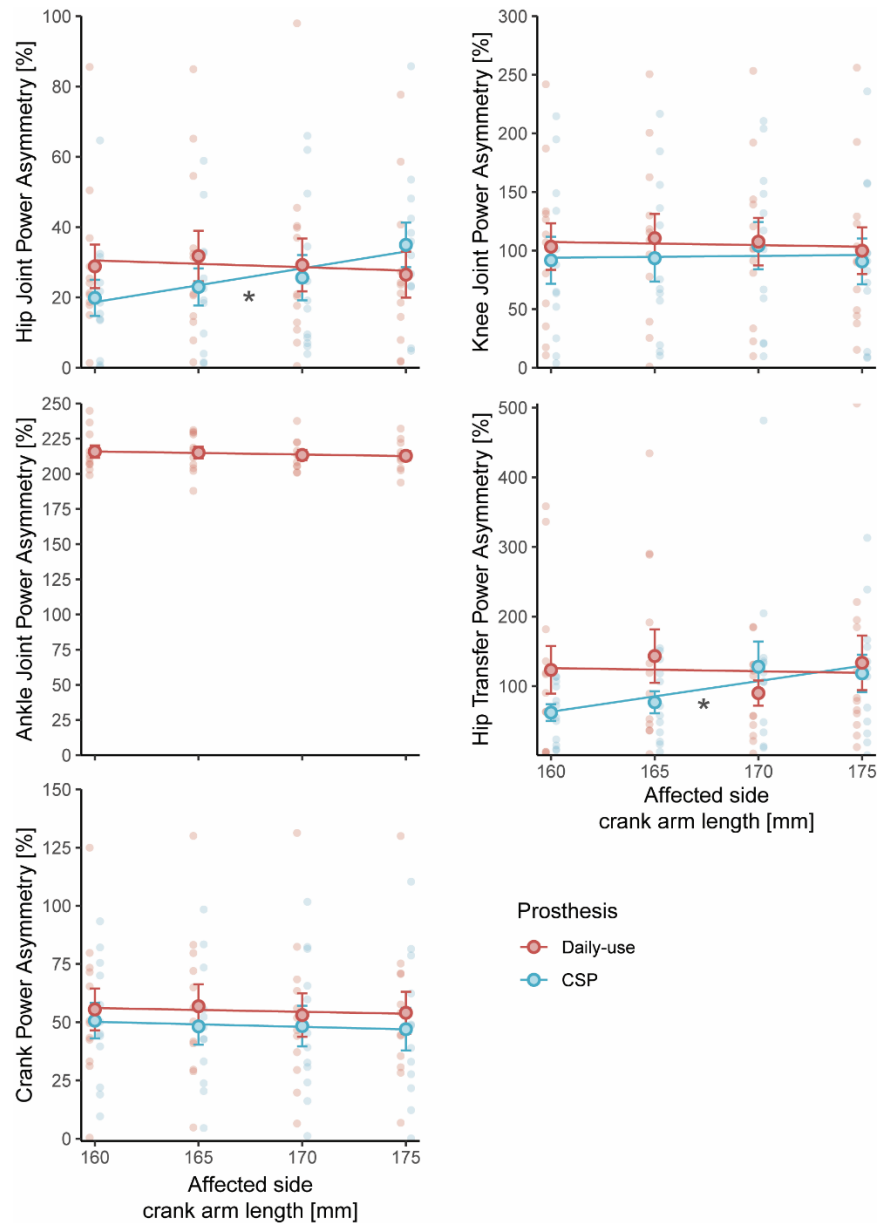


Figure 3.4 Average \pm s.e. percent asymmetry of hip joint, knee joint, ankle joint, hip transfer, and crank power for cyclists with a unilateral transtibial amputation using a daily-use (red) and cycling-specific (CSP; blue) prosthesis. Lines represent the linear mixed-effect models. Small points represent participant responses with ± 0.25 mm offset along the x-axis for visual clarity. Note the different y-axes for each subpanel. * indicates a significant effect of shorter affected side crank arm length.

3.3.3 Net Efficiency

We found no significant effect of shorter affected side crank arm length ($p=0.65$) or prosthesis type ($p=0.82$) on net efficiency (**Figure 3.5**). Across the different affected side crank arm lengths, mean net efficiency was $21.7 \pm 0.4\%$ and $22.4 \pm 0.4\%$ using a daily-use prosthesis and CSP, respectively.

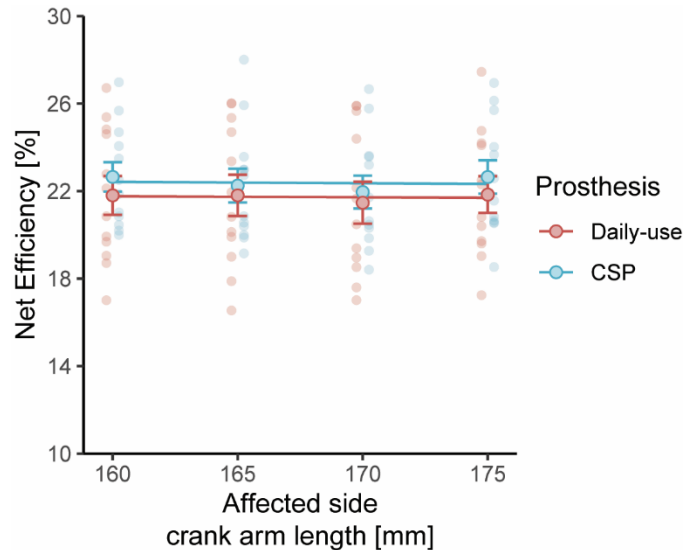


Figure 3.5 Average \pm s.e. net efficiency for cyclists with unilateral transtibial amputation using a daily-use (red) or cycling-specific (CSP; blue) prosthesis. Lines represent the linear mixed-effect models. Small points represent participant responses with ± 0.25 mm offset along the x-axis for visual clarity.

3.4 Discussion

We compared the effects of cycling with equal and shorter affected side crank arm lengths and two types of prostheses in recreational cyclists with a unilateral transtibial amputation (TTA) on joint and crank power, joint and crank power asymmetry, and net efficiency. Contrary to our hypothesis, our results show that neither cycling with shorter affected side crank arm lengths nor using a cycling specific prosthesis (CSP) significantly alters average crank power or average joint power while riding at a moderate power output ($1.5 \text{ W}\cdot\text{kg}^{-1}$). We also found that shorter affected side crank arm length does not affect joint power asymmetry while riding using a daily-use prosthesis. However, the combined effect of shorter affected side crank arm length while using a

cycling specific prosthesis reduced hip joint power and hip transfer power asymmetry. Despite these changes in asymmetry at the hip, we found that net efficiency did not change with shorter affected side crank arm length or cycling using different types of prostheses (daily-use and CSP).

3.4.1 Power and asymmetry

Our results are in agreement with the previous findings of Childers and colleagues (Childers and Kogler, 2014), who showed that a shorter affected side crank arm length reduced kinematic asymmetries in cyclists with a TTA, but did not reduce kinetic asymmetries at the crank or lower-limb joints. We found that cyclists with a TTA produced 42.2% less average crank power on their affected side compared to their unaffected side while riding at $1.5 \text{ W}\cdot\text{kg}^{-1}$ regardless of crank arm length. The difference in average crank power between legs was likely due to the affected side producing 61.7% and 58.7% less average knee joint and hip transfer power compared to the unaffected side. Similar to Childers et al. (Childers and Kogler, 2014), we found that shorter affected side crank arm length does not alter average crank or joint power, or reduce crank or joint power asymmetry while using a daily-use prosthesis. However, we found that the combination of shorter affected side crank arm length from 175 mm to 160 mm and using a CSP can reduce hip joint and hip transfer power asymmetry from 35% to 20%, and 118% to 62%, respectively. While these results initially seem at odds with our finding that average joint power was not significantly affected by a shorter affected side crank arm length or prosthesis type, they might be explained by nonsignificant, incremental changes in hip joint and hip transfer power of both legs and the combined result is a reduction in asymmetry. Additionally, average hip transfer power is very small and makes up less than ~4% of the average crank power over the pedal cycle, and small changes in hip transfer power magnitude in one or both legs can result in large changes in asymmetry while not changing crank power.

Cycling with shorter affected side crank arms or using a CSP did not elicit changes in average crank or joint power but did affect instantaneous crank and joint power. Compared to 175 mm crank arm length, cycling with a 160 mm affected side crank arm length resulted in 5% lower peak positive crank power during the downstroke and 16% lower peak negative crank power magnitude during the upstroke. Shorter crank arm length reduces the crank's moment arm; therefore, the magnitude of peak positive and negative crank power would decrease at a constant cadence (**Table 3.1**). Increasing the affected side crank arm length would likely increase the magnitude of peak positive and negative crank power; however, this is not a viable strategy for cyclists with a TTA who would be required to increase knee and hip extension of the affected side or roll/drop their hips off the saddle to reach the bottom of the crank cycle. We also found that use of a CSP resulted in 15% greater peak knee power during the downstroke and 3% lower peak negative crank power magnitude during the upstroke compared to a daily-use prosthesis. While not statistically significant, we noted that use of a CSP resulted in an 8% numerical reduction in peak positive hip power on the affected side, which coincided near-simultaneously with the 15% greater peak positive knee power (~90-100 degrees, **Figure 3.2**). Therefore, use of a CSP might reduce peak hip power output during the downstroke and redistribute that power to the knee, however, future studies with greater number of participants or increased total mechanical power output are needed to determine how power is transferred within a leg during cycling.

3.4.2 Net efficiency

Similar to previous studies that show efficiency is independent of changes in crank arm length in non-amputee cyclists (Ferrer-Roca et al., 2017; McDaniel et al., 2002; Morris and Londeree, 1997), we found that there was no significant effect of shorter affected side crank arm lengths from 175 mm to 160 mm on net efficiency in cyclists with a TTA. Additionally, we found

that use of a CSP does not change net efficiency compared to a daily-use prosthesis. This result is similar to previous literature that found that altering cleat position from the forefoot to the heel or midfoot does not influence efficiency in non-amputee cyclists (Bartlett, 2007; Van Sickle and Hull, 2007).

Previous research has suggested that net efficiency could be affected by crank arm length due to changes in joint angle and pedal speed (the product of crank arm length and crank angular velocity), which could affect muscle fascicle operating lengths (Barrat et al., 2016) and shortening velocity in uni-articular muscles (Martin et al., 2000). Although we found no significant effects, shorter affected side crank arm lengths from 175 mm to 160 mm numerically decreased peak knee joint and hip joint extension by 6° and 4° at the bottom of the crank cycle, respectively, and decreased peak knee flexion by 2° at the top of the crank cycle (**Figure 3.6**). Moreover, though not significant, cycling using a CSP resulted in 11 - 14° greater knee extension angles throughout the entire crank cycle compared to a daily-use prosthesis, which may have a greater effect on changing muscle fascicle operating lengths than a shorter crank arm length. However, we found no significant effect of shorter affected side crank arm length or cycling using a CSP versus daily-use prosthesis on average joint power or net efficiency. It is possible that these conditions did not elicit large enough changes in joint angles to alter muscle operating length or shortening velocity, as previous research has suggested that equal 140-150 mm crank arm lengths might minimize joint moments and metabolic power (Gonzalez and Hull, 1989; McDaniel et al., 2002). It is also possible that changing the crank arm length on one side may elicit changes in muscle dynamics at the knee joint and hip joint only on the affected side, but these changes may have been too small to influence net efficiency.

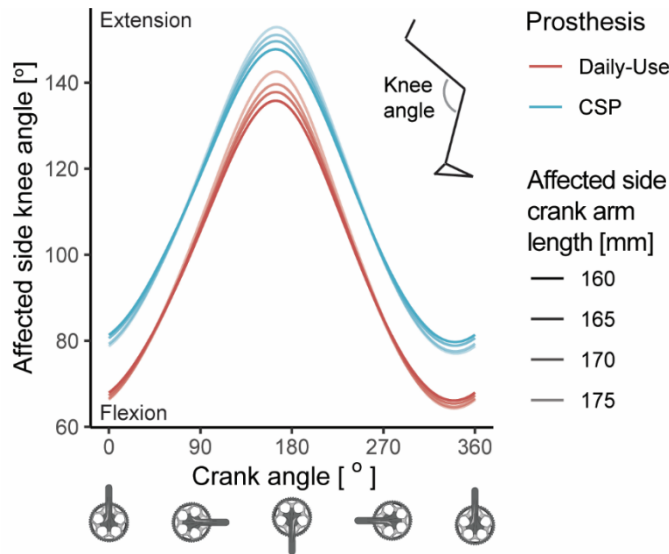


Figure 3.6 Average knee joint angle on the affected side for cyclists with unilateral transtibial amputation using a daily-use (red) or cycling-specific (CSP; blue) prosthesis.

Large biomechanical asymmetries between legs are often presumed to worsen efficiency, however we found that cyclists with a TTA have similar efficiency compared to non-amputees, despite large asymmetries between legs. Previously, Bartlett and Kram (Bartlett, 2007) showed that gross efficiency of competitive, non-amputee cyclists range from 17.1 – 18.6% when riding from 100 – 115 W. If we compare our data after converting to gross efficiency and absolute mechanical power, our participants exhibited an average (\pm s.e.) gross efficiency of $17.8 \pm 0.2\%$ while riding at 112 ± 2 W. These results suggest that cyclists with a TTA are not less efficient even though they exhibit asymmetric kinematics and kinetics at moderate power outputs. Future studies that require higher mechanical power outputs are needed to determine if this finding is consistent across workloads.

3.4.3 Prosthesis and Equipment Considerations

We found that when cycling at a moderate power output ($1.5 \text{ W}\cdot\text{kg}^{-1}$) with shorter affected side crank arm lengths or using a CSP does not change net efficiency compared to symmetric crank arm lengths or using a daily-use prosthesis. Therefore, recreational cyclists with a TTA may not need specialized cranks or a CSP to optimize their performance. Instead, cyclists with a TTA

should likely choose a bike fit and prosthesis that maximizes perceived comfort. Anecdotally, some of the participants reported that they preferred the shortest affected side crank arm length (160 mm) because this configuration did not result in the socket pinching or digging into the back of their knee, especially at the top of the crank cycle during peak knee flexion. The participants who did not report this discomfort had a larger posterior cut-out in the socket that allowed them to flex their knee without discomfort at the top of the crank cycle. Individuals with a TTA who are interested in cycling for exercise or competition may consider a socket with a larger posterior cutout design that allows knee flexion.

Given that shorter affected side crank arm length reduced kinematic asymmetries (Childers and Kogler, 2014) but not crank or joint power asymmetries in cyclists with a TTA, future research should investigate the effects of cycling with non-circular chainrings. Non-circular chainrings, such as oval chainrings, increase the effective chainring diameter and significantly vary crank angular velocity within the crank cycle (Leong et al., 2017). In non-amputee cyclists, oval chainrings do not affect efficiency compared to circular chainrings (Leong et al., 2021), nor do they significantly increase peak crank or joint power because the multiple degrees of freedom in the leg allow non-amputee cyclists to manipulate ankle joint velocity in a manner that counters the effects of increased effective chainring diameter (Leong et al., 2017). However, in a population with large asymmetries between legs due to use of a prosthesis and the absence of degrees of freedom, non-circular chainrings – specifically an oblique chainring (egg-shaped) with an asymmetric shape – may improve crank and joint power asymmetry in cyclists with a TTA. An optimized oblique chainring may alter crank and joint power asymmetries by applying a standard effective chainring diameter to the downstroke of the unaffected side, but an increased effective chainring diameter

during the downstroke of the affected side, thus increasing peak positive crank power on the affected side while not significantly altering the unaffected side.

Future research should consider the effect of CSP geometry on instantaneous crank power. The CSP we used in this study was created by attaching a straight metal pylon directly to the bottom of the participant's daily-use socket and some participants reported increased discomfort on the distal end of their residual limb during the downstroke. Instead, adjusting the angle between the socket and pylon might improve comfort and influence crank power. For example, extending the pylon and then moving the distal end of the pylon to a more anterior position relative to the socket would allow a cyclist to directly connect their CSP to the pedal, while keeping the shank in a similar position as if there was a prosthetic foot attached. In addition, shifting the socket-nylon interface from the bottom of the socket towards the front of the socket may allow some of the pedal reaction force to be distributed over the anterior surface of the shank rather than the distal end of the residuum. These changes in CSP geometry may allow a cyclist with a TTA to apply more force to the cranks during the downstroke if pain is a limiting factor.

3.4.4 Potential limitations

The movement of the residual limb within the prosthesis may influence instantaneous knee joint kinematics and kinetics. Childers and colleagues (Childers et al., 2012; Childers et al., 2014) estimated that cyclists with a TTA experience ~2-4 mm of socket pistoning during the downstroke of the affected side. This magnitude of displacement is within the measurement error of motion capture systems and does not likely affect joint moment calculations in cycling (Childers et al., 2012). However, the prosthetic socket also rotates anteriorly by ~5° about the distal end of the residual limb, particularly during peak knee flexion at the top of the crank cycle and the beginning of the downstroke (Childers et al., 2012). This effectively translates the proximal end of the socket

anteriorly from the knee joint center and may influence the calculation of knee joint kinematics and kinetics on the affected side if reflective markers are placed directly on the socket. Participants used their own prosthetic socket in the current study, so we placed reflective markers directly on the socket to identify the knee joint center (Childers et al., 2012) and assumed a rigid connection between the residual limb and prosthetic socket, which may have affected our results. We calculated knee joint kinematics and kinetics for all trials assuming similar error, and used a repeated measures design that should account for these assumptions and errors.

We did not find any significant differences in average crank power or net efficiency using a daily-use prosthesis or CSP when riding a cycling ergometer. However, when cycling outdoors, there are other factors to consider that will affect cycling performance when using a prosthesis, such as aerodynamic drag or total mass (Martin et al., 1998). The design of a CSP can exhibit reduced mass and aerodynamic drag compared to a daily-use prosthesis (Dyer and Disley, 2020; Dyer and Woolley, 2017), which would allow a cyclist with a TTA to increase their cycling velocity for a given mechanical power output. Previously, Dyer and colleagues (Dyer and Disley, 2020; Dyer and Woolley, 2017) showed that using a CSP with a lightweight airfoil pylon (7.1 N) reduced the finishing time of a Paralympic cyclist by 23 seconds over a 16.1 km time trial compared to their daily-use prosthesis (18.2 N). Therefore, future studies are needed to determine the effects of using a CSP versus daily-use prosthesis for riding outside.

It is unclear how much of the reduction in the magnitude of negative crank power during the upstroke on the affected limb can be attributed to the influence of using a CSP, rather than the difference in weight between prosthesis types. The average weight of the daily-use prosthesis used by our participants was 17.9 N including a cycling shoe. To create the CSP, we removed the prosthetic foot and cycling shoe from the participant's daily-use prosthesis. The weight of a

prosthetic foot scales with size, but an average sized, prosthetic foot with a cosmesis (Ottobock, Restore: size – 43EU/9.5US) and Sworks7 cycling shoe weighs 8.8N (foot – 6.6 N; shoe – 2.2 N). Therefore, we estimate that the average CSP in this study weighed ~9.1 N, about half of the average daily-use prosthesis weight. Therefore, future studies using weight-matched prostheses may be necessary to fully understand the influence of using a CSP compared to a daily-use prosthesis.

Finally, cyclists may utilize different neuromuscular control strategies to ride at higher total mechanical power outputs compared to moderate power outputs. Previously, Ericson (Ericson, 1988) showed that a greater reliance was placed on hip extension to provide power to the crank as total mechanical power output increased from 120 – 240 W. However, data from Elmer et al. (Elmer et al., 2011) suggest that the relative contribution of the ankle, knee, and hip remain constant over a crank cycle when cycling at 250 – 850 W, but an exchange occurs at the knee where non-amputee cyclists decrease relative knee extension power while simultaneously increasing relative knee flexion power. Additionally, peak crank moment asymmetry has been shown to decrease with increasing mechanical power output in non-amputee cyclists riding with equal crank arm lengths (Carpes et al., 2010). Cycling with shorter affected side crank arm lengths or using a CSP may have a different effect at higher total mechanical power outputs compared to moderate power outputs, and future studies with greater mechanical power output are required to determine the effects of shorter affected side crank arm length and prosthesis type on crank and joint power.

3.5 Conclusion

While cycling at a moderate power output, shorter affected side crank arm length and use of a CSP versus a daily-use prosthesis do not significantly change average crank power, average joint power, or net efficiency in cyclists with a TTA. However, small non-significant changes in

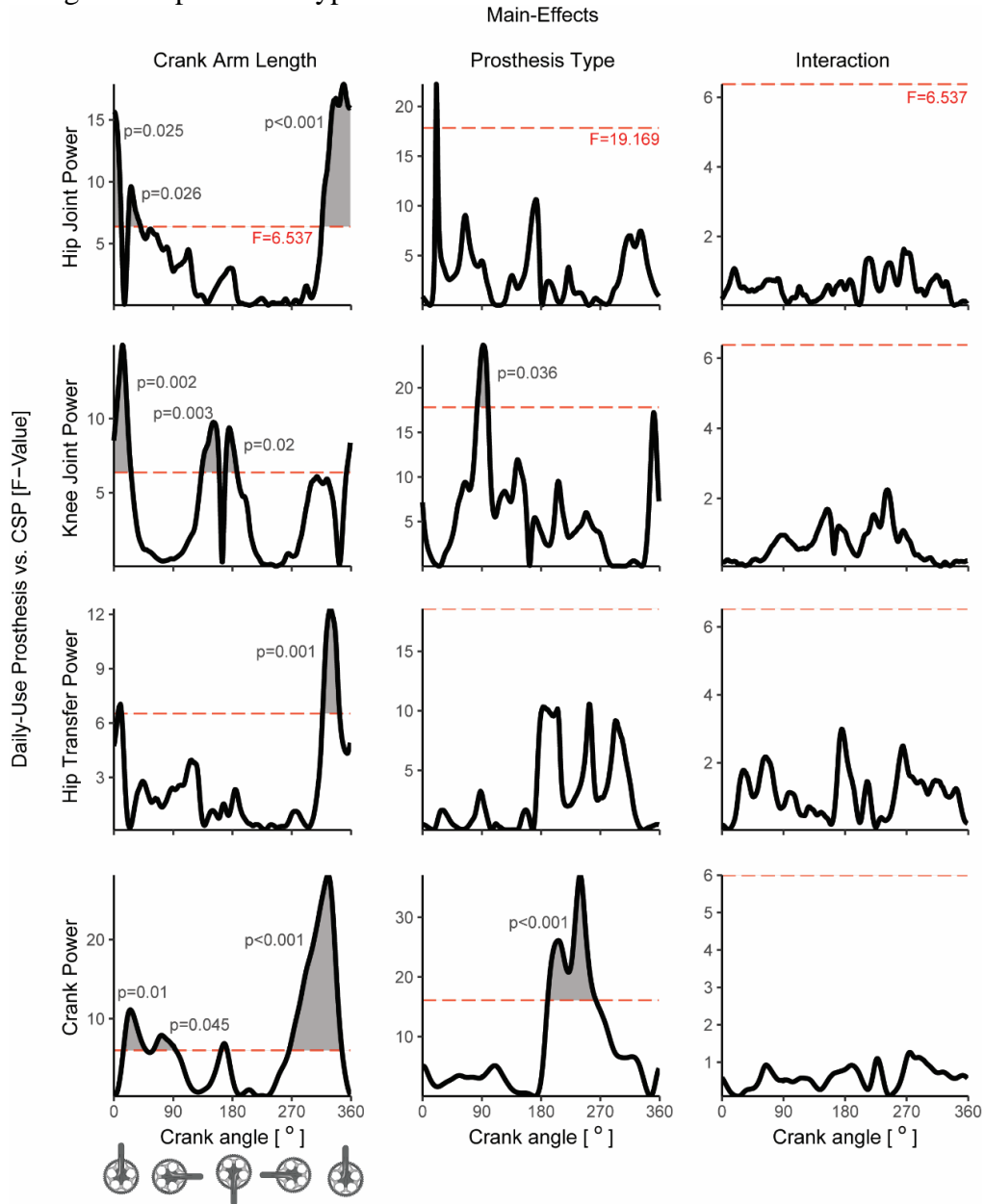
average hip joint power while cycling with shorter affected side crank arm lengths reduced hip joint power asymmetry. Additionally, small non-significant changes in average hip transfer power while cycling with shorter affected side crank arm lengths while using a CSP reduced hip transfer power asymmetry. However, these changes in hip asymmetry do not translate to improvements in crank power asymmetry, therefore, recreational cyclists with a TTA may choose crank arm lengths or prosthesis types based on personal comfort.

3.5.1 Funding

This study was funded by a Department of Veterans Affairs research grant awarded to A.M.G (VA RR&D Service RX0030101-01A1).

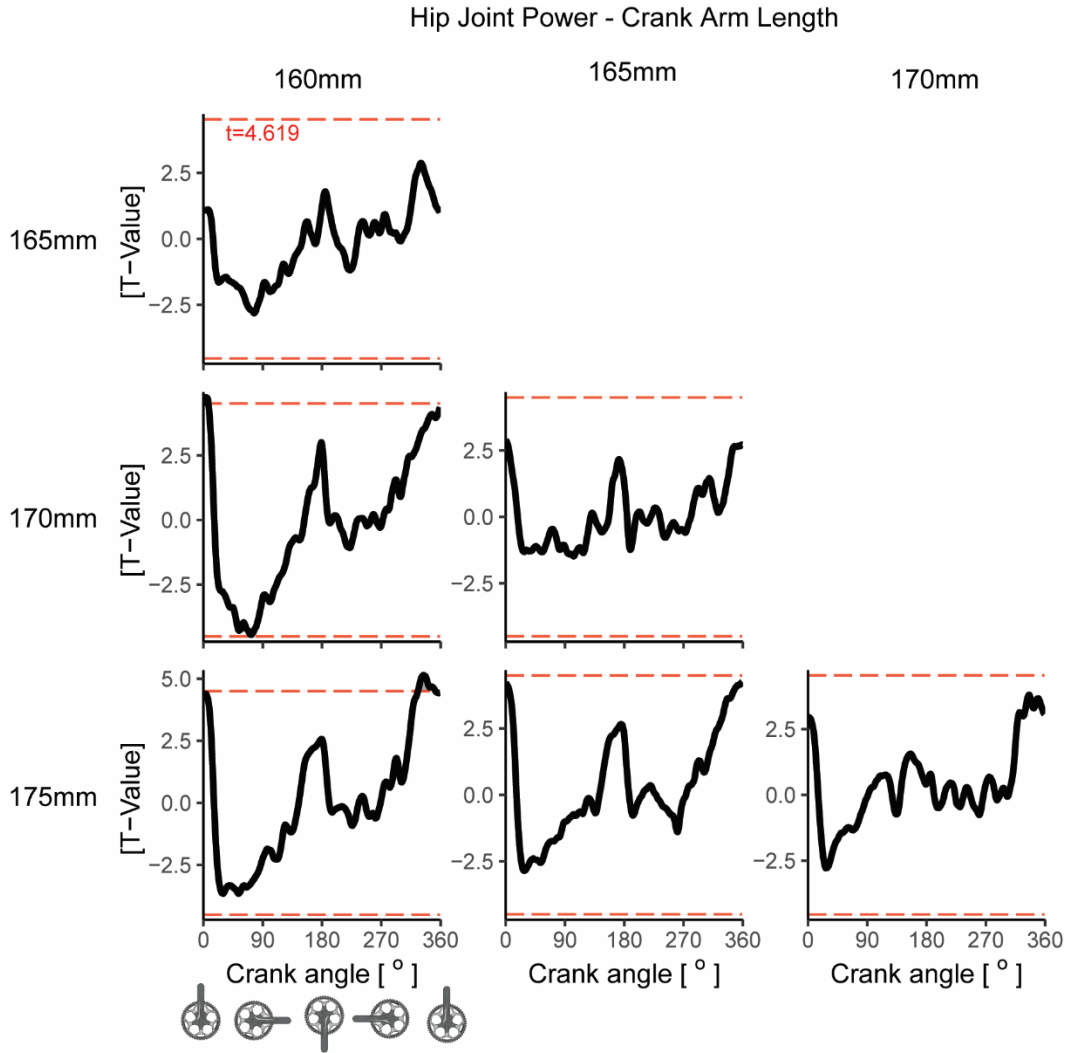
3.6 Supplemental Materials

Digital Supplementary Content 3.1: 2 way, repeated-measures SPM ANOVA for instantaneous hip joint, knee joint, hip transfer, and crank power between shorter affected side crank arm lengths and prosthesis types.

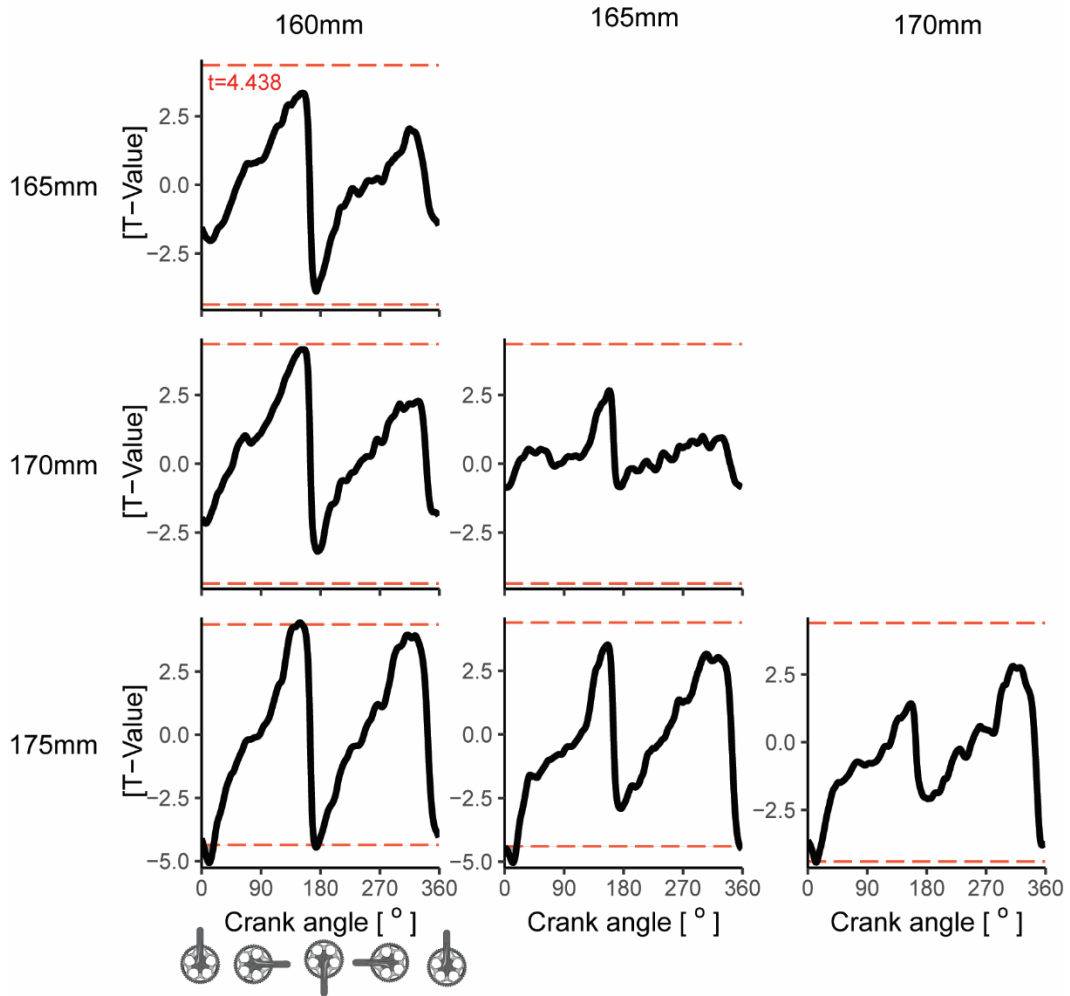


Supplemental Figure 3.1 2 way, repeated-measures SPM ANOVA for instantaneous hip joint, knee joint, hip transfer, and crank power throughout the crank cycle. Red dashed lines indicate the significance threshold for each main effect, and the grey shading indicates areas where a significant effect was found in the crank cycle. Signals where the area of interest was due to one point crossing the significance threshold (i.e., hip power, main-effect of prosthesis) were considered non-significant.

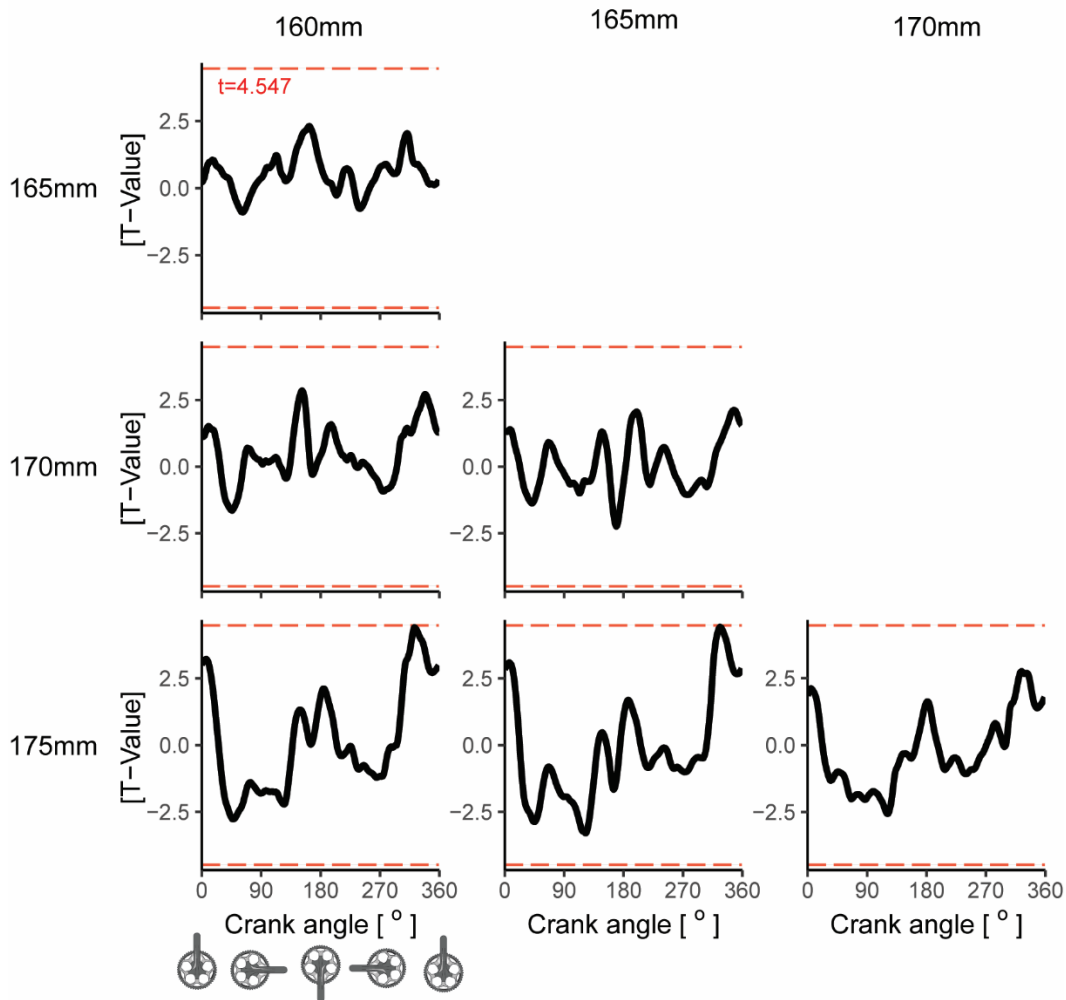
Digital Supplementary Content 3.2: Pairwise t-test SPM comparisons of crank arm length for instantaneous hip joint, knee joint, hip transfer, and crank power.

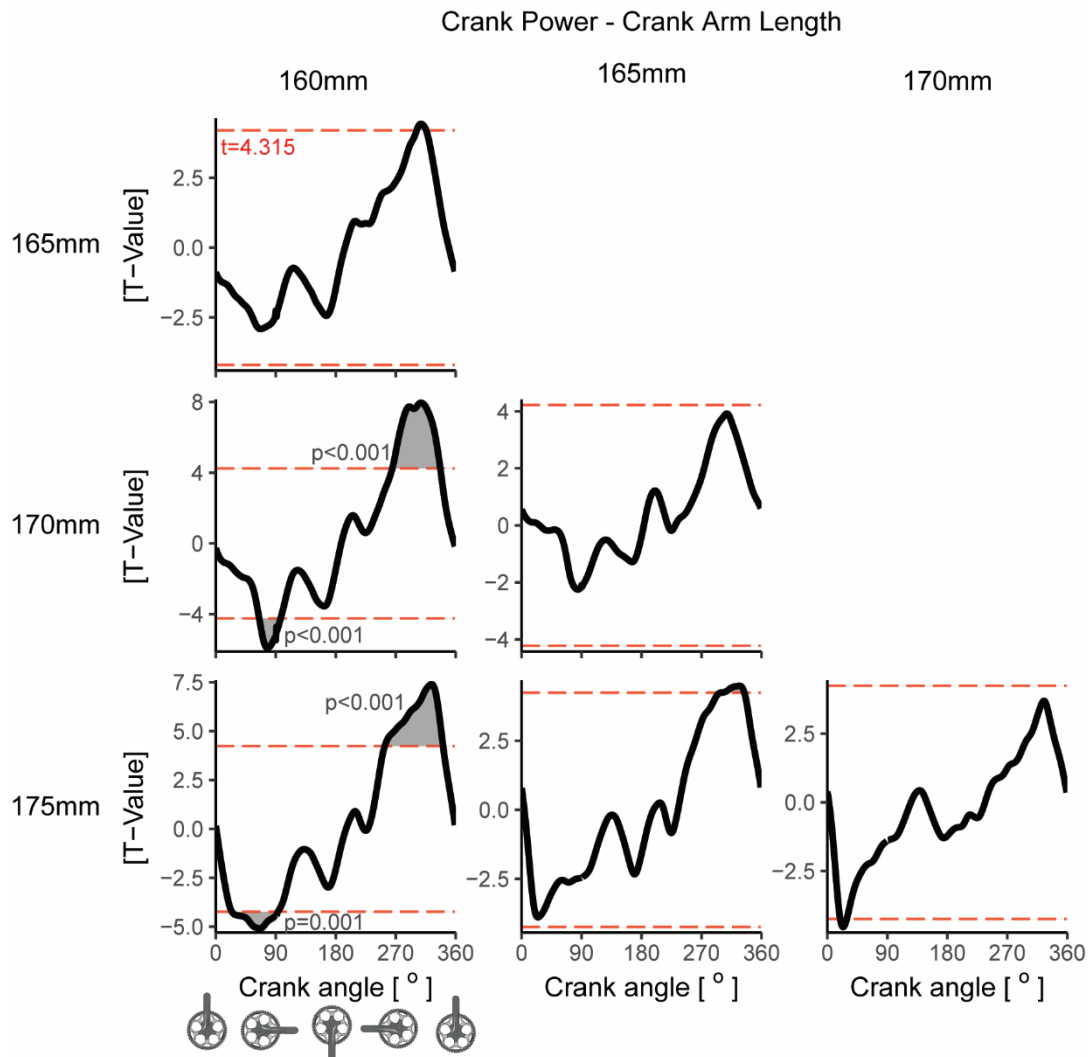


Knee Joint Power - Crank Arm Length



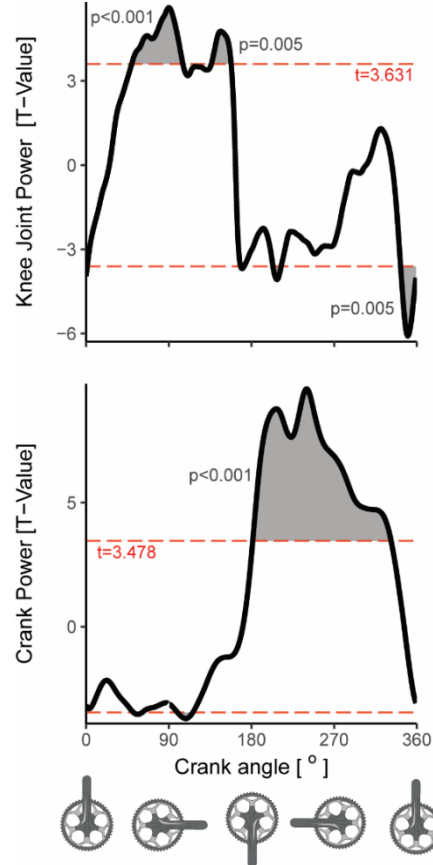
Hip Transfer Power - Crank Arm Length





Supplemental Figure 3.2 Two-tailed, SPM paired t-tests with a Dunn-Šidák correction to evaluate the main effect of crank arm length on hip joint, knee joint, hip transfer, and crank power of the affected side throughout the crank cycle. Red dashed lines indicate the significance threshold, and the grey shading indicates areas of the crank cycle where a significant effect was found. Signals where the area of interest was due to one point crossing the significance threshold were considered non-significant.

Digital Supplementary Content 3.3: Pairwise t-test SPM comparisons of prosthesis type for instantaneous knee and crank power.



Supplemental Figure 3.3 Two-tailed, SPM paired t-tests with a Dunn-Šidák correction to evaluate the main effect of prosthesis type on hip joint, knee joint, hip transfer, and crank power throughout the crank cycle. Red dashed lines indicate the significance threshold, and the grey shading indicates areas of the crank cycle where a significant effect was found. Signals where the area of interest was due to one point crossing the significance threshold were considered non-significant.

Chapter 4: The effect of increased prosthetic leg length and cycling-specific prostheses in cyclists with a unilateral transtibial amputation

In preparation – with intent to submit to *Medicine and Science in Sports and Exercise*

Due in part to the inability of a passive prosthesis to replicate ankle joint movement, cyclists with a unilateral transtibial amputation (TTA) have kinematic and kinetic asymmetries between their affected and unaffected sides that may influence efficiency. Altering bicycle geometry by increasing prosthetic effective leg length and/or using a cycling-specific prosthesis (CSP) may reduce asymmetries and improve cycling performance. **Purpose:** We determined the biomechanical and metabolic effects of increasing prosthetic effective leg length and using two types of prostheses on joint kinematics and kinetics, asymmetry, and net efficiency. **Methods:** 12 cyclists with a TTA rode at 1.5 W kg^{-1} at a standard effective prosthetic leg length and at 5, 10, and 15 mm longer than a standard leg length while using a daily-use prosthesis and CSP. **Results:** Increased prosthetic effective leg length of 15 mm decreased average knee angle by 3° ($p=0.02$). Use of a CSP increased average knee angle on the affected side by 12.5° ($p<0.001$), decreased knee angle asymmetry by 6.7 percentage points ($p<0.001$), and improved net efficiency by 0.9 percentage points ($p=0.014$) compared to a daily-use prosthesis. Average joint and crank power and power asymmetry were not influenced by increased prosthetic effective leg length or prosthesis type. **Conclusions:** Compared to a daily-use prosthesis, use of a CSP improves net efficiency in cyclists with a TTA by increasing the average knee angle on the affected side. CSPs might shift the knee extensor muscles into a more favorable region of the force-length curve and produce force more economically. These findings suggest that riders could increase prosthetic effective leg length up to 15 mm without affecting performance, and that use of a CSP improves cycling performance over a daily-use prosthesis.

4.1 Introduction

During cycling, mechanical power at the crank is produced by the muscles surrounding the ankle, knee, and hip joints, with additional power transferred from the upper body through the hip (Fregly and Zajac, 1996; van Ingen Schenau et al., 1990). When cyclists without an amputation ride at mechanical power outputs of 250-850 W, the ankle, knee, hip, and hip transfer powers contribute 14-26%, 37-41%, 37-46%, and 3-8% of the average crank power throughout the crank cycle, respectively (Elmer et al., 2011; Ericson, 1988; Wilkinson et al., 2020), and the ankle dorsi- and plantarflexes the foot by $\sim 20^\circ$ during the power production phase to assist with the transfer of power from the proximal joints to the crank (Childers and Kogler, 2014; Kautz et al., 1991). The movement of and muscles surrounding the biological ankle during the crank cycle allows cyclists to use multiple pedaling techniques to apply tangential force to the crank through different pedal orientations (Kautz et al., 1991) and/or control a target power output throughout perturbations, such as cycling with noncircular chainrings (Leong et al., 2017).

Cyclists with a unilateral transtibial amputation (TTA) require the use of a prosthesis to transfer power from the proximal joints to the crank. Many cyclists with a TTA choose to use their daily-use prosthesis, which is comprised of a socket that surrounds the residual limb and a stiff pylon connecting the socket to a passive-elastic, carbon fiber prosthetic foot. Due to the structural and muscular differences between the affected and unaffected sides, cyclists with a TTA are unable to dorsi- or plantarflex their prosthetic foot during the crank cycle, which contributes to asymmetric kinematics and kinetics between legs (Childers et al., 2009, Allen et al. - Chapter 3). Cyclists with a TTA who use a daily-use prosthesis have been shown to produce 59%, 54%, and 41% less average knee power, hip transfer power, and crank power in their affected side compared to their unaffected side while riding at 1.5 W kg^{-1} (Allen et al. - Chapter 3), and these

biomechanical asymmetries presumably worsen efficiency (the ratio of mechanical power to metabolic power) (Childers et al., 2009; Forte et al., 2020).

Cycling equipment modifications can alter the bicycle and rider geometry (“bicycle fit”) to influence rider performance. For example, competitive cyclists may use specialized handlebars to adopt a forward aerodynamic riding posture and increase their riding velocity by reducing the projected frontal area and aerodynamic drag (García-López et al., 2008; Martin et al., 1998). Also, declining the saddle (‘nose down’) 8° while riding up an 8° incline can improve gross efficiency by 1.4% (Wilkinson and Kram, 2022), and decreasing seat tube angle from 80° to 68° can worsen gross efficiency by $\sim 2.5\%$ (Price and Donne, 1997). In cyclists with a TTA, optimizing the bicycle fit and/or prosthesis configuration may reduce the kinematic and kinetic asymmetries between legs and potentially improve efficiency. Childers and Kogler (Childers and Kogler, 2014) showed that riding with shorter crank arms (165 mm) on the affected side compared to equal 175 mm crank arms reduced average knee and hip angle asymmetry between affected and unaffected sides in cyclists with a TTA. However, these improvements in kinematic and kinetic asymmetries did not translate to improvements in crank power asymmetry or efficiency (Childers and Kogler, 2014, Allen et al. - Chapter 3).

The mechanical asymmetries in cyclists with a TTA might be affected by changing the effective leg length of the prosthesis, defined as the distance from the joint center of rotation to the center of the cycling cleat (**Figure 4.1**) (Childers et al., 2009). Daily-use prostheses are often adjusted so that the standard pylon length allows an individual with a TTA to have an affected leg length that matches their unaffected leg length during standing. However, because the cycling cleat is placed approximately under the metatarsal heads and the biological ankle dorsi- and plantarflexes, cyclists change the effective leg length of the unaffected side dynamically

throughout the crank cycle, whereas riders with a TTA cannot change effective leg length of their affected side. In a simulated model of a cyclist with a TTA riding at 200 W, the dorsi- and plantarflexion of the biological ankle results in a ~15-20 mm increase in effective leg length of the unaffected side when the crank was near the bottom of the crank cycle (~140-215°) (Childers et al., 2009). A prosthesis is unable to replicate this increase in effective leg length and may contribute to kinematic asymmetries between the affected and unaffected sides because a cyclist with a TTA must increase affected side knee and hip extension to reach the bottom of the crank cycle (Childers et al., 2009), especially when saddle height is based on the unaffected side.

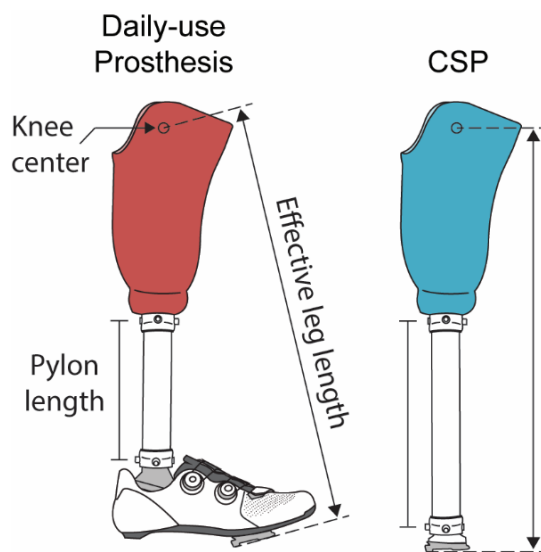


Figure 4.1 Illustration of pylon length and effective leg length in a daily-use prosthesis and a cycling-specific prosthesis (CSP).

Increasing the prosthetic effective leg length of a cyclist with a TTA may alter joint and crank power, and efficiency, through changes in lower-limb kinematics of the affected side. To our knowledge, no study has investigated the effects of changing effective leg length in cycling, however, previous research on the effects of saddle height can provide insight, as changes in saddle height alter the minimum and maximum angles of the ankle, knee, and hip and effect efficiency (Nordeen-Snyder, 1977; Price and Donne, 1997; Rankin and Neptune, 2010). Previously, Nordeen-Snyder (Nordeen-Snyder, 1977) showed that a $\pm 5\%$ change in saddle height (relative to

trochanteric height) could alter peak knee extension by 35% and increase the rate of oxygen consumption by 5-8% in cyclists without an amputation. Similarly, a $\pm 2\%$ change in saddle height away from preferred saddle height worsens gross efficiency in cyclists without an amputation by $\sim 1\%$ during submaximal cycling (Ferrer-Roca et al., 2014). Presumably, these changes in efficiency with knee and hip angle occur due to altered muscle force-length-velocity relationships (Rankin and Neptune, 2010; Yoshihuku and Herzog, 1996). Rankin and Neptune (Rankin and Neptune, 2010) used a musculoskeletal model that maximized average crank power to show that setting saddle height ± 40 mm away from the optimal height can increase or decrease the average knee and hip angle, which places the muscle fibers of the vastus group in a sub-optimal position on the force-length curve for producing power, and ultimately decreases average crank power. While increasing or decreasing saddle height affects the kinematics on both legs, increasing the prosthetic effective leg length may allow cyclists with a TTA to directly alter knee and hip joint kinematics on their affected side. An increase in prosthetic effective leg length may decrease average knee or hip angle, and could influence joint and crank power, joint and crank power asymmetry, and efficiency.

Cyclists with a TTA use either a daily-use prosthesis that includes a prosthetic foot or a cycling-specific prosthesis (CSP), which removes the prosthetic foot and connects the pylon directly to pedal (**Figure 4.1**) and the type of prosthesis likely influences joint kinematics and kinetics. For example, use of a CSP with an effective leg length that matches the unaffected side increased peak knee power by $\sim 15\%$ during the downstroke ($\sim 50-175^\circ$) and numerically increased knee angle by $\sim 11-14^\circ$ throughout the crank cycle compared to a daily-use prosthesis, but there was no significant change in average joint or crank power, or net efficiency (Allen et al. - Chapter 3). Additionally, increasing effective prosthetic leg length in a CSP might mitigate the change in

knee angle provided by a CSP compared to a daily-use prosthesis. Thus, the interaction of use of a CSP and increasing leg length may reduce asymmetry and affect efficiency in cyclists with a TTA.

The purpose of this study was to assess the effects of increased prosthetic effective leg length on joint angle, joint and crank power, joint and crank power asymmetry, and efficiency in cyclists with a TTA while riding using a daily-use prosthesis compared to a CSP. This information will inform prescription of bicycling components and/or prosthetic configurations that minimize asymmetry and improve efficiency. We hypothesized that increased prosthetic effective leg length would 1a) decrease average knee and hip joint angle on the affected side, and reduce kinematic asymmetries between legs, 2a) increase average joint and crank power on the affected side, and reduce joint and crank power asymmetries, and 3a) increase net efficiency (the ratio of mechanical power to net metabolic power). We also hypothesized that use of a CSP would 1b) increase knee and hip angle, and increase knee and hip angle asymmetry, 2b) not change average joint or crank power on the affected side, or joint or crank power asymmetry, and 3b) not change net efficiency compared to using a daily-use prosthesis.

4.2 Methods

4.2.1 Participants

12 healthy individuals with a TTA (6 males/6 females, mean \pm s.d age: 39.4 ± 8.7 years, height: 1.72 ± 0.08 m, mass: 73.2 ± 17.9 kg) and no additional cardiovascular, neurological, or musculoskeletal impairments enrolled in the study. Participants for this study were not required to have previous cycling experience, but self-reported at least 30 minutes of moderate exercise, 3 times per week while using a prosthesis for at least 3 years. All participants provided written

informed consent according to the protocol approved by the Colorado Multiple Institutional Review Board and the Department of Veterans Affairs (COMIRB 18-2783).

4.2.2 Bicycle ergometer setup

We used the same fitting protocol as in our previous study (Allen et al. - Chapter 3). Briefly, participants with a TTA rode a fully adjustable, bicycle ergometer (Retül Müve; Boulder, CO, USA) that we fit to them according to a protocol developed by Retül for individuals without an amputation. We initially set the ergometer to match the geometry of a Specialized Tarmac bicycle, and then scaled the size and dimensions according to a web-based app developed by Retül, which uses sex and standing height as input measures (Bike Sizing App | Specialized.com). We then sized the bike to the participants based on their unaffected side. We had participants ride the ergometer with symmetric 175 mm crank arms while we adjusted the saddle height and fore-aft position so that the unaffected knee angle was 150-160° when the crank was at bottom-dead-center (directly below the bottom bracket), and the tibial tuberosity was directly over the pedal spindle when a plumb line was dropped with the crank at 90°. We allowed minor adjustments for comfort but kept the seat-tube angle constant. We set the handlebar position and stem angle so that the participant's torso was leaning forward with their elbows slightly bent when resting their hands on top of the handlebars. We did not standardize torso angle to allow for individual participant comfort. Simultaneously, a certified prosthetist adjusted the prosthesis alignment to ensure the knee was tracking vertically and the shoe would not rub or hit the crank arm during the crank cycle.

We set the target mechanical power output to 1.5 W kg⁻¹ using an electronic stationary trainer (CycleOps PowerBeam Pro Electronic Trainer; Saris; Madison, WI, USA), and equipped the ergometer with 6-component instrumented clip-in pedals (I-CrankSet; ICS-RM Look Keo2;

Sensix, Poitiers, France; 1000 Hz) to measure individual 3D pedal forces and moments. After six participants successfully completed the protocol with this setup, the trainer could not maintain the target mechanical power output, so we replaced it (Kickr Smart Trainer, Wahoo, Atlanta, GA, USA) for the remaining participants. We calibrated each trainer prior to the testing sessions following manufacturer instructions. During the fitting process and experimental trials, participants wore their own road cycling shoes and Look-style cleats, or shoes and cleats that we provided if they did not have their own (S-Works 7, Specialized Bicycle Components, Morgan Hill, CA, USA; Keo Cleat with 9° float, Look, Nevers, France). For the trials with the daily-use prosthesis, participants wore shoes on both feet. For trials with the CSP, we removed the prosthetic foot and shoe, and secured a cleat directly to the bottom of the pylon. We provided participants with extended pylons for the CSP, so that the effective leg length matched that of their daily-use prosthesis.

4.2.3 Experimental protocol

Participants performed a total of eight, 5-minute trials of seated cycling at 1.5 W kg^{-1} over two days wearing their daily-use prosthesis and a CSP. We selected 1.5 W kg^{-1} as a target power output because it is a moderate power output that is achievable by a wide population of participants using aerobic metabolism. For each prosthesis, participants performed a baseline trial using their standard prosthetic effective leg length, and then we increased the effective leg length of each prosthesis in a randomized order by increasing pylon length by +5, +10, and +15 mm using adjustable-length pylons or placing shims in the tube clamps (**Figure 4.1**). We kept the gear ratio constant (53:24), however, the trainers dynamically adjusted resistance to the participant's freely selected cadence so that target mechanical power output was constant.

4.2.4 Data collection

At the beginning of each day, we placed reflective markers on the pelvis and legs. We placed markers on the anterior superior and posterior iliac spines and midway along the iliac crests of the pelvis, bilaterally on the femoral epicondyles and malleoli, and on the shoes at the calcaneus, and 1st and 5th metatarsal heads. We secured rigid clusters of four markers around each thigh and shank segment, and additional tracking markers on the dorsum of the foot. We positioned the markers on the prosthesis and prosthetic foot to mirror the unaffected side: bilateral knee markers were placed on the outside of the prosthetic socket over the visual axis of rotation, bilateral “malleoli” markers were placed on the prosthesis at the same height as the unaffected side, and the markers of 1st and 5th metatarsal heads were placed on the shoe to match the unaffected side. We established a global coordinate system relative to the bicycle by placing four markers on the base of the ergometer and tracked pedal position and orientation with four markers on each pedal square. We collected 15 seconds of lower body kinematic data from the first, fourth, and fifth minute of each trial using a 10-camera motion capture system (Vicon Nexus 2.3, Oxford, UK; 200 Hz) simultaneously with left and right pedal forces and moments.

Before the start of the experimental trials, we measured the participant’s rates of oxygen consumption and carbon dioxide production at rest using indirect calorimetry (TrueOne 2400, Parvo Medics, Salt Lake City, UT) while the participant was stationary and seated on the ergometer. We measured the participant’s rates of oxygen consumption and carbon dioxide production throughout each trial. We instructed participants to refrain from exercising 24 hours prior to the experimental session and be at least two hours post-prandial at the start of the session. We also conducted the experimental sessions at the same time of day to minimize variability in metabolic rates.

4.2.5 Data analysis

We labeled 3D motion capture marker trajectories in Vicon and exported them to Visual 3D (C-Motion Inc., Germantown, MD) along with pedal forces. We filtered motion and forces using a zero-lag, 2nd-order lowpass Butterworth filter with a 12 Hz cut-off (Wilkinson et al., 2020). We measured joint angle as the inter-segment angle, where an increase in joint angle represents extension. Average joint angle was measured over one crank cycle, where the crank starts and ends at top-dead-center (directly above the bottom bracket), and joint range of motion was measured as the difference between the minimum and maximum angles. We converted the local pedal forces to the global coordinate system using a 3D rotation matrix that accounted for the crank and pedal position. The origin of the global pedal forces was determined by a marker on the pedal square in line with the pedal spindle, and then offset to the midline of the pedal. We calculated instantaneous crank forces (tangential and radial) by transforming the global pedal forces with respect to crank position.

We assumed the pedal free-moment to be zero and calculated joint kinetics for each leg in Visual 3D using 10 crank cycles from the last minute of each trial. We multiplied tangential crank force by the length of the crank arm and its angular velocity to calculate instantaneous crank power for each leg. Angular joint power was defined as the dot product of joint moment and angular velocity, and hip transfer power from the upper body was defined as the dot product of the hip joint reaction force and linear velocity (van Ingen Schenau et al., 1990). We averaged the sum of instantaneous crank powers to get total mechanical power output over a complete crank cycle. We defined the average joint and crank power for each leg as the average power over a complete crank cycle. Because there was no “ankle” to define on the CSP, we did not calculate ankle joint power during the CSP trials. We quantified average joint and crank power asymmetry as the percent difference between the affected (AS) and unaffected (US) side (Eq. 4.1),

$$\% \textit{Asymmetry} = \left| \frac{US - AS}{0.5(US + AS)} \right| \cdot 100 \quad [4.1]$$

where perfect symmetry between legs is represented as 0%.

Finally, we calculated metabolic power (Péronnet and Massicotte, 1991) from the rates of oxygen consumption and carbon dioxide production averaged during the last two minutes of each trial and subtracted resting metabolic power to get net metabolic power. We determined net efficiency as the quotient of average total mechanical power output and net metabolic power.

4.2.6 Statistics

We constructed linear mixed-effect models ($\alpha=0.05$) to determine the effect of increased effective leg length (continuous) and prosthesis type (categorical) on average knee and hip angle of the affected side, average joint and crank power from both legs, joint and crank power asymmetry, and net efficiency. We considered the increase in effective leg length, prosthesis type, and side (affected vs. unaffected) as fixed effects and participant as a random effect. We performed all linear mixed-effect model analyses in R (version 3.6.3) (Kuznetsova et al., 2017; R Core Team, 2022).

4.3 Results

For all changes in effective leg length, the average (\pm s.e.) total mechanical power output and cadence for cycling using a daily-use prosthesis was $1.54 \pm 0.10 \text{ W}\cdot\text{kg}^{-1}$ and 73.9 ± 1.7 rpms and using a CSP was $1.56 \pm 0.12 \text{ W}\cdot\text{kg}^{-1}$ and 73.7 ± 1.5 rpms, respectively (**Table 4.1**).

Table 4.1. Average (\pm s.e.) net efficiency, total mechanical power, and cadence while riding with standard (+0 mm) and increased prosthetic effective leg lengths

Δ Prosthetic effective leg length [mm]	Net Efficiency [%]		Power [W·kg ⁻¹]		Cadence [rpm]	
	Daily-use	CSP [#]	Daily-Use	CSP	Daily-Use	CSP
+0	21.8 \pm 0.8	22.6 \pm 0.8	1.55 \pm 0.03	1.55 \pm 0.04	74.2 \pm 3.7	72.3 \pm 3.0
+5	21.0 \pm 0.8	22.3 \pm 0.9	1.53 \pm 0.03	1.57 \pm 0.04	73.1 \pm 3.8	74.1 \pm 3.4
+10	21.2 \pm 0.9	22.2 \pm 0.8	1.53 \pm 0.03	1.56 \pm 0.04	73.3 \pm 3.3	74.2 \pm 2.8
+15	21.3 \pm 0.9	22.0 \pm 0.7	1.55 \pm 0.03	1.56 \pm 0.03	75.1 \pm 3.4	74.1 \pm 3.3

CSP: cycling-specific prosthesis. [#]Effect of prosthesis.

4.3.1 Joint angle

We found that cyclists with a TTA decreased average knee joint angle on the affected side by $0.2 \pm 0.1^\circ$ ($p=0.02$) for every 1 mm increase in prosthetic effective leg length (**Figure 4.2**). Additionally, use of a CSP increased average knee joint angle on the affected side by $12.5 \pm 1.1^\circ$ ($p<0.001$) compared to a daily-use prosthesis. The average knee joint angle on the unaffected side was not influenced by increased prosthetic effective leg length or prosthesis type ($p\geq 0.21$) and was $108.7 \pm 0.05^\circ$ across all trials. Across all prosthetic effective leg lengths, average knee joint angle on the affected side using a daily-use prosthesis was $11.0 \pm 0.8^\circ$ less than the unaffected side ($p<0.001$). However, there was no difference in average knee joint angle between legs when cycling using a CSP ($p=0.35$). As such, we found no significant change in knee joint angle asymmetry with increased prosthetic effective leg length ($p=0.26$) for either prosthesis (**Table 4.2**). However, use of a CSP decreased knee joint angle asymmetry by 6.7 ± 1.4 percentage points ($p<0.001$) compared to a daily-use prosthesis (**Table 4.2**).

We found no significant differences in average hip joint angle on the affected side with increased prosthetic effective leg length ($p=0.22$) or between prosthesis types ($p=0.93$; **Figure 4.2**). Average hip joint angle for all prosthetic effective leg lengths was $69.5 \pm 1.5^\circ$ using a daily use prosthesis and $69.2 \pm 1.4^\circ$ using a CSP. The average hip joint angle for the affected side was

$7.3 \pm 1.8^\circ$ greater than the unaffected side ($p < 0.001$). We also found no significant change in hip joint angle asymmetry (**Table 4.2**) with increased prosthetic effective leg length ($p = 0.74$), and no differences between prosthesis types ($p = 0.27$). Average hip joint asymmetry for all prosthetic effective leg lengths was $11.8 \pm 0.5\%$ while using a daily-use prosthesis, and $14.8 \pm 0.7\%$ using a CSP.

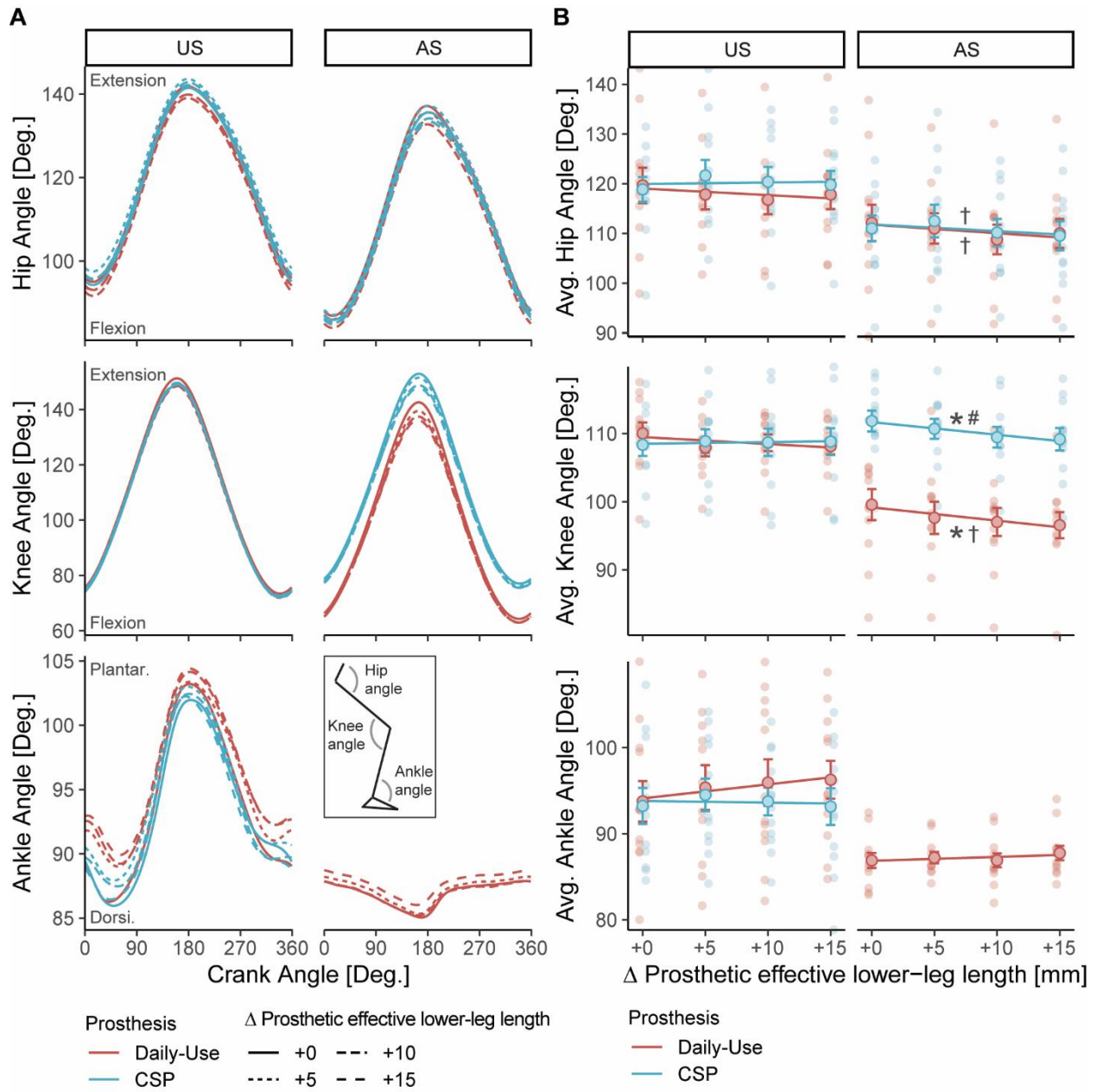


Figure 4.2 Instantaneous (A) and average \pm s.e. (B) hip, knee, and ankle joint angle throughout the crank cycle for the unaffected side (US) and affected side (AS) of cyclists with a unilateral transtibial amputation using a daily-use (red) or cycling-specific (CSP; blue) prosthesis. Ankle joint angle data are not related to our hypotheses but are provided for reference. Colored lines in panel B represent the linear mixed model, and small points represent participant-specific responses with a ± 0.25 mm offset along the x-axis for visual clarity. Note the different y-axes. *Effect of increased prosthetic effective leg length, # effect of prosthesis, † effect of side. There were no interaction effects.

Table 4.2 Average (\pm s.e.) asymmetry between affected and unaffected sides

Asymmetry [%]	Prosthesis	Δ Prosthetic effective leg length [mm]			
		+0	+5	+10	+15
Hip Joint Angle	Daily-Use	12.1 \pm 1.0	10.6 \pm 1.3	12.1 \pm 0.9	12.2 \pm 1.2
	CSP	12.2 \pm 1.3	14.9 \pm 1.5	16.3 \pm 1.7	15.9 \pm 1.2
Knee Joint Angle	Daily-Use	10.2 \pm 1.5	11.0 \pm 1.6	11.7 \pm 1.7	11.8 \pm 1.4
	CSP [#]	3.7 \pm 1.0	3.0 \pm 0.9	2.2 \pm 0.9	2.2 \pm 0.8
Hip Joint Power	Daily-Use	26.5 \pm 6.6	26.1 \pm 6.6	32.2 \pm 7.5	30.5 \pm 8.9
	CSP	35.0 \pm 6.3	28.8 \pm 6.5	29.8 \pm 6.1	26.4 \pm 7.5
Knee Joint Power	Daily-Use	99.9 \pm 19.0	85.2 \pm 13.7	101.4 \pm 19.0	102.5 \pm 19.0
	CSP [#]	90.8 \pm 19.5	92.8 \pm 18.5	90.5 \pm 22.1	94.2 \pm 20.2
Ankle Joint Power	Daily-Use	222.9 \pm 9.6	229.6 \pm 10.8	219.6 \pm 4.7	220.9 \pm 6.5
	CSP	-	-	-	-
Hip Transfer Power	Daily-Use	133.5 \pm 39.1	246.8 \pm 175.9	140 \pm 40.4	213.1 \pm 40.4
	CSP	118.4 \pm 26.8	134.7 \pm 31.3	114.0 \pm 22.1	116.0 \pm 33.2
Crank Power	Daily-Use	54.4 \pm 9.0	49.3 \pm 8.5	54.7 \pm 9.1	58.4 \pm 9.3
	CSP	47.0 \pm 9.2	51.6 \pm 8.9	51.9 \pm 8.1	54.3 \pm 9.0

CSP: cycling-specific prosthesis. There were no significant differences in asymmetry due to increased prosthetic effective leg length ($p \geq 0.18$ for all) or interaction effects ($p \geq 0.08$). [#] Effect of prosthesis.

4.3.2 Power

We found no significant difference in average ankle joint ($p=0.99$), knee joint ($p=0.98$), hip joint ($p=0.94$), hip transfer ($p=0.17$), or crank ($p=0.98$) power for either leg with increased prosthetic effective leg length (**Figure 4.3**). Similarly, we found that use of a CSP did not change average knee joint ($p=0.64$), hip joint ($p=0.73$), hip transfer ($p=0.14$), or crank ($p=0.76$) power for either leg compared to a daily-use prosthesis. We found that average ankle joint, knee joint, hip transfer, and crank power were influenced by side (affected vs. unaffected) ($p < 0.001$ for all), where the affected side produced 0.09 ± 0.01 W kg⁻¹ less average ankle joint power, 0.22 ± 0.01 W kg⁻¹ less average knee joint power, 0.02 ± 0.00 W kg⁻¹ less average hip transfer power, and 0.40 ± 0.02 W kg⁻¹ less average crank power than the unaffected side while using a prosthesis across all

conditions. However, across all conditions we found no difference in average hip joint power ($p=0.38$) between the affected and unaffected sides when cycling using a prosthesis, with the affected side producing $0.35 \pm 0.01 \text{ W kg}^{-1}$ and the unaffected side producing $0.37 \pm 0.01 \text{ W kg}^{-1}$.

We found that increased prosthetic effective leg length did not significantly change average power asymmetry (**Table 4.2**) at the ankle joint ($p=0.67$), knee joint ($p=0.79$), hip joint ($p=0.15$), hip transfer ($p=0.93$), or crank ($p=0.051$) for either prosthesis. Likewise, we found that using a CSP did not have a significant effect on average knee joint ($p=0.32$), hip joint ($p=0.10$), hip transfer ($p=0.65$), or crank ($p=0.12$) power asymmetry compared to a daily-use prosthesis. Ankle joint power asymmetry was $222.9 \pm 4.0\%$ while using a daily-use prosthesis. Knee joint, hip joint, hip transfer and crank power asymmetry were $94.7 \pm 6.6\%$, $29.4 \pm 2.4\%$, $151 \pm 24.6\%$, and $52.7 \pm 3.1\%$, respectively, averaged from both prostheses across all prosthetic effective leg lengths.

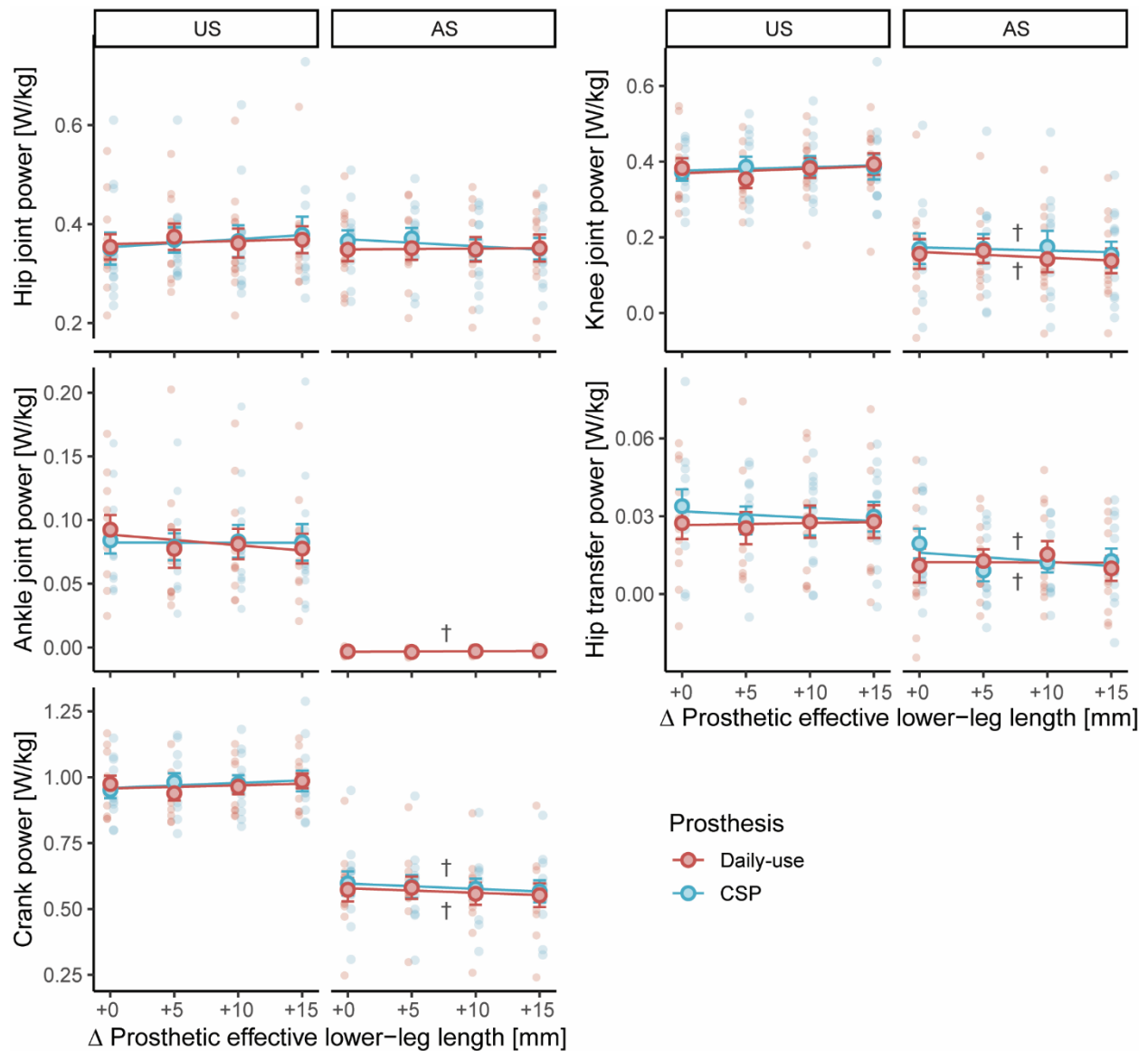


Figure 4.3 Average (\pm s.e.) joint and crank power of the affected side (AS) and unaffected side (US) for cyclists with a unilateral transtibial amputation using a daily-use (red) and cycling-specific (CSP; blue) prosthesis. Colored lines represent the linear mixed model results, and small points represent participant-specific responses with a ± 0.25 mm offset along the x-axis for visual clarity. Note the different y-axes for each subpanel. † effect of side.

4.3.3 Net Efficiency

There was no significant change in net efficiency (**Table 4.1**) with increased prosthetic effective leg length ($p=0.16$). However, compared to using a daily-use prosthesis, using a CSP improved net efficiency from 21.4% to 22.3% across all conditions ($p=0.014$).

4.4 Discussion

We determined the effects of increased prosthetic effective leg length in cyclists with a unilateral transtibial amputation (TTA) at 1.5 W kg^{-1} using a daily-use or cycling-specific prosthesis (CSP). In partial support of our first hypothesis, our results show that a 15 mm increase in prosthetic effective leg length resulted in a 3° decrease in average knee joint angle of the affected side, but this change was not large enough to affect knee joint angle asymmetry. In comparison, cycling using a CSP resulted in a 12.5° increase in average knee joint angle on the affected side, which led to a 6.7 percentage point decrease in knee joint angle asymmetry. We also found that average hip joint angle was not affected by increased prosthetic effective leg length or prosthesis type, therefore, we found no changes in hip joint angle asymmetry.

Cycling using a daily-use prosthesis likely altered the knee and hip joint kinematics of the affected side compared to the unaffected side because a prosthesis cannot emulate biological ankle dorsi- and plantarflexion. We initially assumed that using a daily-use prosthesis would increase average knee and hip joint angle on the affected side compared to unaffected side, because the affected side would be more extended to reach the bottom of the crank cycle if saddle height was based on the unaffected side (Childers et al., 2009). However, contrary to our expectations, we found that the average knee and hip joint angle on the affected side were (avg. \pm s.e.) $10.5 \pm 1.5^\circ$ and $7.5 \pm 0.5^\circ$ less than the unaffected side, respectively (**Figure 4.2**), and indicates that the affected side was more flexed than the unaffected side. Similarly, Childers and Kogler (Childers and Kogler, 2014) reported that cyclists with a TTA using a daily-use prosthesis had an affected side average knee joint angle $\sim 4^\circ$ lower than the unaffected side using equal 172 mm crank arms. However, they also reported that participants increased their hip joint range of motion on the affected side by $\sim 4^\circ$ between the top and bottom of the crank cycle. We did not initially examine

range of motion, but our participants exhibited a similar knee and hip joint range of motion between affected (knee: $78.4 \pm 1.3^\circ$, hip: $50.5 \pm 1.5^\circ$) and unaffected (knee: $78.0 \pm 1.6^\circ$, $47.0 \pm 1.1^\circ$) sides using a daily-use prosthesis.

If cycling with the use of a daily-use prosthesis reduces extension of the affected side, cyclists with a TTA may utilize different motor control strategies than non-amputee cyclists to change their joint kinematics and kinetics. In non-amputee cyclists, redundant degrees-of-freedom within the leg-pedal-crank system allows riders to utilize different joint kinematics throughout the crank cycle to manipulate how mechanical power is transferred to the pedal (Elmer et al., 2011; Martin and Brown, 2009; Yoshihuku and Herzog, 1996). For example, at high mechanical power outputs (>550 W), non-amputee cyclists increase ankle joint duty cycle (the relative time a joint is in extension vs. flexion) so that the ankle is plantarflexed for more than half of the crank cycle (Elmer et al., 2011). Also, when using non-circular chainrings that vary instantaneous crank angular velocity, non-amputee cyclists alter ankle joint angular velocity to maintain constant efficiency and mechanical power from the knee and hip joints (Leong et al., 2017; Leong et al., 2021). The multiple degrees-of-freedom within the leg-pedal-crank system are provided by the non-fixed position of the hip and dorsi- and plantarflexion of the ankle (Yoshihuku and Herzog, 1996), which allows riders without an amputation to vary lower-limb segment trajectories to maintain a constant mechanical power output (Martin and Brown, 2009). A prosthesis removes one degree-of-freedom, so cyclists with a TTA may use another strategy to limit affected side knee and hip joint extension but still allow the cleat to reach the bottom of the crank cycle, such as sitting off-center from the midline of the saddle so that the hip joint center on the affected side is lower, or tilting the pelvis to provide extra leg length (Price and Donne, 1997). Cyclists with a TTA may limit knee and hip joint extension on the affected side to minimize the potential for

injury risk due to increased strain of the knee and hip joint extensors. Future studies are needed to investigate the rider's frontal-plane position on the saddle and its effects on joint kinematics and kinetics.

We found that increased prosthetic effective leg length or cycling with a CSP while riding at a moderate power output (1.5 W kg^{-1}) results in changes to average knee joint angle compared to a daily-use prosthesis. Increased prosthetic effective leg length by +15 mm for both prosthesis types decreased average knee joint angle by 3° on the affected side, thus the affected knee joint was slightly more flexed throughout the crank cycle (**Figure 4.2**). While not part of our hypotheses, we observed that the +15 mm increase in prosthetic effective leg length numerically decreased peak knee joint angle by $6.5 \pm 1.3^\circ$ using a daily-use prosthesis and $5.2 \pm 0.9^\circ$ using a CSP (**Figure 4.2**). Use of a CSP increased average knee joint angle on the affected side by 12.5° so that the leg was more extended, and knee joint angle asymmetry decreased by 6.7 percentage points compared to a daily-use prosthesis. But this change in affected side knee joint angle did not alter average hip joint angle on the affected side or average knee and hip joint angle on the unaffected side (**Figure 4.2**).

Despite the reduction in knee joint angle asymmetry using a CSP versus daily-use prosthesis, our findings do not support our second hypothesis. We found that joint and crank power asymmetry did not change with increased prosthetic effective leg length using a daily-use prosthesis or a CSP (**Table 4.2**), because there was no change in average joint and crank power for either leg (**Figure 4.3**). These results support previous findings (Childers and Kogler, 2014; Allen et al. - Chapter 3) that decreased kinematic asymmetries do not always lead to improvements in joint or crank power asymmetry in cyclists with a TTA. Additionally, we found no evidence of an interaction between increased prosthetic effective leg length and using a CSP. In the previous

chapter (Chapter 3), Allen et al. found that cycling at 1.5 W kg^{-1} using a CSP and shorter affected side crank arm lengths reduced hip joint and hip transfer power asymmetry through small non-significant changes from one or both legs. Our findings indicate that cyclists with a TTA who choose to use a CSP may increase prosthetic effective leg length by up to 15 mm without changing joint or crank power production.

Finally, our results partially support our third hypothesis; net efficiency did not change with increased prosthetic effective leg length, but use of a CSP increased net efficiency by 0.9 percentage points compared to a daily-use prosthesis (**Table 4.1**). It is likely that a 15 mm increase in prosthetic effective leg length is not large enough to elicit changes in knee extensor force-length-velocity relationships to significantly affect joint power, crank power, or efficiency. Whereas the 0.9 percentage point increase in net efficiency when using a CSP is likely attributed to the 12.5% increase in average knee joint angle on the affected side. Previous musculoskeletal modelling studies have demonstrated that an $\sim 11^\circ$ increase in average knee joint angle (due to increasing saddle height) is large enough to shift the vastus muscle fibers into a sub-optimal region of the force-length relationship for producing power and increase the muscle shortening velocity, which leads to a decrease in average crank power (Rankin and Neptune, 2010). While we did not observe a change in joint or crank power when participants used a CSP, increasing the average knee joint angle from $97.7 \pm 2.2^\circ$ using a daily-use prosthesis to $110.3 \pm 1.5^\circ$ using a CSP may have placed the knee extensors in a more favorable state for producing force more economically. This value closely coincides with theoretical studies, showing that crank power is maximized with an average knee angle of 113° in cycling models without a foot segment (Yoshihuku and Herzog, 1996).

We found that net efficiency improved when participants used a CSP compared to daily-use prosthesis across all prosthetic effective leg lengths, whereas our previous study found a non-

significant improvement of 0.7 percentage points in net efficiency when cyclists with a TTA used a CSP versus daily-use prosthesis with different affected side crank arm lengths (Allen et al. - Chapter 3). Previously, Noordhof et al. (Noordhof et al., 2010) showed that the smallest change in gross efficiency (the ratio of mechanical power to gross metabolic power) that can be reliably measured in submaximal cycling via indirect calorimetry is ~0.6 percentage points, and that measures of gross efficiency are not significantly affected by day-to-day variations in metabolism. After reanalyzing our data, we found that use of a CSP provided a significant 0.6 ± 0.2 percentage point (avg \pm s.e., CI_{95%} [0.10 to 1.05], $p=0.02$) improvement in gross efficiency over a daily-use prosthesis (from 17.4% to 18.0%). This improvement in gross efficiency is similar to previous cycling studies (Ferrer-Roca et al., 2014), which reported that non-amputee cyclists significantly worsened gross efficiency by 0.5% when riding at ~70-75% of their VO_{2max} with decreased saddle height from 105% to 102% of trochanteric length (~30 mm difference between the two conditions). When considered together, these results suggest that use of a CSP may improve efficiency over a daily-use prosthesis in cyclists with a TTA while riding at 1.5 W kg^{-1} , but these effects are at the threshold of what can be reliably detected, and further research is required. Future studies of the effects of using CSPs would benefit from using a single absolute workload. Gross efficiency in cycling increases non-linearly with absolute mechanical power output (Ettema and Lorås, 2009; Reger et al., 2013) and may explain why the results of our protocol, that used mass-normalized mechanical power output, results in changes in efficiency that is close to the smallest detectable change for sub-maximal cycling (Noordhof et al., 2010). Our participants rode over a range of 80-150 W, and it is unknown if the potential metabolic benefits provided by a CSP are workload dependent.

4.4.1 Potential limitations

Previous studies found that a prosthetic socket moves relative to the residual limb during cycling (Childers et al., 2012; Childers et al., 2014). The prosthetic socket rotates $\sim 5^\circ$ about the distal end of the residual limb and causes the proximal end of the socket to move anterior to the knee joint center when the knee is maximally flexed at the top of the crank cycle (Childers et al., 2014). Because participants used their own prosthetic socket for this study, we placed markers on the outside of the prosthesis and assumed a rigid connection between the residual limb and the socket. Therefore, we likely measured a greater instantaneous knee joint flexion angle at the top of the crank cycle, which may have affected our measures of average knee joint angle. We assumed a similar error and performed this calculation in all trials and used a repeated measures design, which should account for our comparisons. Future studies are needed to quantify how the movement of the residual limb within a prosthetic socket and how the non-rigid connection affect joint kinematics and kinetics in cyclists with a TTA.

Use of a CSP led to an increase in knee joint angle and net efficiency for cyclists with a TTA, but other bicycle fit manipulations may affect average knee joint angle, such as saddle height (Ferrer-Roca et al., 2014; Nordeen-Snyder, 1977; Price and Donne, 1997; Rankin and Neptune, 2010; Yoshihuku and Herzog, 1996). We set saddle height based on the unaffected side during a static position, but previous studies have suggested that efficiency is optimized with saddle heights set at 98-100% of the trochanteric length (the distance from the greater trochanter to the ground during standing). The optimal saddle height for cyclists with a TTA may differ from that of non-amputees and the net efficiency due to use of a CSP may depend on saddle height. Future research is needed to understand how saddle height and use of a CSP affects knee joint angle and efficiency.

4.5 Conclusion

Increased prosthetic effective leg length up to 15 mm or use of a CSP does not alter average joint or crank power or joint or crank power asymmetry in cyclists with a TTA riding at a moderate power output (1.5 W kg^{-1}). However, increased prosthetic effective leg length of 15 mm decreases the average knee joint angle on the affected side by 3° . Moreover, use of a CSP increases average knee joint angle by 12.5° , reduces knee joint angle asymmetry by 6.7 percentage points, and improves net efficiency by 0.9 percentage points compared to a daily-use prosthesis. Therefore, recreational cyclists with a TTA could increase prosthetic effective leg length by up to 15 mm without changing performance and use a CSP to improve efficiency and thus performance. These findings are useful for riders, coaches, and clinicians to make informed decisions about bicycle fitting components to select or prescribe and may also encourage individuals with a TTA to engage in cycling as form of exercise and promote improvements in overall health.

4.5.2 Funding

This study was funded by a Department of Veterans Affairs research grant awarded to A.M.G (VA RR&D Service RX0030101-01A1).

Conclusions

In Chapter 1, I determined how active muscle volume changed with step frequency in humans during stationary, two-legged hopping and running (at 3.0 m s^{-1}) on level ground. I found that active muscle volume decreased by 26% and 20% during hopping and running, respectively, when step frequency increased from 85% of preferred step frequency to 115% of preferred step frequency. The largest reductions in active muscle volume occurred at the knee in both bouncing gaits through changes in effective mechanical advantage and/or duty factor. Moreover, accounting for the changes in active muscle volume resulted in a near-constant metabolic cost-coefficient, indicating that the primary mechanical determinants of metabolic power (the rate of force generation and active muscle volume) well-describe changes in metabolic power across step frequencies. These findings add to a growing body of research suggesting that changes in effective mechanical advantage influence active muscle volume and the metabolic power in bouncing gaits.

In Chapter 2, I quantified lower-limb joint mechanics during human hopping using a passive, full-leg exoskeleton with three different spring stiffness profiles compared to normal, unassisted two-legged hopping. I found that a passive full-leg design that acts in parallel with the legs primarily assists the muscles surrounding the ankle, followed by the knee, due the length of the average exoskeleton moment arm during the stance phase. Additionally, use of degressive stiffness springs provide the greatest reductions to ankle and knee joint moment and positive power compared to linear or progressive stiffness springs. Finally, the distribution of total average positive power is unchanged when hopping using a passive, full-leg exoskeleton compared to unassisted hopping. The practical application of these data may inform future assistive device designs, especially the development of passive, full-leg exoskeletons that assist running during the ground contact phase.

In Chapter 3, I evaluated the effects of shortened affected side crank arm length and prosthesis type (daily-use vs. cycling-specific prostheses [CSP]) on joint and crank power, joint and crank power asymmetry, and net efficiency in cyclists with a unilateral transtibial amputation (TTA). I found that shorter affected side crank arm lengths and use of a CSP do not significantly change average joint or crank power, or net efficiency while riding at 1.5 W kg^{-1} . However, shorter affected side crank arm lengths while using a CSP provide a small reduction in hip joint power and hip transfer power asymmetry compared to a daily-use prosthesis. These findings suggest that recreational cyclists with a TTA may choose affected side crank arm lengths or prosthesis types based on personal comfort without significantly affecting performance.

In Chapter 4, I evaluated the effects of increased prosthetic effective leg length while using a daily-use prosthesis or a CSP in cyclists with a TTA. I found that increased prosthetic effective leg length decreased average knee joint angle. However, increased prosthetic leg length using either prosthesis does not significantly influence joint or crank power, joint or crank power asymmetry, or net efficiency. Instead, I found that use of a CSP increased average knee joint angle on the affected side, decreased knee joint angle asymmetry, and improved net efficiency compared to a daily-use prosthesis. These findings suggest that cyclists with a TTA can increase prosthetic effective leg length up to 15 mm without affecting performance and use of a CSP provides a performance benefit over a daily-use prosthesis, possibly due to a shift in the knee extensor muscles to a more favorable region of the force-length-velocity curve for producing force more economically.

In conclusion, this dissertation furthers our understanding of the biomechanics and energetics of human locomotion and the influence of assistive devices. These findings provide a

foundation for the future development of assistive devices for bouncing gaits and cycling that can improve performance, promote physical activity and improve overall health.

References

- Alcantara, R. S. (2019). Dryft: A Python and MATLAB package to correct drifting ground reaction force signals during treadmill running. *J. Open Source Softw.* 4, 1910.
- Alexander, R. M. and Bennet-Clark, H. C. (1977). Storage of elastic strain energy in muscle and other tissues. *Nature* 265, 114–117.
- Allen, S. P. and Grabowski, A. M. (2019). Hopping with degressive spring stiffness in a full-leg exoskeleton lowers metabolic cost compared with progressive spring stiffness and hopping without assistance. *J. Appl. Physiol.* 127, 520–530.
- Arampatzis, A., Brüggemann, G.-P. and Metzler, V. (1999). The effect of speed on leg stiffness and joint kinetics in human running. *J Biomech* 32, 1349–1353.
- Arellano, C. J. and Kram, R. (2014). Partitioning the metabolic cost of human running: a task-by-task approach. *Integr Comp Biol* 54, 1084–98.
- Arnold, E. M., Ward, S. R., Lieber, R. L. and Delp, S. L. (2010). A model of the lower limb for analysis of human movement. *Ann Biomed Eng* 38, 269–279.
- Barclay, C. J. (2017). Energy demand and supply in human skeletal muscle. *J. Muscle Res. Cell Motil.* 38, 143–155.
- Barrat, P. R., Martin, J. C., Elmer, S. J. and Korff, T. (2016). Effects of Pedal Speed and Crank Length on Pedaling Mechanics during Submaximal Cycling. *Med. Sci. Sports Exerc.* 48, 705–713.
- Bartlett, J. L. (2007). Muscle function in walking, running and cycling. [Doctoral Dissertation, University of Colorado, Boulder]. *ProQuest Dissertations*.
<http://www.proquest.com/pqdtglobal/docview/304889654/abstract/15BA9B305B114099PQ/2>
- Batliner, M. E., Kipp, S., Grabowski, A. M., Kram, R. and Byrnes, W. C. (2018). Does Metabolic Rate Increase Linearly with Running Speed in all Distance Runners? *Sports Med Int Open* 2, E1–E8.
- Beck, O. N., Gosyne, J., Franz, J. R. and Sawicki, G. S. (2020). Cyclically producing the same average muscle-tendon force with a smaller duty increases metabolic rate. *Proc. R. Soc. B*.
- Beck, O. N., Punith, L. K., Nuckols, R. W. and Sawicki, G. S. (2019). Exoskeletons improve locomotion economy by reducing active muscle volume. *Exerc Sport Sci Rev* 47, 237–245.
- Bergstrom, M. and Hultman, E. (1988). Energy cost and fatigue during intermittent electrical stimulation of human skeletal muscle. *J. Appl. Physiol.* 65, 1500–1505.
- Biewener, A. A. (1989). Scaling body support in mammals: Limb posture and muscle mechanics. *Science* 245, 45–48.

Biewener, Andrew. A., Farley, C. T., Roberts, T. J. and Temaner, M. (2004). Muscle mechanical advantage of human walking and running: implications for energy cost. *J. Appl. Physiol.* 1985 97, 2266–74.

Bike Sizing App | Specialized.com Spec. Bicycle Compon. USA.
<https://www.specialized.com/us/en/bike-sizing/app>

Blickhan, R. (1989). The spring-mass model for running and hopping. *J Biomech* 22, 1217–1227.

Bragaru, M., Dekker, R. and Geertzen, J. H. (2012). Sport prostheses and prosthetic adaptations for the upper and lower limb amputees: an overview of peer reviewed literature. *Prosthet. Orthot. Int.* 36, 290–296.

Carpes, F. P., Mota, C. B. and Faria, I. E. (2010). On the bilateral asymmetry during running and cycling – A review considering leg preference. *Phys. Ther. Sport* 11, 136–142.

Cavagna, G. A. (1975). Force platforms as ergometers. *J Appl Physiol* 39, 174–179.

Cavagna, G. A. and Kaneko, M. (1977). Mechanical work and efficiency in level walking and running. *J Physiol* 268, 467–481.

Cavagna, G. A. and Legramandi, M. A. (2015). Running, hopping and trotting: tuning step frequency to the resonant frequency of the bouncing system favors larger animals. *J. Exp. Biol.* 218, 3276–3283.

Cavagna, G. A., Franzetti, P., Heglund, N. C. and Willems, P. (1988). The determinants of the step frequency in running, trotting and hopping in man and other vertebrates. *J. Physiol.* 399, 81–92.

Cavagna, G. A., Mantovani, M., Willems, P. A. and Musch, G. (1997). The resonant step frequency in human running. *Pflüg. Arch. Eur. J. Physiol.* 434, 678–684.

Cavanagh, P. R. and Williams, K. R. (1982). The effect of stride length variation on oxygen uptake during distance running. *Med. Sci. Sports Exerc.* 14, 30–35.

Childers, W. L. and Gregor, R. J. (2011). Effectiveness of force production in persons with unilateral transtibial amputation during cycling: *Prosthet. Orthot. Int.* 35, 373–8.

Childers, W. L., Perell-Gerson, K. L. and Gregor, R. J. (2012). Measurement of Motion Between the Residual Limb and the Prosthetic Socket During Cycling. *JPO J. Prosthet. Orthot.* 24, 19–24.

Childers, W. L., Prilutsky, B. I. and Gregor, R. J. (2014). Motor adaptation to prosthetic cycling in people with trans-tibial amputation. *J. Biomech.* 47, 2306–2313.

- Childers, W. L., Kistenberg, R. S. and Gregor, R. J. (2011). Pedaling Asymmetries in Cyclists With Unilateral Transtibial Amputation: Effect of Prosthetic Foot Stiffness. *J. Appl. Biomech.* 27, 314–321.
- Childers, W. L. and Kogler, G. F. (2014). Symmetrical kinematics does not imply symmetrical kinetics in people with transtibial amputation using cycling model. *J. Rehabil. Res. Dev.* 51, 1243–1254.
- Childers, W. L., Kistenberg, R. S. and Gregor, R. J. (2009). The Biomechanics of Cycling with a Transtibial Amputation: Recommendations for Prosthetic Design and Direction for Future Research: *Prosthet. Orthot. Int.* 33, 256–71.
- Cherry, M. S., Kota, S., Young, A. and Ferris, D. P. (2016). Running with an elastic lower limb exoskeleton. *J Appl Biomech* 32, 269–77.
- Daly, D. J. and Cavanagh, P. R. (1976). Asymmetry in bicycle ergometer pedalling. *Med. Sci. Sports* 8, 204–208.
- Datta, D. (2017). blandr: a Bland_Altman Method Comparison package for R.
- Deans, S., Burns, D., McGarry, A., Murray, K. and Mutrie, N. (2012). Motivations and barriers to prosthesis users participation in physical activity, exercise and sport: a review of the literature. *Prosthet. Orthot. Int.* 36, 260–269.
- Doke, J. and Kuo, A. D. (2007). Energetic cost of producing cyclic muscle force, rather than work, to swing the human leg. *J. Exp. Biol.* 210, 2390–2398.
- Doke, J., Donelan, J. M. and Kuo, A. D. (2005). Mechanics and energetics of swinging the human leg. *J. Exp. Biol.* 208, 439–445.
- Dontje, M. L., Dall, P. M., Skelton, D. A., Gill, J. M. R., Chastin, S. F. M. and Team, on behalf of the S. U. (2018). Reliability, minimal detectable change and responsiveness to change: Indicators to select the best method to measure sedentary behaviour in older adults in different study designs. *PLOS ONE* 13, e0195424.
- Dyer, B. (2016). Cycling with an amputation: A systematic review. *Prosthet. Orthot. Int.* 40, 538–544.
- Dyer, B. and Woolley, H. (2017). Development of a high-performance transtibial cycling-specific prosthesis for the London 2012 Paralympic Games. *Prosthet. Orthot. Int.* 41, 498–502.
- Dyer, B. and Disley, B. X. (2020). The aerodynamic impact of a range of prostheses designs when cycling with a trans-tibial amputation. *Disabil. Rehabil. Assist. Technol.* 15, 577–581.
- Elmer, S. J., Barratt, P. R., Korff, T. and Martin, J. C. (2011). Joint-Specific Power Production during Submaximal and Maximal Cycling. *Med. Sci. Sports Exerc.* 43, 1940.

- Ericson, M. O. (1988). Mechanical muscular power output and work during ergometer cycling at different work loads and speeds. *Eur. J. Appl. Physiol.* 57, 382–387.
- Ettema, G. and Lorås, H. W. (2009). Efficiency in cycling: a review. *Eur. J. Appl. Physiol.* 106, 1–14.
- Farley, C. T., Blickhan, R., Saito, J. and Taylor, R. C. (1991). Hopping frequency in humans: a test of how springs set stride frequency in bouncing gaits. *J Appl Physiol* 1985 71, 2127–2132.
- Farley, C. T. and González, O. (1996). Leg stiffness and stride frequency in human running. *J. Biomech.* 29, 181–186.
- Farley, C. T. and Morgenroth, D. C. (1999). Leg stiffness primarily depends on ankle stiffness during human hopping. *J. Biomech.* 32, 267–273.
- Farley, C. T., Houdijk, H. H., Van Strien, C. and Louie, M. (1998). Mechanism of leg stiffness adjustment for hopping on surfaces of different stiffnesses. *J Appl Physiol* 1985 85, 1044–1055.
- Farris, D. J., Robertson, B. D. and Sawicki, G. S. (2013). Elastic ankle exoskeletons reduce soleus muscle force but not work in human hopping. *J Appl Physiol* 1985 115, 579–585.
- Farris, D. J. and Sawicki, G. S. (2012a). Linking the mechanics and energetics of hopping with elastic ankle exoskeletons. *J Appl Physiol* 1985 113, 1862–1872.
- Farris, D. J. and Sawicki, G. S. (2012b). The mechanics and energetics of human walking and running: a joint level perspective. *J R Soc Interface* 9, 110–8.
- Farris, D. J., Hicks, J. L., Delp, S. L. and Sawicki, G. S. (2014). Musculoskeletal modelling deconstructs the paradoxical effects of elastic ankle exoskeletons on plantar-flexor mechanics and energetics during hopping. *J Exp Biol* 217, 4018–28.
- Ferrer-Roca, V., Bescós, R., Roig, A., Galilea, P., Valero, O. and García-López, J. (2014). Acute Effects of Small Changes in Bicycle Saddle Height on Gross Efficiency and Lower Limb Kinematics. *J. Strength Cond. Res.* 28, 784.
- Ferrer-Roca, V., Rivero-Palomo, V., Ogueta-Alday, A., Rodríguez-Marroyo, J. A. and García-López, J. (2017). Acute effects of small changes in crank length on gross efficiency and pedalling technique during submaximal cycling. *J. Sports Sci.* 35, 1328–1335.
- Ferris, D. P. and Farley, C. T. (1997). Interaction of leg stiffness and surface stiffness during human hopping. *J Appl Physiol* 1985 82, 15–22.
- Ferris, D. P., Bohra, Z. A., Lukos, J. R. and Kinnaird, C. R. (2006). Neuromechanical adaptation to hopping with an elastic ankle-foot orthosis. *J Appl Physiol* 1985 100, 163–70.

- Forte, P., Marinho, D. A., Silveira, R., Barbosa, T. M. and Morais, J. E. (2020). The Aerodynamics and Energy Cost Assessment of an Able-Bodied Cyclist and Amputated Models by Computer Fluid Dynamics. *Medicina (Mex.)* 56, 241.
- Franz, J. R., Wierzbinski, C. M. and Kram, R. (2012). Metabolic cost of running barefoot versus shod: is lighter better? *Med Sci Sports Exerc* 44, 1519–25.
- Frederick, E., Daniels, J. and Hayes, J. (1984). The effect of shoe weight on the aerobic demands of running. In *Curr Top Sports Med Proc World Congr Sports Med* (ed. Bachl, N.), Prokop, L.), and Suckert, R.), p. Vienna: Urban and Schwarzenberg.
- Fregly, B. J. and Zajac, F. E. (1996). A state-space analysis of mechanical energy generation, absorption, and transfer during pedaling. *J. Biomech.* 29, 81–90.
- Full, R. J., Zuccarello, D. A. and Tullis, A. (1990). Effect of variation in form on the cost of terrestrial locomotion. *J. Exp. Biol.* 150, 233–246.
- García-López, J., Rodríguez-Marroyo, J. A., Juneau, C.-E., Peleteiro, J., Martínez, A. C. and Villa, J. G. (2008). Reference values and improvement of aerodynamic drag in professional cyclists. *J. Sports Sci.* 26, 277–286.
- Gonzalez, H. and Hull, M. L. (1989). Multivariable optimization of cycling biomechanics. *J. Biomech.* 22, 1151–1161.
- Grabowski, A. M. and Herr, H. M. (2009). Leg exoskeleton reduces the metabolic cost of human hopping. *J. Appl. Physiol.* 1985 107, 670–8.
- Griffin, T. M., Roberts, T. J. and Kram, R. (2003). Metabolic cost of generating muscular force in human walking: insights from load-carrying and speed experiments. *J. Appl. Physiol.* 1985 95, 172–183.
- Gutmann, A. K. and Bertram, J. E. A. (2017a). The apparently contradictory energetics of hopping and running: the counter-intuitive effect of constraints resolves the paradox. *J. Exp. Biol.* 220, 167–170.
- Gutmann, A. K. and Bertram, J. E. A. (2017b). Metabolic cost of human hopping. *J. Exp. Biol.* 220, 1654–1662.
- Heglund, N. C. and Taylor, C. R. (1988). Speed, stride frequency and energy cost per stride: how do they change with body size and gait? 18.
- Heil, D. P., Derrick, T. R. and Whittlesey, S. (1997). The relationship between preferred and optimal positioning during submaximal cycle ergometry. *Eur. J. Appl. Physiol.* 75, 160–165.
- Herzog, W., Nigg, B. M., Read, L. J. and Olsson, E. (1989). Asymmetries in ground reaction force patterns in normal human gait. *Med. Sci. Sports Exerc.* 21, 110–114.

- Hewson, A., Dent, S. and Sawers, A. (2020). Strength deficits in lower limb prosthesis users: A scoping review. *Prosthet. Orthot. Int.* 44, 323–340.
- Hogan, M. C., Ingham, E. and Kurdak, S. S. (1998). Contraction duration affects metabolic energy cost and fatigue in skeletal muscle. *Am. J. Physiol.-Endocrinol. Metab.* 274, E397–E402.
- Hothorn, T., Bretz, F. and Westfall, P. (2008). Simultaneous Inference in General Parametric Models. *Biom. J.* 50, 346–363.
- Hoy, M. G., Zajac, F. E. and Gordon, M. E. (1990). A musculoskeletal model of the human lower extremity: The effect of muscle, tendon, and moment arm on the moment-angle relationship of musculotendon actuators at the hip, knee, and ankle. *J. Biomech.* 23, 157–169.
- Högberg, P. (1952). How do stride length and stride frequency influence the energy-output during running. *Arbeitsphysiologie* 14, 437–441.
- Hull, M. L. and Gonzalez, H. (1988). Bivariate optimization of pedalling rate and crank arm length in cycling. *J. Biomech.* 21, 839–849.
- Kaneko, K., Matsumoto, M., Ito, A. and Fuchimoto, T. (1987). Optimum step frequency in constant speed running. In *Biomechanics X-B* (ed. Johnson, B.), p. Champaign, IL: Human Kinetics.
- Kautz, S. A., Feltner, M. E., Coyle, E. F. and Baylor, A. M. (1991). The Pedaling Technique of Elite Endurance Cyclists: Changes with Increasing Workload at Constant Cadence. *J. Appl. Biomech.* 7, 29–53.
- Kerdok, A. E., Biewener, A. A., McMahon, T. A., Weyand, P. G. and Herr, H. M. (2002). Energetics and mechanics of human running on surfaces of different stiffnesses. *J Appl Physiol* 1985 92, 469–78.
- Kessler, S. E., Lichtwark, G. A., Welte, L. K. M., Rainbow, M. J. and Kelly, L. A. (2020). Regulation of foot and ankle quasi-stiffness during human hopping across a range of frequencies. *J. Biomech.* 108, 109853.
- Kipp, S., Byrnes, W. C. and Kram, R. (2018a). Calculating metabolic energy expenditure across a wide range of exercise intensities: the equation matters. *Appl. Physiol. Nutr. Metab.* 43, 639–642.
- Kipp, S., Grabowski, A. M. and Kram, R. (2018b). What determines the metabolic cost of human running across a wide range of velocities? *J. Exp. Biol.* 221,.
- Kram, R. and Taylor, C. R. (1990). Energetics of running: A new perspective. *Nature* 346, 265–267.

- Kuitunen, S., Ogiso, K. and Komi, P. V. (2011). Leg and joint stiffness in human hopping. *Scand J Med Sci Sports* 21, e159-67.
- Kuznetsova, A., Brockhoff, P. B. and Christensen, R. H. B. (2017). lmerTest Package: Tests in Linear Mixed Effects Models. *J. Stat. Softw.* 82, 1–26.
- Lai, A., Lichtwark, G. A., Schache, A. G., Lin, Y.-C., Brown, N. A. T. and Pandy, M. G. (2015). In vivo behavior of the human soleus muscle with increasing walking and running speeds. *J Appl Physiol* 118, 1266–1275.
- Leong, C.-H., Elmer, S. J. and Martin, J. C. (2017). Noncircular Chainrings Do Not Influence Maximum Cycling Power. *J. Appl. Biomech.* 33, 410–418.
- Leong, C.-H., Elmer, S. J. and Martin, J. C. (2021). Noncircular Chainrings Do Not Influence Physiological Responses During Submaximal Cycling. *Int. J. Sports Physiol. Perform.* 17, 407–414.
- Mai, P. and Willwacher, S. (2019). Effects of low-pass filter combinations on lower extremity joint moments in distance running. *J. Biomech.* 95, 109311.
- Malcolm, P., Galle, S., Derave, W. and De Clercq, D. (2018). Bi-articular Knee-Ankle-Foot Exoskeleton Produces Higher Metabolic Cost Reduction than Weight-Matched Mono-articular Exoskeleton. *Front. Neurosci.* 12,.
- Marsh, R. L., Ellerby, D. J., Carr, J. A., Henry, H. T. and Buchanan, C. I. (2004). Partitioning the energetics of walking and running: Swinging the limbs is expensive. *Science* 303, 80–83.
- Martin, J. C., Brown, N. A., Anderson, F. C. and Spirduso, W. W. (2000). A governing relationship for repetitive muscular contraction. *J. Biomech.* 33, 969–974.
- Martin, J. C. and Spirduso, W. W. (2001). Determinants of maximal cycling power: crank length, pedaling rate and pedal speed. *Eur. J. Appl. Physiol.* 84, 413–418.
- Martin, J. C. and Brown, N. A. T. (2009). Joint-specific power production and fatigue during maximal cycling. *J. Biomech.* 42, 474–479.
- Martin, J. C., Milliken, D. L., Cobb, J. E., McFadden, K. L. and Coggan, A. R. (1998). Validation of a Mathematical Model for Road Cycling Power. *J. Appl. Biomech.* 14, 276–291.
- McDaniel, J., Durstine, J. L., Hand, G. A. and Martin, J. C. (2002). Determinants of metabolic cost during submaximal cycling. *J. Appl. Physiol.* 93, 823–828.
- McMahon, T. A. and Cheng, G. C. (1990). The mechanics of running: how does stiffness couple with speed? *J Biomech* 23, 65–78.

- Moed, B. and Kram, R. (2005). Metabolic costs of forward propulsion and leg swing at different running speeds. p. Cleveland, OH.
- Monte, A., Nardello, F. and Zamparo, P. (2021). Mechanical advantage and joint function of the lower limb during hopping at different frequencies. *J. Biomech.* 118, 110294.
- Morris, D. M. and Londeree, B. R. (1997). The effects of bicycle crank arm length on oxygen consumption. *Can. J. Appl. Physiol. Rev. Can. Physiol. Appl.* 22, 429–438.
- Nasiri, R., Ahmadi, A. and Ahmadabadi, M. N. (2018). Reducing the energy cost of human running using an unpowered exoskeleton. *IEEE Trans Neural Syst Rehabil Eng* 26, 2026–2032.
- Noordhof, D. A., de Koning, J. J., van Erp, T., van Keimpema, B., de Ridder, D., Otter, R. and Foster, C. (2010). The between and within day variation in gross efficiency. *Eur. J. Appl. Physiol.* 109, 1209–1218.
- Nordeen-Snyder, K. S. (1977). The effect of bicycle seat height variation upon oxygen consumption and lower limb kinematics. *Med. Sci. Sports Exerc.* 9, 113.
- Oja, P., Titze, S., Bauman, A., de Geus, B., Krenn, P., Reger-Nash, B. and Kohlberger, T. (2011). Health benefits of cycling: a systematic review. *Scand. J. Med. Sci. Sports* 21, 496–509.
- Orekhov, G., Robinson, A. M., Hazelwood, S. J. and Klisch, S. M. (2019). Knee joint biomechanics in transtibial amputees in gait, cycling, and elliptical training. *PLoS ONE* 14, e0226060.
- Pataky T. C. (2010). Generalized n-dimensional biomechanical field analysis using statistical parametric mapping. *J Biomech.* 43, 1976–82.
- Péronnet, F. and Massicotte, D. (1991). Table of nonprotein respiratory quotient: An update. *Can. J. Sport Sci.* 16, 23–29.
- Perry, A. K., Blickhan, R., Biewener, A. A., Heglund, N. C. and Taylor, R. C. (1988). Preferred speeds in terrestrial vertebrates: Are they equivalent? *J. Exp. Biol.* 137, 207–219.
- Pierson-Carey, C. D., Brown, D. A. and Dairaghi, C. A. (1997). Changes in Resultant Pedal Reaction Forces Due to Ankle Immobilization During Pedaling. *J. Appl. Biomech.* 13, 334.
- Pinheiro, J., Bates, D., DebRoy, S., Sarkar, D. and R Core Team (2020). nlme: Linear and Nonlinear Mixed Effects Models.
- Poonsiri, J., Dekker, R., Dijkstra, P. U., Hijmans, J. M. and Geertzen, J. H. B. (2021). Cycling in people with a lower limb amputation. *BMC Sports Sci. Med. Rehabil.* 13, 75.
- Price, D. and Donne, B. (1997). Effect of variation in seat tube angle at different seat heights on submaximal cycling performance in man. *J. Sports Sci.* 15, 395–402.

- R Core Team (2020). R: A language and environment for statistical computing.
- Raburn, C. E., Merritt, K. J. and Dean, J. C. (2011). Preferred movement patterns during a simple bouncing task. *J. Exp. Biol.* 214, 3768–3774.
- Rall, J. A. (1985). Energetic aspects of skeletal muscle contraction: implications of fiber types. *Exerc Sport Sci Rev* 13, 33–74.
- Rankin, J. W. and Neptune, R. R. (2010). The Influence of Seat Configuration on Maximal Average Crank Power during Pedaling: A Simulation Study. *J. Appl. Biomech.* 26, 493–500.
- Rasske, K., Thelen, D. G. and Franz, J. R. (2017). Variation in the human Achilles tendon moment arm during walking. *Comput. Methods Biomech. Biomed. Engin.* 20, 201–205.
- Reger, M., Peterman, J. E., Kram, R. and Byrnes, W. C. (2013). Exercise efficiency of low power output cycling. *Scand. J. Med. Sci. Sports* 23, 713–721.
- Revelle, W. (2019). psych: Procedures for Personality and Psychological Research.
- Roberts, T. J., Chen, M. S. and Taylor, C. R. (1998a). Energetics of bipedal running II. Limb design and running mechanics. *J. Exp. Biol.* 201, 2753–2762.
- Roberts, T. J., Kram, R., Weyand, P. G. and Taylor, C. R. (1998b). Energetics of bipedal running I. Metabolic cost of generating force. *J. Exp. Biol.* 201, 2745–2751.
- Roberts, T. J., Marsh, R. L., Weyand, P. G. and Taylor, R. C. (1997). Muscular force in running turkeys: the economy of minimizing work. *Science* 275, 1113–1115.
- Robertson, B. D., Farris, D. J. and Sawicki, G. S. (2014). More is not always better: modeling effects of elastic exoskeleton compliance on underlying ankle muscle-tendon dynamics. *Bioinspir Biomim* 9, 046018.
- Sargeant, A. J. and Davies, C. T. (1977). Forces applied to cranks of a bicycle ergometer during one- and two-leg cycling. *J. Appl. Physiol.* 42, 514–518.
- Sawicki, G. S., Lewis, C. L. and Ferris, D. P. (2009). It Pays to Have a Spring in Your Step. *Exerc. Sport Sci. Rev.* 37, 130.
- Sawicki, G. S., Beck, O. N., Kang, I. and Young, A. J. (2020). The exoskeleton expansion: improving walking and running economy. *J. NeuroEngineering Rehabil.* 17, 25.
- Schache, A. G. and Baker, R. (2007). On the expression of joint moments during gait. *Gait Posture* 25, 440–452.

- Sepp, L. A., Baum, B. S., Nelson-Wong, E. and Silverman, A. K. (2020). Joint work and ground reaction forces during running with daily-use and running-specific prostheses. *J. Biomech.* 101, 109629.
- Simpson, C. S., Welker, C. G., Uhlrich, S. D., Sketch, S. M., Jackson, R. W., Delp, S. L., Collins, S. H., Selinger, J. C. and Hawkes, E. W. (2019). Connecting the legs with a spring improves human running economy. *J Exp Biol* 222,.
- Smak, W., Neptune, R. R. and Hull, M. L. (1999). The influence of pedaling rate on bilateral asymmetry in cycling. *J. Biomech.* 32, 899–906.
- Snyder, K. L. and Farley, C. T. (2011). Energetically optimal stride frequency in running: the effects of incline and decline. *J. Exp. Biol.* 214, 2089–2095.
- Swinnen, W., Mylle, I., Hoogkamer, W., De Groot, F. and Vanwanseele, B. (2021). Changing Stride Frequency Alters Average Joint Power and Power Distributions during Ground Contact and Leg Swing in Running. *Med. Sci. Sports Exerc.* 53, 2111–2118.
- Taylor, C. R., Heglund, N. C., McMahon, T. A. and Looney, T. R. (1980). Energetic cost of generating muscular force during running. 10.
- Taylor, C. R. (1985). Force development during sustained locomotion: A determinant of gait, speed and metabolic power. *J. Exp. Biol.* 115, 253–262.
- Taylor, C. R. (1994). Relating mechanics and energetics during exercise. *Adv. Vet. Sci. Comp. Med.* 38A, 181–215.
- Umberger, B. R., Gerritsen, K. G. M. and Martin, P. E. (2003). A Model of Human Muscle Energy Expenditure. *Comput. Methods Biomech. Biomed. Engin.* 6, 99–111.
- Too, D. and Landwer, G. E. (2000). The effect of pedal crank arm length on joint angle and power production in upright cycle ergometry. *J. Sports Sci.* 18, 153–161.
- Umberger, B. R. and Rubenson, J. (2011). Understanding Muscle Energetics in Locomotion: New Modeling and Experimental Approaches. *Exerc. Sport Sci. Rev.* 39, 59.
- van den Bogert, A. J. (2003). Exotendons for assistance of human locomotion. *Biomed. Eng. OnLine* 2, 17.
- van Ingen Schenau, G. J., van Woensel, W. W. L. M., Boots, P. J. M., Snackers, R. W. and de Groot, G. (1990). Determination and interpretation of mechanical power in human movement: application to ergometer cycling. *Eur. J. Appl. Physiol.* 61, 11–19.
- Van Sickle, J. R. and Hull, M. L. (2007). Is economy of competitive cyclists affected by the anterior–posterior foot position on the pedal? *J. Biomech.* 40, 1262–1267.

- Veilleux, L.-N., Rauch, F., Lemay, M. and Ballaz, L. (2012). Agreement between vertical ground reaction force and ground reaction force vector in five common clinical tests. *J. Musculoskelet. Neuronal Interact.* 12, 219–23.
- Vigotsky, A. D., Zelik, K. E., Lake, J. and Hinrichs, R. N. (2019). Mechanical misconceptions: Have we lost the “mechanics” in “sports biomechanics”? *J. Biomech.* 93, 1–5.
- Wickham, H. (2016). *ggplot2: Elegant Graphics for Data Analysis*.
- Wilkinson, R. D. and Kram, R. (2022). Nose-down saddle tilt improves gross efficiency during seated-uphill cycling. *Eur. J. Appl. Physiol.* 122, 409–414.
- Wilkinson, R. D., Lichtwark, G. A. and Cresswell, A. G. (2020). The Mechanics of Seated and Nonseated Cycling at Very-High-Power Output: A Joint-Level Analysis. *Med. Sci. Sports Exerc.* 52, 1585–1594.
- Witte, K. A., Fiers, P., Sheets-Singer, A. L. and Collins, S. H. (2020). Improving the energy economy of human running with powered and unpowered ankle exoskeleton assistance. *Sci. Robot.*
- Wright, S. and Weyand, P. G. (2001). The application of ground force explains the energetic cost of running backward and forward. *J. Exp. Biol.* 204, 1805–1815.
- Yandell, M. B., Quinlivan, B. T., Popov, D., Walsh, C. and Zelik, K. E. (2017). Physical interface dynamics alter how robotic exosuits augment human movement: implications for optimizing wearable assistive devices. *J Neuroeng Rehabil* 14, 40.
- Yoshihuku, Y. and Herzog, W. (1996). Maximal muscle power output in cycling: A modelling approach. *J. Sports Sci.* 14, 139–157.
- Zhou, T., Xiong, C., Zhang, J., Hu, D., Chen, W. and Huang, X. (2021). Reducing the metabolic energy of walking and running using an unpowered hip exoskeleton. *J. NeuroEngineering Rehabil.* 18, 95.